DROPLET ANALYSIS AND FLAME PROPAGATION STUDY FOR PARAFFIN AEROSOLS GENERATED BY IMPROVED ELECTROSPRAY DEVICE

A Dissertation

by

YAN-RU LIN

Submitted to the Office of Graduate and Professional Studies of
Texas A&M University
in partial fulfillment of the requirements for the degree of

DOCTOR OF PHILOSOPHY

Chair of Committee,	M. Sam Mannan
Committee Members,	Zhengdong Cheng
	James Holste
	Eric Petersen
Head of Department,	M. Nazmul Karim

May 2017

Major Subject: Chemical Engineering

ABSTRACT

Throughout the process industries, there have been numerous fire and explosion incidents related to aerosols. Aerosols may form from rapid condensation of vapor or accidental leakage of pressurized liquid. However, their hazards are relatively unfocused and the data pertinent to aerosols are scarce compared to vapor and dust. In this research, the electrospray system used to generate aerosol was improved, and the major controlling parameters which affect aerosol quality were studied. Finally, the flame speed of aerosol was researched based on the improvement and findings of stable operation parameters.

The main objective of this study was to advance the understanding of aerosol flame propagation behavior, which provides insight regarding reaction kinetics and pressure rise per unit time. This was made possible by modifying a previous electrospray device. The electrospray was improved by redesigning the whole system. The nozzle packing density was increased by five times, and the electrical force on each nozzle was more uniform. The concentration of aerosol was further promoted by applying a flat grounded mesh and a cylindrical grounded mesh.

The operating parameters of electrospray were also discussed, including additive, liquid flow rate and applied voltage. Amongst the four types of additives tested, Stadis 450 was the most effective one to facilitate the breakup of droplets. The amount of additive also affected the droplet size distribution. Therefore, the type and amount of additive should

be selected carefully to reach the balance of small droplet size and uniform size distribution. This also applied to the liquid flow rate and voltage, and a stable operating region was proposed based on the liquid flow rate and voltage. Electrospray should be operated in this region to conduct consistent studies.

Enhanced aerosol flame speed was observed in a certain “transition droplet size range.” A theoretical calculation was provided to describe the aerosol flame propagation. Although it failed to predict the location of transition range, the estimation of flame speed was improved. An empirical analysis was also proposed to correlate the relationship between the aerosol flame speed, droplet size and liquid properties. The fitting to the experimental results was fairly successful, which indicates the proposed relationship can be considered to further improve the theoretical models.

DEDICATION

To my parents, Kuo-Jiang Lin and Bai-Yin Lin

my wife, Min-Chi Hsieh and my daughter, Emily Lin

for all of their love, understanding and support

ACKNOWLEDGEMENTS

I never thought I would pursue and complete a doctorate degree. It is a long journey and I cannot finish it without all of these kind help. I truly appreciate the people I met, the suggestions I received and also the challenges I encountered.

First of all, I want to sincerely acknowledge my advisor, Dr. M. Sam Mannan, who has offered unconditional support to me throughout these years. He creates an intellectual environment for students to discover the possibility to contribute to process safety. I feel deeply grateful that I had the chance to join Mary Kay O'Connor Process Safety Center in the Chemical Engineering department, Texas A&M University.

I would also like to thank my committee members, Dr. Zhengdong Cheng, Dr. James Holste and Dr. Eric Petersen for their guidance and advice throughout the course of this exploration. Special thanks also go to Dr. Zhengdong Cheng's group with regard to the high speed camera and the set of high voltage generation, which are the essential part of my instrumentation.

It has been a great pleasure to receive guidance and useful suggestions from Dr. Hans Pasman and Dr. Simon Waldram for any question I may have. I also want to express my thanks to my team leaders, Dr. Xiaodan Gao and Dr. Hao Chen, who provided me direction at the beginning of my research and continuously supported my work. I would also like to

thank Dr. Chad Mashuga for discussing electrospray and aerosol with me and inspiring me some great ideas.

I also like to show my appreciation to the pioneers in the field of aerosol research, Dr. Peng Lian and Dr. Szu-ying Huang, for their teaching and coaching. I also want to extend my thanks to the staff in the Mary Kay O'Connor Process Safety Center, Ms. Valerie Green and Ms. Alanna Scheinerman for their assistance and support. My thanks also go to the members in the Mary Kay O'Connor Process Safety Center. They made my experience in the center unforgettably interesting. I would also like to thank my friends, especially those in College Station, who enriched my life here.

My deepest appreciations go to my parents, Kuo-Jiang Lin and Bai-Yin Lin. I want to thank them for the unlimited support and care in every stage of my life. I would not be here without their love. I also want to thank my brother, Wen-Yen Lin, for the joy and tears we had gone through. I want to express my great appreciation to my wife, Min-Chi Hsieh for her help and support during these years. She is always so patient and kind to me. The same thanks also go to her family for treating me as their own. Finally, a special thank is for my daughter, Emily Lin, who makes my happier each and every single day.

CONTRIBUTORS AND FUNDING SOURCES

Contributors

This work was supervised by a dissertation committee consisting of Professors Sam Mannan, Zhengdong Cheng and James Holste of the Department of Chemical Engineering and Professor Eric Petersen of the Department of Mechanical Engineering.

All work for the dissertation was completed independently by the student.

Funding Sources

This research was supported by Mary Kay O'Connor Process Safety Center, Artie McFerrin Department of Chemical Engineering, Texas A&M University.

TABLE OF CONTENTS

Page

Page

Page

LIST OF FIGURES

Page

Page

Page

LIST OF TABLES

Page

CHAPTER I

INTRODUCTION [*]

Fire and explosion hazards of liquids are often classified by their flash points. A liquid is defined as "flammable" if its flash point is under 37.8 ^{o}C as in NFPA 30 [1], or under 93 ^{o}C in the GHS standard [2]. Liquids with flash points above these values are called "combustible liquids," and attention to such liquids is usually less than that of "flammable liquids." The difference reveals the concept of "flammable or combustible" is subjective and prone to change. Table 1 shows the difference between these standards. It can be seen there is a significant gap in defining "flammable liquid." Attention is also needed when following regulations or guidelines to avoid non-compliance.

However, the real hazards depend on the properties of the liquids and the operating conditions of the processes involving the liquids, not solely on their flash points. For combustible liquids, including higher flash point liquids, their flammability can be drastically increased when they are under high pressure and temperature, which is common in the process industries. When a liquid is released under such circumstances, an aerosol or mist often forms. Once an aerosol forms, its properties are significantly different from the properties of the bulk liquid or vapor.

---

[*] Part of this section is reprinted with permission from "Improved electrospray design for aerosol generation and flame propagation analysis" by Y.-R. Lin, H. Chen, C. Mashuga and M.S. Mannan, 2015. *Journal of Loss Prevention in the Process Industries*, 38, 148-145, Copyright 2015 by Elsevier

Table 1. Definition of flammable and combustible liquids under NFPA 30 and GHS

Flash point (^{o}C)	NFPA 30	GHS
Below 22.8 ℃; boiling point below 37.8 ℃	Flammable, Class IA	Flammable, Category 1
Below 22.8 ℃; boiling point at or above 37.8 ℃	Flammable, Class IB	Flammable, Category 2
At or above 22.8 ℃, but below 37.8 ℃	Flammable, Class IC	**Flammable, Category 3**
At or above 37.8 ℃, but below 60 ℃	**Combustible, Class II**	
At or above 60 ℃, but below 93 ℃	**Combustible, Class IIIA**	**Flammable, Category 4 But hazard statement is Combustible liquid**
At or above 93 ℃	Combustible, Class IIIB	Combustible

Since the droplet size is much smaller than the bulk liquid, the surface area will be much higher and evaporation rate will increase dramatically, facilitating the ignition process and combustion. Furthermore, the probability of reaching an ignition source is also increased due to the ease of aerosol dispersion. Given that the hazards associated with the high flash

point liquids are relatively overlooked, aerosol hazards may not be appropriately managed, which may lead to severe incidents. There are many processes in both onshore and offshore facilities that can lead to aerosol formation.

For example, heat transfer fluids (HTFs), a group of high flash point liquids widely used in the industry, have been involved in many incidents. Factory Mutual Engineering and Research (FME&R) reported there were 54 HTFs-related fires and explosions in a ten-year period, which caused $150 million in loss [3]. In 1995, a severe fire and explosion occurred in Milliken & Company's Live Oak/Milstar Complex and Carpet Service Center, causing a total loss of more than $400 million. The direct cause was leakage of hot oil with 350 ^{o}F flash point, and the dense white aerosol cloud spread and quickly reached an ignition source [4]. Moreover, more than 200 incidents involving HTFs had been reported in the past 20 years [5].

One industrial scenario for mist formation is superheated liquid flashovers, in which the liquid vaporizes, expands and cools down to form fine liquid droplets. Another scenario is a liquid stream breaks down into coarse droplets due to the friction force between the liquid surface and air, as demonstrated in literature [6-8].

In standards or codes, only transportation of aerosol dispensers is listed as an aerosol hazard in GHS, and it is classified by flammable components, heat of combustion, and ignition distance test or foam test. If aerosol dispensers contain any component which is

classified as flammable according to GHS criteria (*i.e.*, flammable vapors, flammable liquids, and flammable solids), they should be considered for classification as flammable aerosol in GHS standard. It is important to note that this criterion does not include "combustible liquids." Moreover, aerosols not only form from aerosol dispensers, but may also form due to accidental leakage of liquids/vapors from high pressure and high temperature pipes or vessels in the process facilities, as mentioned previously.

1.1. Statement of the problem

Although it is well known that aerosols pose great threats to the process industries and have been studied for decades, their flammable behavior and mechanisms are not completely understood. There are consensus standards and apparatuses with regard to vapor and dust; however, no consensus has been established to study aerosol flammability, hence aerosol data are much less prevalent than vapor or dust.

Flame speed is an important factor in hazard evaluation of a material. It is generally understood that flame speed increases as aerosol size decreases. However, there is no systematic way to investigate aerosol flame speed. In a previous study, only 83~89 μm droplets of a heat transfer fluid were studied, which may not be sufficient to reveal a clear flame speed pattern [9]. Therefore, it is critical to utilize a reliable device capable of producing high quality droplets to study fundamental aerosol behavior.

In previous studies [9-11], the generated aerosols are not sufficiently small enough for a wider range of flammability study. Also the aerosols are too poly-dispersed and not uniform, and the aerosol concentration is low. In order to further investigate aerosol flammability, it is critical to improve the capability of the device to examine a more complete range of aerosol flammability fundamentals. Only after the improvement has been achieved can the trend of aerosol flame propagation be studied to provide insight and valuable information for managing aerosol hazards.

1.2. Objectives and methodology

The lack of experimental data impedes thorough understanding of aerosol combustion behavior. Therefore, the ultimate goal of this research was to study flammability data of aerosols to assist in the establishment of better preventative and mitigative strategies. In order to achieve the goal, good quality (monodispersed droplet size, high concentration, uniform distribution in the chamber, small droplet size and stable) aerosols were required to generate reproducible and consistent flammability data.

As in previous studies, an electrospray device was used to generate aerosols because it is relatively easy to control the aerosol formation conditions. The first objective of this work was to modify the existing equipment to improve the aerosol quality. The modification consisted of three major physical changes, including setting of spraying nozzles,

utilization of flat ground mesh and cylindrical ground mesh, and adjustment of ignition source.

The second objective was to explore operating parameters for high quality aerosols, including electrical conductivity of liquid, applied voltage and liquid flow rate. Electrical conductivity and other physical properties of liquid were adjusted by additive type and additive concentration. Optimization of the three parameters is essential to obtain monodispersed and stable aerosols. An optimal operating region was outlined for stable operation.

After the first and second objectives were complete, good quality aerosols were generated to allow the study of aerosol flame propagation. Three hydrocarbons (*n*-octane, *n*-decane and *n*-dodecane) were investigated to provide the overview of aerosol flame speed. An enhanced flame propagation phenomenon was found within a certain droplet size range, termed the "transition range", which is contradictory to general perception. In the viewpoint of inherently safer design, the transition range should be avoided once there is a release because the aerosol flame speed is at the maximum under this condition. In addition to experimental study, the trend of flame propagation as a function of liquid characteristics was correlated using empirical analysis. A theoretical model was also developed to calculate and predict the magnitude of flame speed. The methodology of this research is presented in Figure 1.

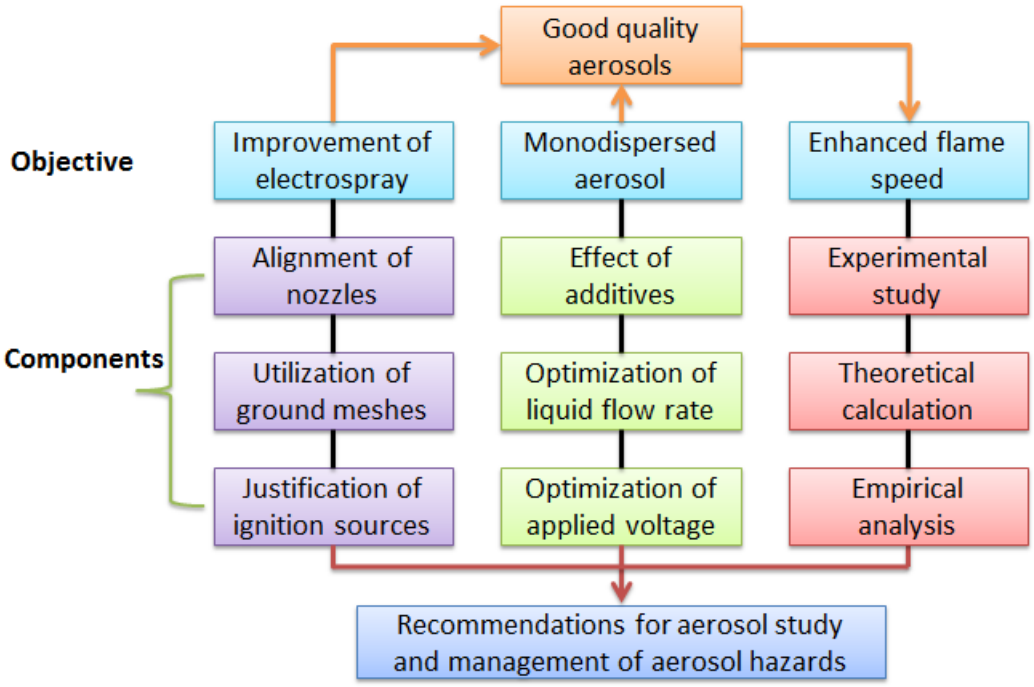

Figure 1. Research methodology

1.3. Organization of the dissertation

The research reported in this dissertation was conducted in Aerosol Laboratory (402 of Jack E. Brown Building) of the Mary Kay O'Connor Process Safety Center at Texas A&M University and parts of it have been published in peer-reviewed journals. There are five additional chapters after the Chapter I Introduction.

Chapter II introduces the holistic review of literature, including formation of aerosol, dispersion of aerosol, the required energy to ignite aerosol, the upper and lower limit of flammable range and flame propagation. Some aerosol incidents are also shown to raise

readers' awareness. Chapter III presents the equipment setup, including electrospray and its modification for high quality aerosols (aerosol generation), Malvern laser system (measurement of droplet size and aerosol concentration), ignition system and high speed camera (for analysis of aerosol flame speed). Chapter IV explores the operating parameters, including the liquid properties (mainly to change electrical conductivity), the applied voltage and the liquid flow rate. It also provides the rationale of additive selection and results of solubility test. Optimization of these parameters is necessary to produce high quality aerosols for fundamental study. Chapter V shows the results of aerosol flame speed tests. The transition range phenomenon has been confirmed in this study by examining three *n*-alkanes. When the droplet sizes are within this range, the flame speed will be even higher than that of smaller droplet size, which is in conflict with people's intuitiveness. The analysis of flame propagation behavior and possible explanation are also given in this chapter. Finally, overall conclusions of this dissertation and tentative future work are provided in Chapter VI.

CHAPTER II

BACKGROUND

The hazards associated with gas explosion and dust explosion have been widely recognized and studied. Centuries ago, gas explosions often occurred in the mining industry and people began to research gas flammability limit and other properties. Sophisticated apparatuses have been set up to explore this field. Dust explosions also grasp public attention, such as the Imperial Sugar dust explosion in 2008 which caused 14 deaths. Dust explosions have an added degree of complexity compared to gas explosions. In addition to the fire triangle in gas explosion, two other cornerstones (confinement and dispersion) are added to create the fire pentagon for dust explosions.

The definition of an aerosol is a group of solid or liquid particles suspended in a gas. This study only focuses on liquid droplets. An aerosol can form as a result of accidental leakage of high pressure and high temperature liquids, or rapid condensation of superheated vapor. Hydrocarbons are widely used in the process industries and many of them are operated under conditions which allow aerosol formation. However, there are no clear metrics to evaluate aerosol hazards, nor a robust apparatus to investigate aerosol properties. Therefore, flash point, fire point and auto-ignition temperature are usually used as criteria to select a fluid or to judge its safety. When a liquid is at its flash point, the vapor concentration can produce a flash fire momentarily once ignited. It is tested based on ASTM D92 or Cleveland Open Cup method. On the other hand, when liquid is at its fire

point, the vapor concentration is sufficient to sustain the combustion. It is tested based on ASTM D93 or Penske Martens Closed Cup method. Nevertheless, this is insufficient to evaluate aerosol hazards and avoid aerosol incidents.

It is a good practice to classify areas in the petroleum installations based on presented hazards and risks. However, there is a concern that industrial fluids operated under their flash points may be classified as non-hazardous under the Institute of Petroleum Model Code of Safe Practice. An example of such a scenario was given in the paper by Bowen and Shirvill [12]. Although the liquids are below their flash points, aerosols could still form and disperse to reach an ignition source. The ensuing fire or explosion can be as devastating as a vapor explosion or a dust explosion. As a result, a holistic literature review is given regarding aerosol formation, dispersion, ignition, flammability limit and its consequences. Some case studies are also provided to depict what aerosol fire/explosion incidents look like.

2.1. Incidents

As mentioned in Chapter I, 54 incidents involving heat transfer fluids (HTFs) were reported in the paper by Febo and Valiulis [3]. Four of these incidents were explosion scenarios. One of those explosions blew out two concrete block walls and moved a third wall by 5 inches. The HTF was used in a 2195 kW heater and the liquid amount was 7.5

m^3. Its flash point was 232 ^oC and the pressure was 4.5 barg. The HTF was sprayed away and ignited after an expansion joint (rated for 10 barg) separated.

In 1974, there was a massive explosion in Flixborough, UK. The explosion killed 28 personnel and injured 36 others. Although the consequences were very severe, they could have been even worse if the explosion had occurred during a normal work day. There were six reactors in series containing cyclohexane and converting it to cyclohexanone and cyclohexanol. The reaction condition was under 8.63 bar and 155 °C. Five days prior to the incident, cyclohexane leaked out of reactor no. 5, and the reactor was removed. A dogleg shaped bypass line was installed to connect reactor no. 4 and no. 6 for continuous production. However, forces arising from the bypass line were not considered, and the bypass line ruptured after startup. A large quantity of superheated cyclohexane flashed and then condensed to form fine droplets. The aerosol cloud found an ignition source and the explosion demolished the plant [13]. Although this is a serious aerosol incident, it is often considered a vapor cloud explosion. Both of these events are devastating, however earlier efforts on aerosol lost attention, resulting in a lack of appropriate aerosol hazard management.

In 2012, a huge white and black cloud was seen at Chevron refinery facility in Richmond, CA. Luckily, only 6 employees were injured from this aerosol fire incident. The pipe rupture and aerosol cloud formation occurred in the “4-sidecut” 8-inch line containing light gas oil at a rate of 5,000 bpd (normally it was 10,800 bpd, but it was reduced by the

shift team leader). The operation conditions were around 640 ^{o}F and 55 psig (flash point of light gas oil: <200 ^{o}F, auto-ignition point: 640 ^{o}F). A small leak was identified in the pipe. As a result, the fire department was called to the scene to establish Incident Command, which is a normal practice at the refinery. Workers removed the insulation in order to evaluate an appropriate method to fix the leak. When they did this, the leak got worse and the light gas oil sprayed out and flashed to form a huge aerosol cloud [14]. Luckily, the leak was identified in the early stage and firefighters had sprayed water over the scene, resulting in consequences that were far less catastrophic than Flixborough.

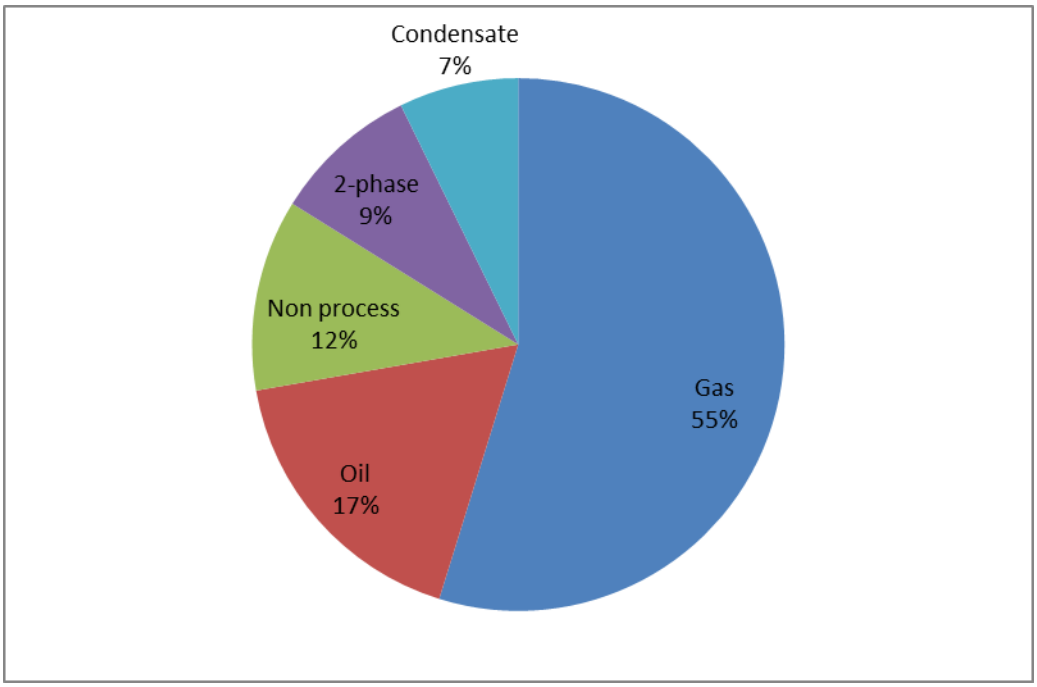

Figure 2. Frequency of hydrocarbon release by type of release

In a ten-year period (1992 to 2002), 2312 hydrocarbon releases in offshore installations had been reported to Hydrocarbon Releases (HCR) Database (belong to Health & Safety Executive, UK) as displayed in Figure 2. More than half of the releases were gas releases and sources from liquid hydrocarbons were 36% (oil + non process + condensate) [15]. Many of these fluid releases have the potential to form aerosol cloud, either from high pressure release or rapid condensation of vapor. Amongst these releases, 143 cases reached ignition and the report provided more detailed information about them. 27 cases out of the 143 cases with a release pressure over 10 barg are listed in Table 2 and the rupture holes were around 1 to 10 millimeters. When a fluid is released under such conditions it has high tendency to produce an aerosol cloud. It should be noted that all such releases were from non-process type, except one was oil type which is indicated in bold font.

As indicated in previous studies [6, 8, 10, 11], high flash point liquids, such as HTFs, can form aerosols and pose fire and explosion threats to people and surroundings. However, any fluids under the right conditions can actually generate aerosols, and they may be more devastating than their vapor form [16-18]. Therefore, a thorough understanding of aerosol properties is needed to manage the associated hazards.

Table 2. Liquid hydrocarbon releases with a pressure over 10 barg [15]

No.	Hydrocarbon type	Release pressure (barg)	Equivalent hole (mm)
16	Heat Trans Oil	10.34	9.53
31	Lub Oil	100.00	1.00
33	Lub Oil	70.00	12.70
40	Diesel	30.00	1.00
41	Fuel Oil	10.00	5.00
46	Diesel	30.00	11.80
47	Diesel	30.00	11.80
48	**Oil**	**250.00**	**25.40**
56	Lub Oil	10.00	2.70
58	Diesel	30.00	1.00
59	Diesel	30.00	2.30
64	Lub Oil	17.24	1.00
70	Diesel	103.45	12.70
71	Diesel	103.45	12.70
72	Diesel	23.00	1.00
82	Diesel	50.00	1.00
84	Diesel	68.97	1.00
91	Lub Oil	100.00	5.00
92	Glycol	10.34	1.00
96	Hydraulic Oil	81.00	3.20
99	Diesel	82.80	1.00
110	Diesel	124.00	1.40
112	Diesel	124.00	1.40
113	Lub Oil	10.00	1.90
121	Diesel	123.99	1.60
122	Diesel	40.00	1.00
123	Diesel	110.00	1.00

2.2. Aerosol formation

In conditions present in industry, aerosols can form from accidental leakage of high pressure processes. Depending on the storage temperature and fluid properties, it can be further divided into mechanical breakup, transition to flashing and full flashing liquid jet [19]. In the laboratory, there are more ways to generate liquid droplets, such as sonic spray, ultrasonic vibration, electrospray, surface acoustic wave (SAW) and vibrating orifice aerosol generation (VOAG). However, this chapter gives only a general idea on atomization from a high pressure orifice. The electrospray generation method will be introduced in chapter III.

Faeth described the breakup regimes and structure of aerosols generated from a high pressure orifice (*i.e.*, non-evaporating round pressure-atomized spray) [20]. Since the breakup mechanism is extremely complicated, the transition criteria for spray regimes are not very clear. The breakup of a liquid stream can be divided into six regions: drip, stable liquid jet, Rayleigh breakup, first wind-induced breakup, second wind-induced breakup and atomization breakup. The extreme case of drip regime happens at very low flow rate where $We_f < 3\sim4$. Another extreme case is stable liquid jet where the viscous force is too large to cause any breakup ($Oh > 2\sim4$). Therefore, dense spray can only occur in the other four regimes as shown in Figure 3.

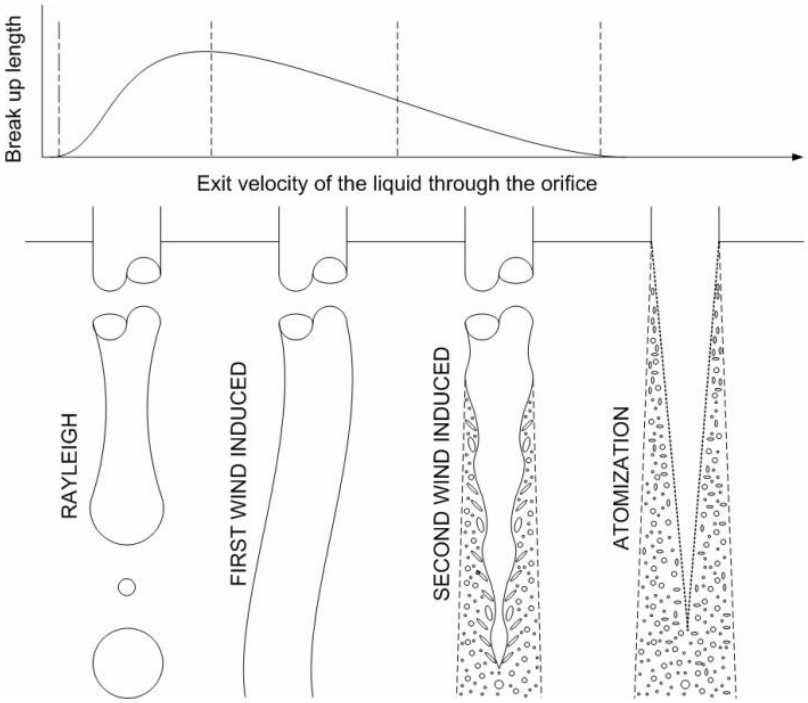

Figure 3. Breakup regimes and associated length for round jets in still gas [7]

These four regimes are based on jet flow rate exiting the orifice, with flow rate increasing left to right. When the flow rate is relatively low, the breakup length (the distance of jet breakup happening from the orifice exit) also increases in the Rayleigh regime. In this regime, the liquid inertia force interacts with surface tension, resulting in a droplet size larger than the orifice diameter. For the remaining three regimes (first wind-induced breakup, second wind-induced breakup, and atomization breakup), gas phase aerodynamics is involved and the breakup length decreases monotonically with increasing liquid flow rate. Droplet size in the first wind-induced regime is similar to the orifice diameter due to the twisting or helical instability in the liquid stream. In the second wind-induced regime, both the helical and surface instability of liquid stream are involved so

the surface shear created by the high relative velocity between gas and liquid tears the liquid stream. The droplet diameter varies in a wide range of sizes up to the orifice diameter. When the shear force continues to increase (increase of the liquid flow rate), the point where spray breakup begins right at the orifice exit is the beginning of the atomization regime [7, 20].

From the viewpoint of potential hazards, the second wind-induced and atomization regimes pose greater threats over others, and the two regimes are generalized in Figure 4 [8]. The distance AB is the breakup length and the distance AC is the aerosol formation distance. In the zone AB, there is liquid only. In the zone BC or disintegration zone, shear force due to relatively high velocity between the liquid stream and still air rips the surface of the liquid column into irregular liquid ligaments, which is the primary breakup. The rate of primary breakup directly affects the length of the liquid core as it disintegrates ligaments from the liquid column. This zone is also called dense spray consisting of a liquid core and a dispersed flow region. These liquid ligaments are not stable and subject to secondary breakup. Finally a dilute spray with smaller and stable droplets are formed due to deformation and further breakup of the liquid droplets [21].

Previous studies particularly focus on the relation of droplet size and liquid condition, especially for high flash point liquids [6, 8, 22]. Figure 5 clearly indicates the atomization process and the required distance for liquid breakup and full development of aerosol droplets. Due to the extreme aerodynamic complexity, dimensional analysis was used to

develop empirical equations for correlation of droplet size, liquid properties and operating condition of the liquid. Suggestions were made on the selection of heat transfer fluids to reduce potential hazards.

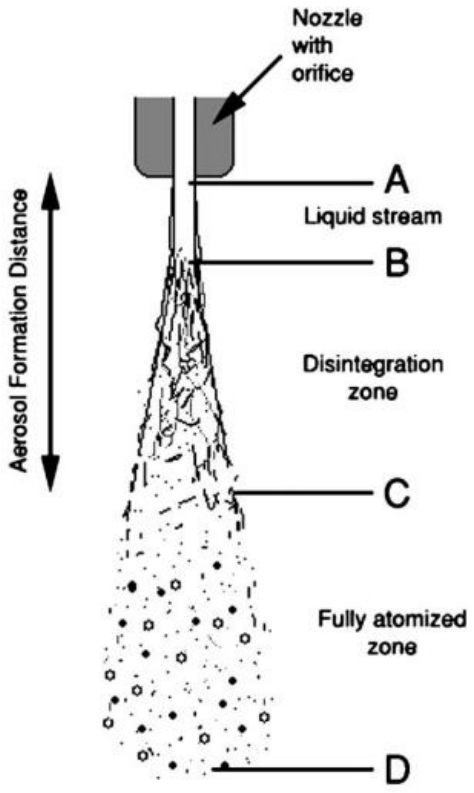

Figure 4. Process of liquid atomization by high pressure [8]

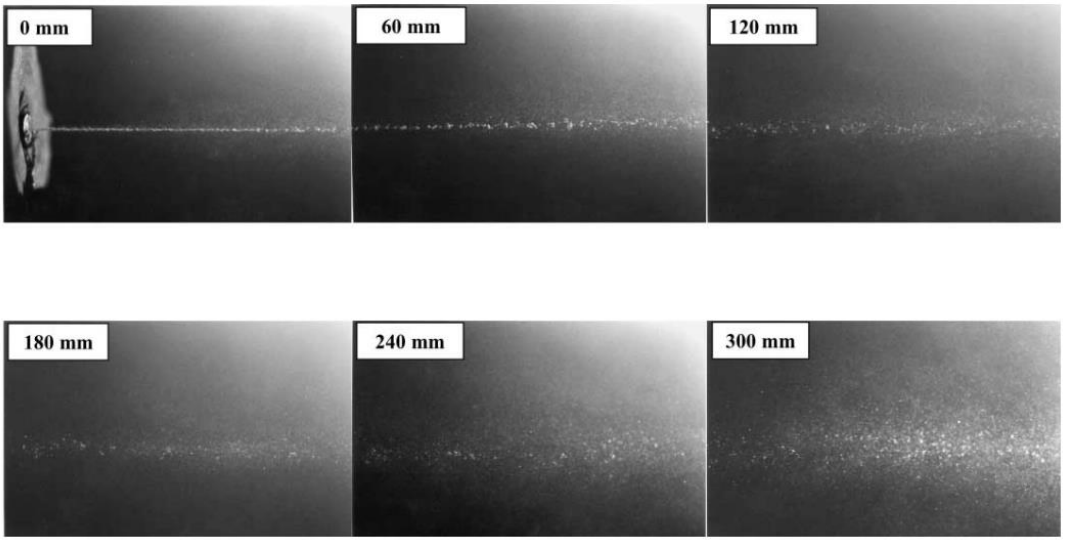

Figure 5. Photographs of atomization process released under high pressure orifice [6]

2.3. Aerosol dispersion

After formation of aerosol due to accidental leakage, the aerosol usually travels some distance due to high pressure in the container, obstacle impingement and wind. Since its droplet size is much smaller than its bulk liquid, it is much easier to disperse and reach an ignition source. As a result, it is important to understand the aerosol dispersion phenomenon. During the dispersion process, the droplet size can change due to heat and mass transfer. Additionally, the droplets may coalescence once they collide together. If the size is too large, the droplets will precipitate (rainout) and decrease aerosol concentration. These dynamic processes depend on fluid properties, ambient temperature, humidity, release condition, wind speed and obstacles, *etc*.

In order to understand and predict aerosol formation and dispersion, a multi-year program had been conducted and supported by the Center for Chemical Process Safety (CCPS). The end result of the research is the RELEASE model, which considers the physical properties of released fluids and release conditions (temperature and pressure), *etc*. When a fluid is released to the atmosphere from high pressure and temperature, the RELEASE model is able to simulate the amount of liquid, vapor or two-phase release generated. However, this model only addresses pure component releases in the horizontal direction, and it does not consider vaporization effect during droplet travel trajectory [23].

Det Norske Veritas Ltd. (DNV) had developed the "Unified Dispersion Model" (UDM) using the PHAST software to predict the two-phase fluids due to accidental atmospheric releases. It can calculate the amount of rainout, pool spreading and re-evaporation, as shown in Figure 6. It could also simulate releases of mixtures. However, it is based on the simple assumption that the properties of mixtures can be reasonably represented by average values. Possible improvement was assessed for UDM in PHAST 6.0, including considering air entrainment, using isentropic expansion or isenthalpic expansion and employing droplet size distribution (currently it is only the average droplet size), *etc*. Also the flashing breakup mechanism is based on the RELEASE model and CCPS data which have some disadvantages [24].

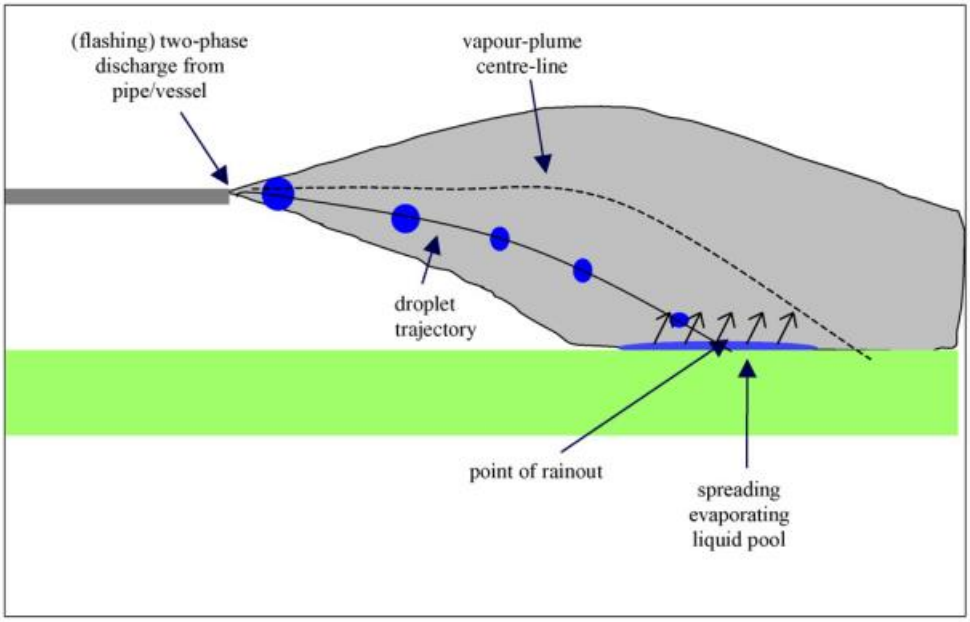

Figure 6. Process of two phase release [25]

2.4. Ignition

After an ignitable aerosol cloud has formed and dispersed, it needs to contact with an ignition source for any possible ignition and combustion (if the fluid is below it auto-ignition temperature). However, there are many ignition sources in any process plant, and most of the time it is difficult to identify all ignition sources. Even when ignition sources are identified, it is impossible to eliminate all of them. As a result, efforts should be made to understand the types of ignition sources, the required energy and the required temperature for ignition so that adequate approaches may be taken to reduce the probability of ignition.

Table 3. Overview of ignition sources and their percentage [26]

Ignition source	Percentage
Electrical (wiring of motors)	23
Friction (bearings or broken parts)	10
Overheated materials (abnormally high temperatures)	8
Hot surfaces (heat from boilers, lamps, etc.)	7
Burner flames (improper use of torches)	7
Combustion sparks (sparks and embers)	5
Cutting and welding (sparks, arc, heat, etc.)	4
Mechanical sparks (grinders, crushers)	2
Static sparks (release of accumulated energy)	1

An overview of ignition sources over 25,000 fires and their percentage had been given in Factory Mutual Engineering Research Corporation's report, as shown in Table 3 [26]. As mentioned in Chapter 2.1, for data from Hydrocarbon Releases (HCR) Database about offshore installments, 27 fires were liquid released with pressure over 10 barg [15]. The types of these ignitions are listed in Table 4. Most of the fires were caused by hot surfaces. Additionally, Santon surveyed several databases and reported 37 incidents related to mists or aerosols and 20 of the incidents resulted in explosions. The possible ignition sources of these incidents are presented in Table 5 [27]. It can be noted there were many unknown sources, and the distribution of the ignition sources is also highly varied from these tables. The possible reason for the high variation is that: the data in Table 4 is biased to offshore

installments. While the number of data points in Table 5 is limited, and there are also many unknown ignition cases.

Table 4. Ignition sources in the 27 fires from HCR database [15]

Ignition source	Cases
Overheated materials (abnormally high temperatures)	1
Hot surfaces	20
Engine induction	4
Gas Burner	1
Not known	1

Table 5. Ignition sources in the 37 incident from Santon's report [27]

Ignition source	Cases
Compression auto-ignition	1
Electric arc	1
Hot surface	3
Static	6
Combustion chamber/igniter/pilot flame	10
Hot work	1
Engine induction	1
Catalyst	1
Naked light	1
Unknown	12

When considering ignition energy for combustible or flammable materials, the main parameter is minimum ignition energy (MIE). It is the minimum energy which can initiate a sustainable flame. It can be affected by many factors for a given chemical or mixture composition, such as temperature, pressure, turbulence and droplet size. It is usually measured by the discharge of energy (J) stored in a capacitor. A schematic view of droplet ignition is shown in Figure 7. A droplet receives a certain amount of energy and the temperature within the droplet increases. Due to the energy and increased temperature, some of the liquid is vaporized, which mixes rapidly with the surrounding air. If the vapor mixture due to vaporization is within the flammability limit and remaining energy is sufficient to ignite the mixture, a flash can be observed. If the rate of heat release from the combustion is higher than the rate of heat loss to surroundings, the combustion will sustain and propagate. MIE is the critical energy limit to a specific chemical at a specific condition.

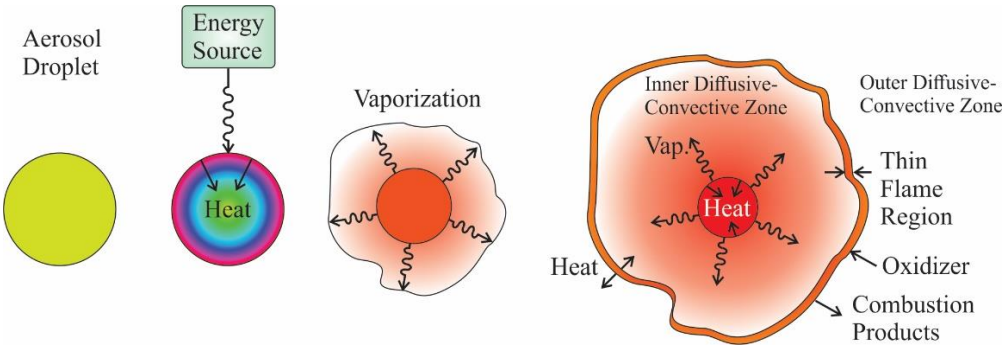

Figure 7. Schematic view of droplet ignition

The concern with aerosols over bulk liquids is the extreme increase in surface area due to their small droplets. This can enhance the rate of mass and energy transfer, thus aerosols can be ignited at temperatures below their liquid flash points. However, it is reported that the MIE of aerosols is normally one or more orders of magnitude higher than gas mixtures due to extra energy needed to vaporize the liquid droplets [28].

Sauter Mean Diameter (SMD) is used to represent the characteristic size of droplets. SMD is a volume-to-surface area ratio for droplets and is widely used in mass and heat transfer studies. Research indicates that droplet size has strong effect on MIE, as shown in Figure 8 [28]. As droplet size decreases, the MIE reduces dramatically for isooctane, diesel and heavy fuel oil within 40 to 100 μm. Nevertheless, some investigation demonstrated that there exists an optimal droplet size for absolute MIE, as displayed in Figure 9 [29]. In Figure 9 the fuel is tretralin and droplet size ranges from 12 to 40 μm. The MIE reaches a minimum at around 24 μm. It is possible that the trend of MIE varies with materials, and the droplet size in Figure 8 is too large. Another explanation is the shock wave in the spark kernel pushes the smaller droplets away in Figure 9, which causes a lean vapor mixture around the smaller droplet size and requires higher MIE for ignition.

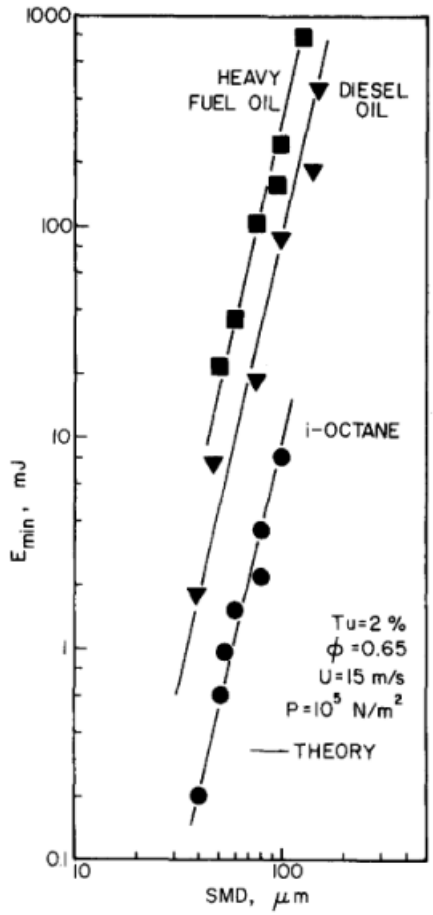

Figure 8. Effect of droplet size on MIE [28]

Another interesting consideration is the definition of successful ignition. Its effect has been demonstrated in Figure 9, and the more clear demonstration is in Figure 10 [30]. Because the definition of successful ignition can significantly change the required energy to ignite aerosols, ignition tests should be conducted with caution (*e.g.*, 50% of ignition at 2 mJ vs. 90% of ignition at 20 mJ in Figure 10).

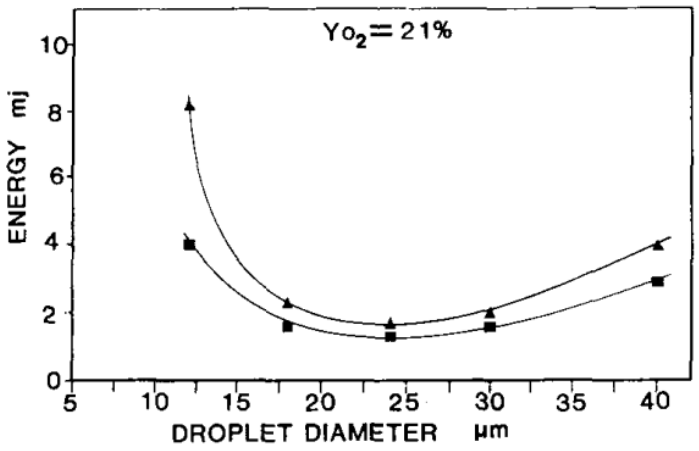

Figure 9. Optimal droplet size on MIE for tetralin aerosols (▲) 70% of ignition frequency (■) 50% of ignition frequency [29]

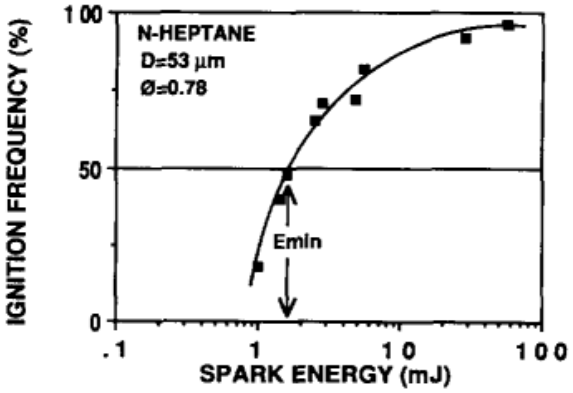

Figure 10. Influence of ignition frequency on ignition energy [30]

Fuel-air equivalence ratio (ϕ) also has a large impact on the MIE. Danis *et al.* pointed out there is an optimum equivalence ratio for pre-vaporized *n*-heptane (*i.e.*, vapor) between ϕ = 1.5 and 2.0. However, the optimum region was not observed for *n*-heptane aerosols (33, 41, 53µm respectively) up to ϕ = 1.8 [30]. Nevertheless, it was reported that there is an optimum equivalence ratio for *n*-decane aerosols. For a droplet size of 40 µm, the optimum

equivalence ratio is around 0.9; for a droplet size of 80 μm, the optimum equivalence ratio is around 1.7 [31].

2.5. Flammability limit

For a fuel to be ignitable, it must be within the upper and lower flammability limit (UFL and LFL). The concept has been widely studied in the vapor phase, and minimum explosive concentration (MEC) is used in dust explosion research. In general people have more concern about LFL as the concentration of accidental released fuel is increased from zero (or near zero) into the flammability limits, and the LFL is more often to encounter.

The measurement of flammability limit is highly affected by experimental method and definition. For UFL and LFL in vapor phase, the ignition energy is usually set as 10 J stored in an electric arc. As a result, an ignition source with much higher energy may ignite a mixture outside of the flammability limits which is measured using 10 J of energy [32]. Although combustion under such situation is not stable and would be extinguished easily by outside disturbance, the determination of flammability should be defined clearly. In the case of MEC in dust explosion, the ignition energy is usually set as 2,500 or 5,000 J stored in pyrotechnic ignitor and tested in a 20 L explosion chamber per ASTM 1515 standard. However, such consensus does not exist for aerosol study due to the difficulty of aerosol formation in a well-controlled manner.

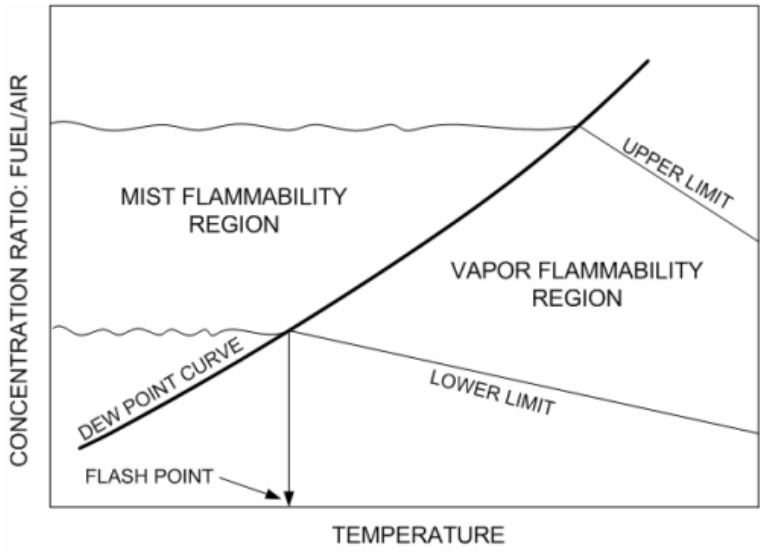

Figure 11. Flammability curve in terms of concentration and temperature [7]

Therefore, the values of aerosol LFL and UFL are described in a conceptual form as shown in Figure 11 [7]. This concept was proposed by Eichhorn in 1955 and raised the concern of aerosol fire and explosion [33]. He thought there were UFL and LFL for aerosols similar to the vapor phase even though the temperature is well below their flash points. Once the concentration of aerosol falls into this range, the aerosol can explode. The dew point curve separates the aerosol and vapor form, and the flammability limit varies with temperature. Although this diagram is an over-simplified concept in 1955, we still cannot answer the question of aerosol flammability limit thoroughly. This indicates that more effort is needed to study aerosols.

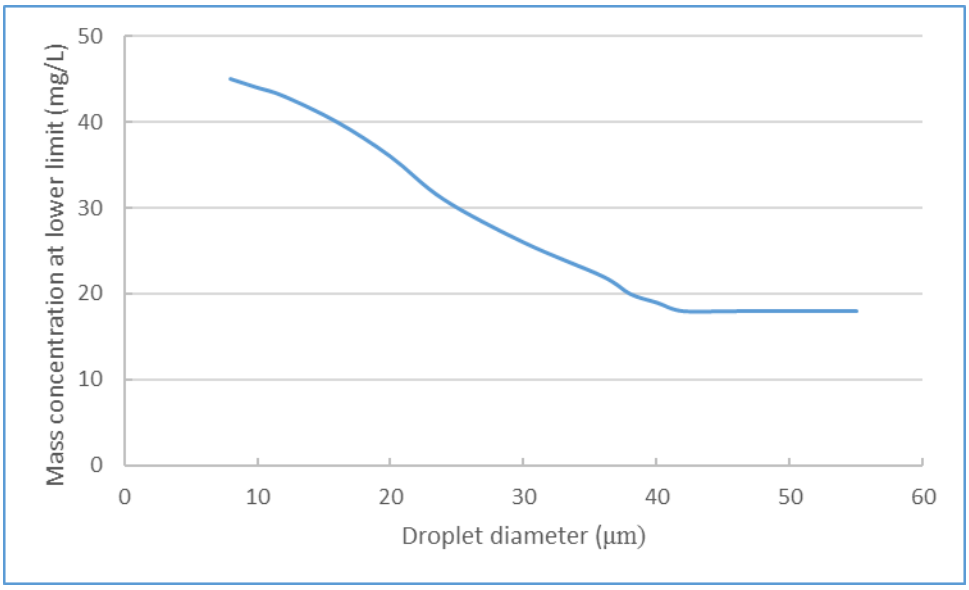

Figure 12. LFL of tetralin aerosols vs. droplet size (figure adapted from [34])

Burgoyne and Cohen studied the relationship between droplet size and LFL using tetralin aerosols with droplet size ranging from 7 to 55 μm as presented in Figure 12. Surprisingly, the LFL (mg/L) decreases with increasing droplet size significantly. For aerosol with very small droplet size (below 10 μm), the LFL is close to that of associated vapor form. The reason is that the small droplets will evaporate ahead of flame front due to extremely high surface area and fast heat transfer. Therefore, its combustion behavior is similar to the corresponding vapor mixture. For droplets above 40 μm, the droplets burn in individual flames as the surface area and rate of heat and mass transfer are too slow. For droplet sizes within 10 to 40 μm, the combustion would be transitional [34].

A similar trend is also observed in literature [35-37]. These experiments were performed using condensation of super-saturated vapor. The droplets fell freely from the top of the

tube and were ignited at the bottom. A possible reason of the decreasing LFL associated with larger droplets is the increase of terminal velocity. As the droplet size increases, the free-fall terminal velocity also increases. If the upward propagating flame is viewed as stationary, then there is more liquid mass per certain time period falling into the flame front for combustion. Therefore, the observed LFL of larger droplets can be lower than that of vapor and smaller droplets since the local fuel concentration is maintained due to the higher falling velocity. An empirical equation was developed to correlate the relationship between LFL and size of free falling droplets as presented in eq. (1)[36]. The C_s is the observed static LFL concentration while C_k is the kinetic LFL concentration after adjusting for flame speed and droplet falling velocity. V_s and V_f are the droplet and flame speed respectively.

$$C_k = C_s \frac{V_s + V_f}{V_f} \tag{1}$$

2.6. Aerosol flame propagation

Fire and explosion are the most serious concerns in the process industries. As a result, much effort has been put into studying the fundamental aspects of fire and explosion characteristics. This is also true for aerosol although it garners less attention as compared to vapor and dust explosion. Beginning in 1954, Burgoyne and Cohen applied the condensation method to produce monodispersed aerosols for aerosol study. In addition to LFL mentioned in Chapter 2.5, they also examined aerosol flame speed. It was found that

the flame speed of larger droplet sizes was higher than that of droplets smaller than 10 μm. However, no clear trend was identified [34].

Hayashi *et al*. conducted droplet burning experiments with aerosols generated by a cloud chamber, which also depended on the condensation of vapor to produce fine and monodispersed droplets. It was found that flame speed of larger droplets would be faster than that of smaller droplets, although the final temperature and overall fuel-air ratio are not the same. However, it was very clear that the flame speed of an aerosol can be higher than that of vapor [38].

On the other hand, Ballal and Lefebvre utilized an atomizer to generate sprays of isooctane, diesel oil and heavy fuel oil, resulting in a wide droplet size distribution. In their paper, it was found that the flame speed would only increase when the droplet size reduced, no matter which fuel or vapor ratios were tested. However, the smallest droplet size was around 30 μm so the full trend of flame propagation was not revealed. They proposed a model to describe the flame propagation and their prediction was fairly successful. The model is based on the fact that the quench time of a flame is equal to the evaporation time of droplets and the reaction time of a gas mixture [39].

Later, Polymeropoulos modified Ballal and Lefebvre's model to predict the trend of aerosol burning velocity. The evaporation time was changed slightly; however, the major difference is to consider simultaneous combustion of vapor fuel and liquid fuel. In Ballal

and Lefebvre's work, all liquid droplets are required to vaporize before combustion. Naturally, the burning velocity of an aerosol will never exceed that of vapor and increases monotonically with reducing droplet size. Nevertheless, if the ignition criterion for droplets is met, the diffusion flame from droplets can also release heat together with the homogeneous combustion of fuel vapor. Combination of diffusion flame can result in enhancement of burning velocity, as demonstrated by the shaded area in Figure 13 [16].

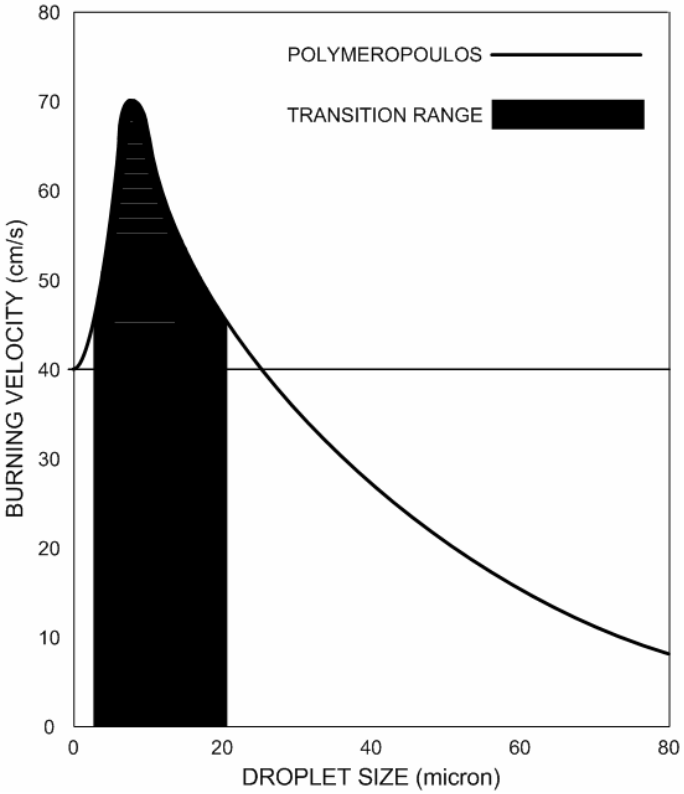

Figure 13. Prediction of aerosol burning velocity with function of droplet size [7]

Chan and Jou also used the condensation method to produce monodispersed tetralin aerosols [17]. It was found that there is a transition range (around 12 to 20 μm) where aerosol flame speed is higher than that of other larger or smaller droplets, as shown in Figure 14. They further modeled the transitional phenomenon by using the concept of a stationary flame, quasi-linearization and a normalization procedure. The modeling results agreed with the experimental data well except underestimating the flame speed at the transition range.

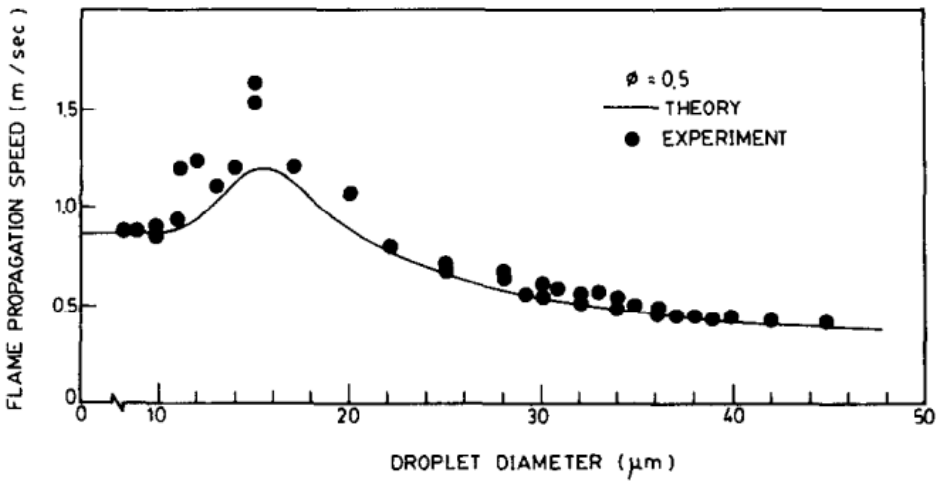

Figure 14. Experimental and simulation results of aerosol flame speed using tetralin aerosols [40]

The possible explanations to the enhanced flame speed in the transition range are (i) droplets in this range are small enough to provide vapor for combustion, while also large enough to wrinkle the flame front. This can increase reaction surface area thus increasing flame speed. (ii) Gas products from burning droplets expand and increase the

transportation process so the reaction is also enhanced. (iii) The local atmosphere of a burning droplet is at the optimum fuel to air ratio so the reaction rate is also at a maximum.

Another interesting finding is that the maximum flame speed would occur when the flame radius of the droplet is equal to the distance between neighboring droplets. This is explained by a droplet array system. At this condition, the flame spreads most efficiently from a droplet to a neighboring droplet. This can be arranged in the normalized flame speed and normalized droplet spacing as shown in Figure 15 [18, 41].

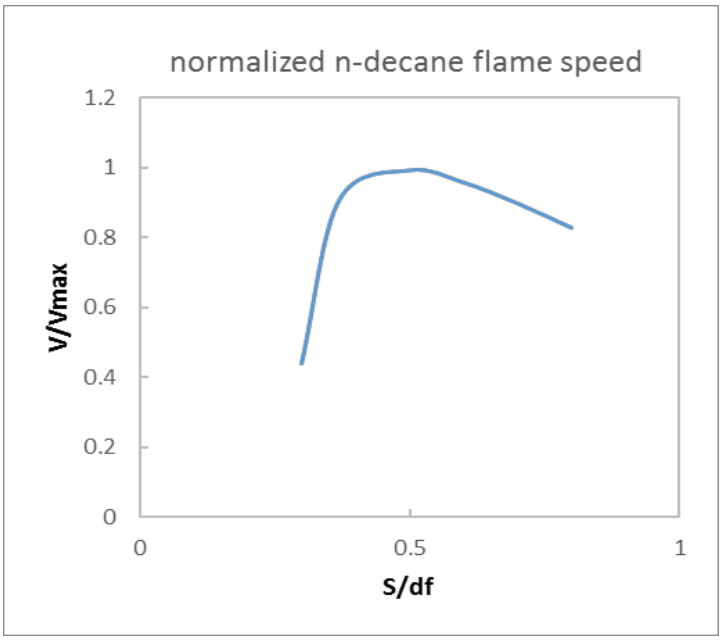

Figure 15. Normalized flame speed versus normalized droplet spacing (figure adapted from [18])

2.7. Summary

In this chapter, the holistic overview of the aerosol problem has been described. Each of the difficulties should be researched appropriately. The hazards and safety considerations are not addressed adequately in the text books due to the scarcity of experimental data and incomplete development of fundamental theories. In this work, interest is put in the transitional phenomenon of aerosol flame speed. In order to study it, the aerosol generation method should be reviewed and improved. In addition, the aerosol cloud should be stable and near-monodispersed for consistent results. Then the high quality aerosols can be used to verify the special flame speed phenomenon. As a result, prevention and mitigation measures can be developed to prevent or reduce the consequences of aerosol formation.

CHAPTER III

IMPROVEMENT OF ELECTROSPRAY DEVICE [*]

3.1. Introduction and review of aerosol generation

In literature there are three major methods to generate aerosols for experimental study:

(i) Spray from fuel injector or sprayer [39, 41, 42]: Similar to real scenarios in the process industries, the aerosol is generated from a pressurized orifice, or sprayed from a fuel injector or sprayer. This is one of the traditional ways to generate aerosols and is widely used by aerosol dispensers or injectors for auto engines. However, the generated aerosols may be poly-dispersed and are not suitable for fundamental study. The aerosol size measured at different distances is also different due to the formation mechanism of aerosols [8].

(ii) Cloud chamber [17, 34, 38]: This is another traditional way to generate aerosols, and the generated aerosols are mono-dispersed. It relies on the rapid condensation of superheated vapor when the chamber is suddenly expanded and cooled down.

[*] Part of this section is reprinted with permission from "Improved electrospray design for aerosol generation and flame propagation analysis" by Y.-R. Lin, H. Chen, C. Mashuga and M.S. Mannan, 2015. *Journal of Loss Prevention in the Process Industries*, 38, 148-145, Copyright 2015 by Elsevier

However, the resulting atmosphere is hard to control to achieve desired droplet size at 1atm and room temperature.

(iii) Electrospray [10, 43, 44]: This method applies a high electrical force to break liquid stream into fine droplets. It can generate mono-dispersed aerosols for fundamental study and is relatively easy to control droplet size. More detailed information will be given in Chapter 3.3. The major problem of electrospray is the low aerosol concentration. In our previous research, the maximum aerosol concentration was only around 0.1 to 0.2 ppm [10]. Due to equipment design and low conductivity of heat transfer fluid, the smallest droplet size was 80 μm for a heat transfer fluid (P-NF), and Lian *et al*. could only study flame speed of droplets size between 80 and 90 μm [9, 10]. Another problem of the previous equipment design is the droplets would be attracted back to the electrospray device, which caused uneven dispersion of aerosols in the chamber and lowered the aerosol concentration. This chapter described how the electrospray device can be improved to generate higher quality aerosols for fundamental study. Results were compared with the previous study to verify this statement.

3.2. Materials

Table 6. Properties of the heat transfer fluid (D-600) and dodecane

	Duratherm 600 (D-600)	**Dodecane**
Appearance	Slight yellow. transparent liquid	transparent colorless liquid
Composition	Hydrotreated mineral oil	$C_{12}H_{26}$
Average molecular weight	372 (kg/kmol)	170.33 (kg/kmol)
Flash point	224˚C	71 ˚C
Fire point	240˚C	205 ˚C
Boiling point	>298˚C	215 – 217 ˚C
LFL	–	0.6% (V)
Density	852.3 kg/m^3 (25˚C)	750 kg/m^3 (25˚C)
Dynamic viscosity	65.9 mPa s (25˚C)	1.34 mPa s (25˚C)
Kinematic viscosity	77.27×10^{-6} m^2/s (25˚C)	1.79×10^{-6} m^2/s (25˚C)
n*	1.5	1.42
k*	0.1	0

*n is the real part of refractive index, and k is the imaginary part of refractive index.

As mentioned in Chapter 1 and Chapter 2, fluids with very high flash point can also create fire and explosion threat to the process industries. Therefore, Duratherm 600 (D-600), a commercial heat transfer fluid, is used in this study to demonstrate the capability of the improved electrospray device. It can also make a direct comparison with the previous study. Its properties are listed in Table 6. However, the range of droplet size generated by

electrospray is highly connected to the nature of liquid properties. In order to examine the ignitibility of ignition sources for droplets less than 60 μm, dodecane is introduced and its properties are also presented in Table 6.

Table 7. Properties of the additive (Stadis 450)

	Stadis 450
Appearance	Amber, transparent liquid
Composition	Toluene: 30-60% Naphtha: 10-30% Dinonylnaphthlysulphonic acid: 10-30% Polymer containing Sulphur: 10-30% Polymer containing Nitrogen: 5-10% Propan-2-ol: 1-5% Naphthalene: 1-5%
Flash point	6˚C
Boiling point	90˚C
Density	920 kg/m^3 (15˚C)
Kinematic viscosity	7×10^{-6} m^2/s (40˚C)

Since the heat transfer fluid is a highly hydrotreated and hydrocracked hydrocarbons, its electrical conductivity is very low. As a result, a highly conductive additive is needed to increase its electrical conductivity for electrospray operation. The additive is Stadis 450 and its properties are shown in Table 7. The amount used in D-600 is only 1 wt% or 2

wt%. It has been shown that small amounts of additive can increase the electrical conductivity drastically without significantly changing other properties of the liquid [45]. The mixture of fuel and additive are stirred about 5 minutes, and the sample usually stands still for a couple of hours to make sure they are miscible.

3.3. Electrospray device for aerosol generation

Figure 16 shows the schematic view of electrospray setup. The concept and operating procedure are similar to our previous research [9-11]. Test fluid is contained in ten 2.5×10^{-6} m^3 syringes, and dispensed with a syringe pump (KDS 220). Ten stainless steel nozzles (2.5×10^{-4} m i.d. and 5.1×10^{-4} m o.d.) were assembled on a small metal plate, which is connected to a high voltage source (HV1). A metal mesh positioned right beneath the metal plate is connected to a second high voltage source (HV2) and serves as a relative ground. Ten 5.1×10^{-4} m i.d. plastic capillaries connect the syringes to the nozzles to transport the test fluid. The high voltages are generated by the function generators (Stanford Research System, DS-345) and then amplified to the desired levels by high voltage amplifiers (Trek Inc. 610E). The voltage difference between HV1 and HV2 is maintained at several kilovolts to energize the test fluid. As liquid stream with sufficient electrical conductivity passes through the nozzles, the liquid meniscus takes a conical shape (cone-jet) and fine droplets are generated.

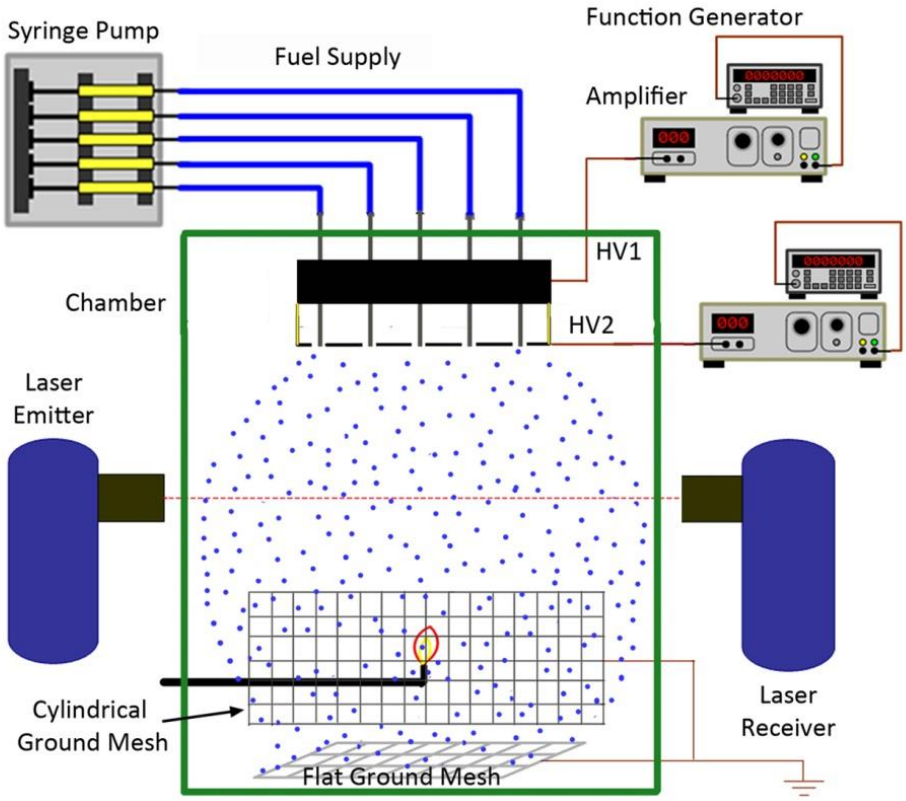

Figure 16. Schematic view of electrospray setup

In our aerosol flammability study, some desired physical properties of aerosols are high concentrations, small mean droplet size, mono-dispersed droplets, stable spray and even droplet dispersion in the test chamber. Attention to equipment details and modification are required to achieve the desired aerosol conditions. First, every nozzle should be positioned at the center of the metal mesh hole to create a uniform electric field. If the electric field is not uniform, the resulting droplet size distribution will be poly-dispersed. The comparison between improved design and previous electrospray setup is shown in Figure 17. In addition, the distance between the nozzles and metal mesh was greatly reduced so that the voltage difference between HV1 and HV2 can be set around 2~3 kV instead of

7~10 kV used in our previous electrospray. Lower voltages are safer and easier to achieve by the equipment.

(a) Previous design: not aligned (b) Current design: aligned

Figure 17. Detailed view of previous and current electrospray devices

Though electrospray is relatively easy to generate aerosols with sufficiently uniform size distribution, the major drawback is that the concentration of generated aerosols is low, which is unfavorable for reaching the lower flammability limit of fluid. In order to increase the aerosol concentration for a variety of test liquids, a multi-nozzle system can be applied. By using microfabrication and etching technology, nozzle number and density can be extremely high [46]. In this work, the nozzle density is about five-fold of previous work [9-11].

The other reason for low concentration in the previous studies is the re-attraction effect of electric field. Since the generated droplets are highly charged, they may be attracted back

to the electrospray device if there is no other guidance electric field. This phenomenon not only created uneven dispersion in the chamber, but also greatly reduced the aerosol concentration. On the other hand, the nature of the charged particles will repulse each other and self-disperse, which prevents them from coalescence if they are not attracted back to the electrospray device. There are three ways to achieve this goal.

First, droplets from the nozzles can be burned directly before being attracted back. However, the distance before attraction should be considered in this case. In the previous design, this distance was about 2 cm, and that space is not enough for ignition and observation of flame propagation. Second, the liquid stream from the nozzle can be directly atomized against a ground collector and the aerosol can be burned in this space [47]. However, in order to place the igniter and observe flame propagation, the distance between the nozzle and ground collector needs to be sufficiently large. Therefore liquids are also required to have higher electrical conductivity and other properties, and this is not practical for paraffin used in this study. Finally, the alternative way is adding the third electrode mesh (ground collector mesh) to guide the charged droplets down such that the re-attraction can be avoided or greatly reduced [46]. This approach was adopted as the optimal solution in this research.

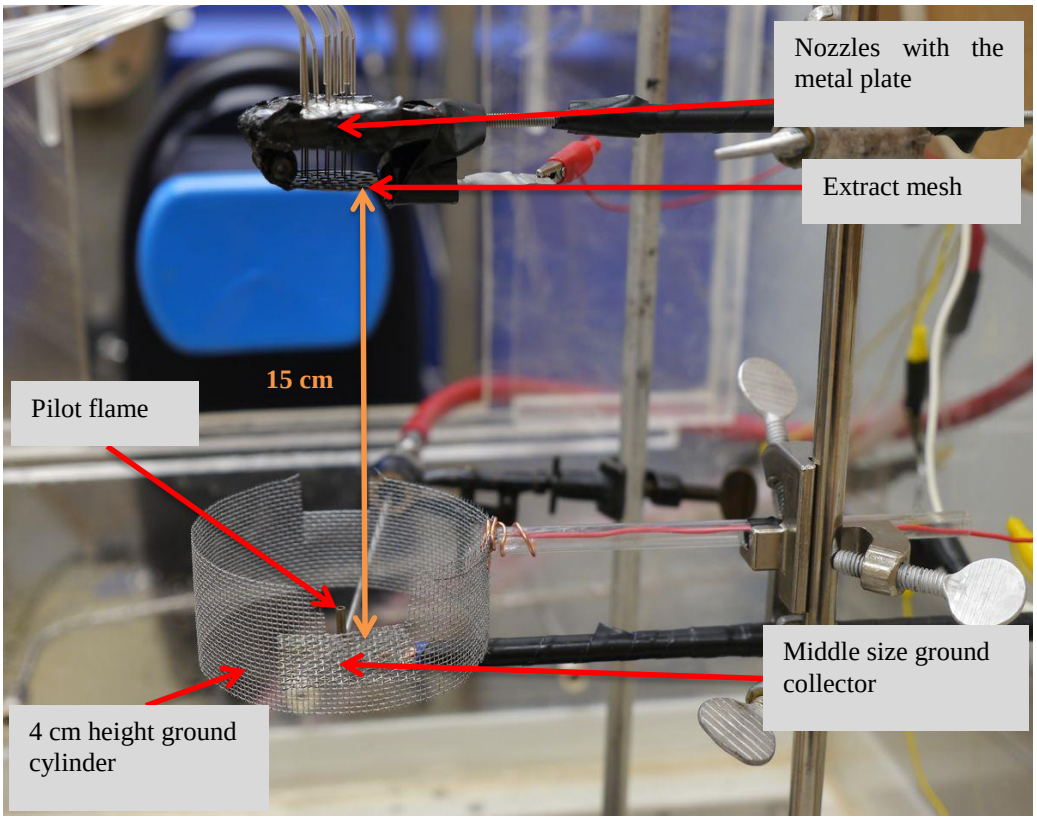

Figure 18. Real electrospray setup

As demonstrated in Figure 18, a flat ground mesh and a cylindrical ground mesh were utilized to guide the charged droplets down for combustion. The flat ground mesh was positioned 15 cm below the metal mesh (HV2) for ignition and flame propagation. Three sizes of the flat ground meshes were tested (large: 15 cm x 15 cm; medium: 4 cm x 4 cm; small: 1.7 cm x 1.7 cm) in this study, the medium size was found to give the most uniform results and was utilized thereafter. For better confinement of the charged particles, a second ground mesh with a cylindrical shape was introduced. Various cylinder heights were tested, with a 4 cm cylinder selected since it created the most uniform dispersion and

droplet velocity. A diameter of 10 cm was selected for the cylinder, which best confined the aerosol plume as compared to a 5 cm diameter cylinder. The real electrospray setup is shown in Figure 18.

3.4. Aerosol characterization

3.4.1. Malvern laser diffraction particle analyzer

Once the droplets are generated and attracted toward the ground meshes, they are continuously monitored by a Laser Diffraction Particle Analyzer (LDPA), which applies laser diffraction techniques for droplet size and aerosol concentration measurements [48]. It consists of a 2 mW He-Ne laser source and diode detectors. The LDPA is classified as 3R laser and suitable laser-protection goggles are needed while operating the equipment for all personnel in the lab.

The benefit of LDPA is the in-situ, non-intrusive measurement of droplet sizes. Without sampling, information about aerosol concentration and droplet size is continuous and instantaneous throughout the testing process. It relies on the fact that particles passing through a laser beam will scatter light at an angle that is directly related to their sizes. As droplet size decreases, the scattering angle of the laser light increases logarithmically. The average droplet size is based on Sauter Mean Diameter (SMD), which is a Surface Area Moment Mean Diameter $D_{[3][2]}$. Scattering intensity is also dependent on particle size,

diminishing with particle projected area, particle optical properties and total particle number. With the ratio of laser intensity before and after spray, aerosol concentration can be calculated using Beer-Lambert law as shown in eq. (2). This relies on Mie theory. Figure 19 shows the schematic view of the scattering behavior.

$$C_v(\times 10^6) = \frac{-2000\mathrm{Ln}(T)}{3\mathrm{b}\sum\frac{Q_i v_i}{d_i}} \tag{2}$$

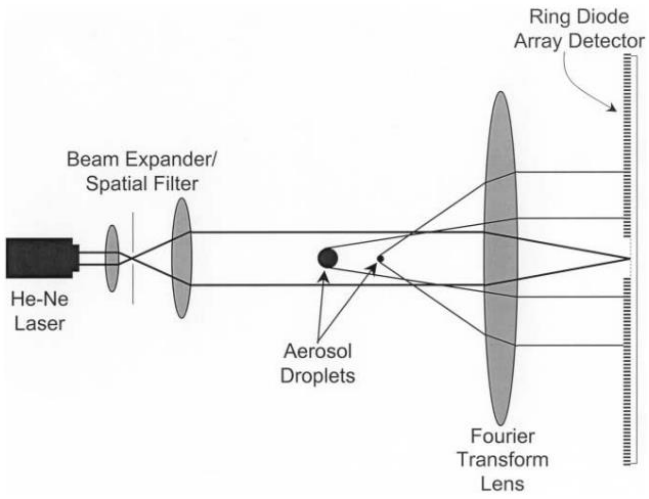

Figure 19. Schematic view of droplet size measurement by Malvern LDPA [6]

Mie theory is used to evaluate an extinction cross-section which relates to particle projected area, particle optical properties, and total particle number. Though Mie theory is more accurate than Fraunhofer approximation, it needs correct refractive index of the material ($n + ik$) to calculate the data. The real part (n) of refractive index describes the amount of light scattered when the light passes through the particles. The imaginary part

(*k*) describes the amount of light absorbed when the laser enters into the droplets. The real part is usually available in MSDS. However, it is not available for D-600. It can be estimated that *n* is equal to 1.5 since D-600 is a high molecular weight and severely hydrocracked hydrocarbon (For example, hexadecane and octane have values of 1.43 and 1.4 respectively). The imaginary part is much more complicated and hard to obtain the exact value. The rule of thumb is that clear liquids can be treated as no absorption (*i.e.*, $k = 0$) and slightly opaque liquids can be estimated as $k = 0.1$ (or 0.01 to 0.2) since there is only slight absorption [49]. The dispersant in this study is air which has a refractive index of $n = 1.0$.

3.4.2. Ignition sources

Aerosols are generated in an open chamber under the extractor mesh and guided downward by other ground meshes. Propane flame is used to ignite the aerosol when its concentration and droplet size stabilize. The ignition source is positioned 15 cm below the metal mesh, and the propane flame is controlled at a length of 1.5 cm. In the later tests, exploding wire, hot NiCr wire and small propane flame were also tested. The exploding wire with 10 J is an ASTM E918 type used the same as Mashuga's apparatus [50]. The material of hot wire is NiCr C (60% Nickel, 16% Chromium and 24% Iron) and the diameter is 0.16 mm (AWG 34). For small propane flame, the length is controlled at 0.5 cm. The size comparison of propane pilot flame is demonstrated in Figure 20, and the simple hot wire is shown in Figure 21.

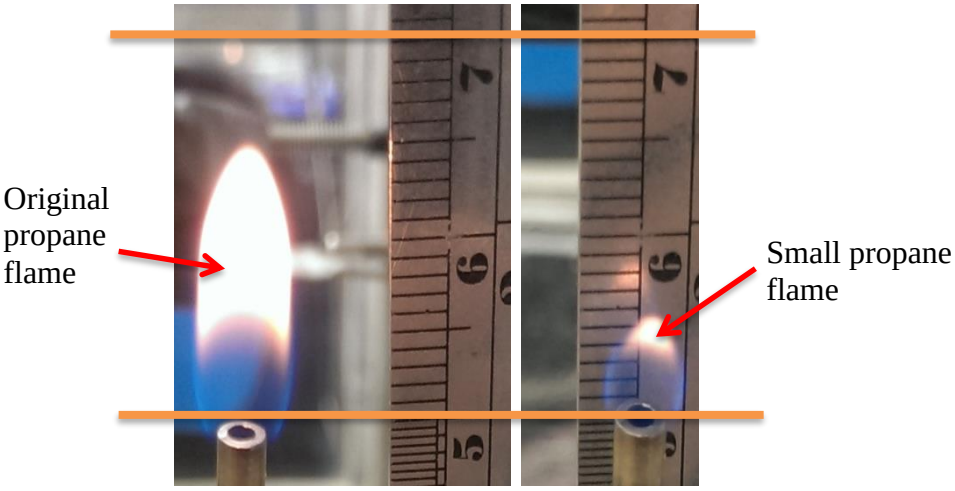

Figure 20. Size comparison of propane pilot flame

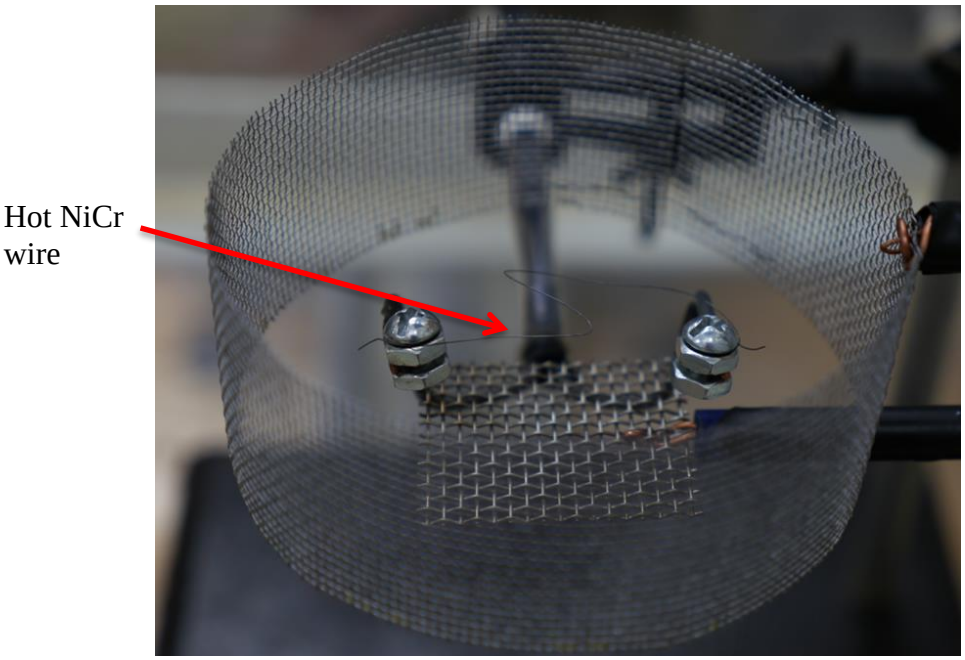

Figure 21. Design of simple hot wire

3.4.3. High speed camera and flame speed calculation

Aerosol ignition and flame propagation was captured by high speed camera (Phantom 4.2, Vision Research Inc.). The lens is DOZ-10×16 from Navitar. Short video (.cin file format) is filmed by sequential pictures (at 512 × 512 pixels resolution, the speed is up to 2,200 frames per second). Desired sections of videos are cut and stored as another format (.avi file format) by Cine Viewer software (v2.3, Vision Research Inc.). The shortened videos are then converted into pictures by Free Video to JPG Converter (5.0.29, Freestudio). Finally, the series of flame pictures are processed and analyzed using ImageJ software (v1.47, National Institutes of Health).

The image processing steps and definition of flame speed are similar to Lian's study [9]. Because flame shape is irregular, it is difficult to analyze flame speed by defining the position of a flat flame plane. Instead, flame speed in this research is defined as the movement of the center of the flame reaction body in the sequential pictures. The following is the detailed description of image processing and analysis used to calculate flame propagation speed.

Due to the reflection of flame light on the steel rod and container wall, and some unrelated flame fragments in different stages, there are some bright areas which should be excluded in the flame speed calculation. The Paintbrush Tool in ImageJ is used to eliminate those areas. Then, the rest of bright flame is highlighted by adjusting a threshold value of

brightness. As a result, all pixels in the flame areas have the same brightness, and other areas are set to be dark. The Wand Tool in ImageJ can select the desired bright spots, and The Measure Tool can calculate the mass center of flame. Y-axis pixel number of mass center of flame is converted into real scale and it represents the vertical position of the flame. The position of the flame is plotted versus time, and the slope of the linear fitting line of this figure represents the flame propagation speed under this test condition. The overview of the experimental setup is shown in Figure 22.

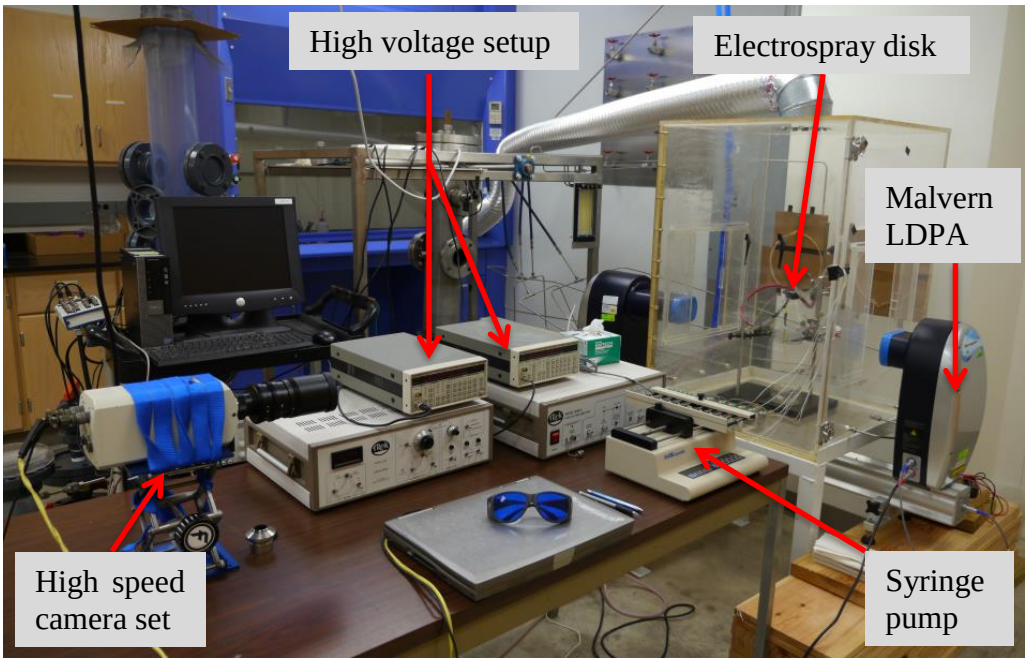

Figure 22. Overview of the experimental setup

3.5. Results and discussion

3.5.1. Aerosol formation and droplet characterization

As mentioned earlier, the previous electrospray device has been modified to generate higher quality aerosol. Some basic parameters are introduced here. C_v is volume-based concentration in ppm. $D_v(10)$, $D_v(50)$ and $D_v(90)$ mean that 10%, 50% and 90% of droplets are smaller than these respective values. Sauter Mean Diameter (SMD) is used to represent the Surface Area Moment Mean Diameter ($D_{[3][2]}$) and it is defined as:

$$\text{SMD } (D_{[3][2]}) = \frac{\sum n_i D_i^3}{\sum n_i D_i^2} \tag{3}$$

In order to compare the droplet size distribution of aerosols, span ratio is introduced. The smaller the span ratio, the narrower the distribution (*i.e.*, mono-size distribution) of the aerosol is. Span ratio is defined as:

$$\text{Span ratio} = \frac{D_v(90) - D_v(10)}{D_v(50)} \tag{4}$$

Table 8 shows a comparison of the span ratio of data obtained in our previous studies and the current study [9, 11]. The sampling rate of Malvern LDPA was 1 Hz in these measurements. Both Huang [11] and this work use the average of a 60-second data set.

However, Lian used single point data and only showed variation of the average droplet sizes in his work [51]. The span ratio of Lian's work might be larger if his average data was available. Smaller SMD and span ratio of aerosols generated by current device in Table 8 demonstrates the improvements of the device can create higher quality aerosols. Eighty percent of droplets were within 56.7 and 71.3 μm. Though the longer distance between the nozzles and mesh in the previous electrospray device would attenuate the effect of non-alignment, the span ratios of our previous electrospray were much higher than that of the current electrospray.

Table 8. Comparison of span ratio of the previous and current devices

	Previous study 1 [9]	**Previous study 2 [11]**	**Improved design**
$D_v(10)$ (μm)	96.3	83.6	56.7
$D_v(50)$ (μm)	120.1	127.4	63.8
$D_v(90)$ (μm)	148.3	193.6	71.3
Span ratio	**0.43**	**0.86**	**0.23**
SMD (μm)	118.4	108.3	63.4

A major issue with the electrospray approach is the low concentration of generated aerosol, which can be improved by applying a multi-nozzle system. Thus the packing density of nozzles is increased by five-fold to increase the aerosol concentration. In addition, ground meshes are applied to guide the charged droplets down for characterization and

combustion. The ground meshes not only make the dispersion more even in the test chamber, but also increase the aerosol concentration. The mesh sizes are defined as large: 15 cm × 15 cm, medium: 4 cm × 4 cm and small: 1.7 cm × 1.7 cm, respectively. The resulting aerosol profiles are depicted in Figure 23. For large mesh, the profile is too wide at the bottom because the mesh is too large. For small mesh, many droplets would escape away because the overall attraction force is too small. Since the medium-size flat ground mesh can generate more uniform aerosol in the test chamber, it is chosen thereafter.

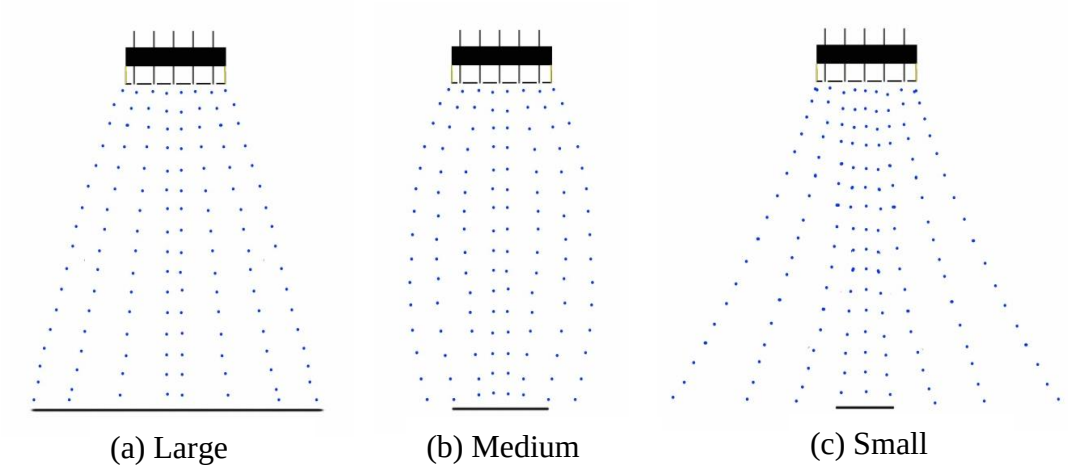

(a) Large (b) Medium (c) Small

Figure 23. Schematic of the resulting aerosol profiles for different sizes of flat ground meshes

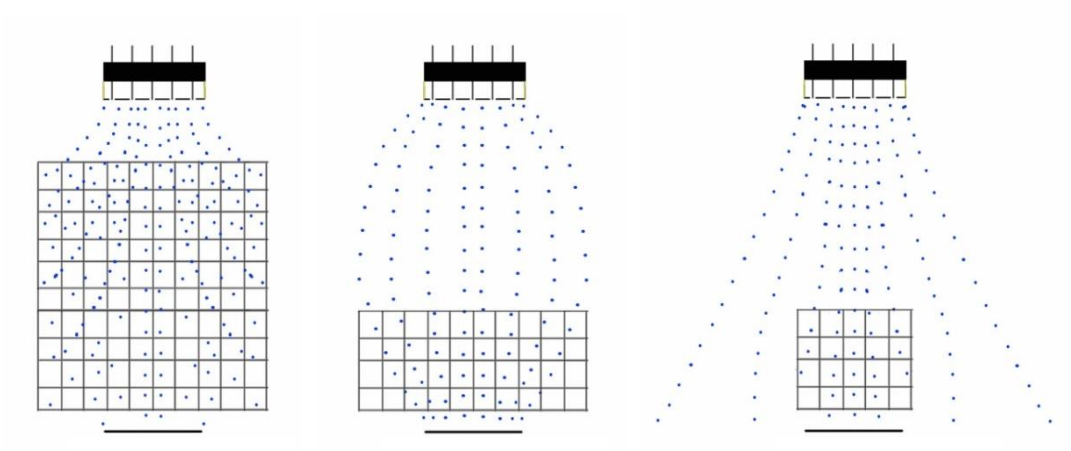

(a) Large (b) Medium (c) Small

Figure 24. Schematic of the resulting aerosol profiles for different sizes of cylindrical ground meshes

Lower flash point hydrocarbons (*e.g.*, *n*-decane and *n*-octane) usually have lower molecular weight and higher lower flammability limit (LFL). As a result, liquid pumping rate needs to increase to reach their LFL and the aerosol plume is also bigger. The medium-size ground mesh alone is not sufficient to confine the aerosol, and the unconfined droplets would contaminate the LDPA lens. Under this condition, the characterization of aerosol is not possible. Therefore a second ground mesh in cylindrical shape is introduced to resolve this problem. The tested cylindrical ground meshes in diameter and height are defined as large: 10 cm × 10 cm, medium: 10 cm × 4 cm and small: 5 cm × 4 cm, respectively. The aerosol profiles are depicted in Figure 24. For large cylindrical ground mesh, the droplet density and velocity of aerosols in the top section are higher than that of the bottom. For small cylindrical ground mesh, some droplets would still escape from the electric field and contaminate the LDPA lens. It is shown that the medium-size cylindrical mesh can better confine the droplets and create an even dispersion. Therefore, the

medium-size cylindrical mesh and medium flat ground mesh are applied in the modified electrospray. The resulting aerosol dispersions from previous electrospray device and current improved design are shown in Figure 25.

(a) Previous design: attracted back and not even (b) Current design: even

Figure 25. Comparison of dispersion between previous and current electrospray devices

Aerosol stability is another important factor in aerosol generation. If the aerosol is not stable in concentration and droplet size, the flammability test results will not be consistent and reproducible, and the mitigation based on inaccurate data to address aerosol hazards may be inappropriate. In the previous study, generated aerosols were not stable enough [9, 11]. Figure 26 presents stable measurements of droplet size and aerosol concentration generated by the modified electrospray device. Stability of the aerosol with the new device was greatly improved. Table 9 summarizes the capability comparisons between the previous and current electrospray devices. With the new design, higher quality data and expanded experimental conditions can be achieved.

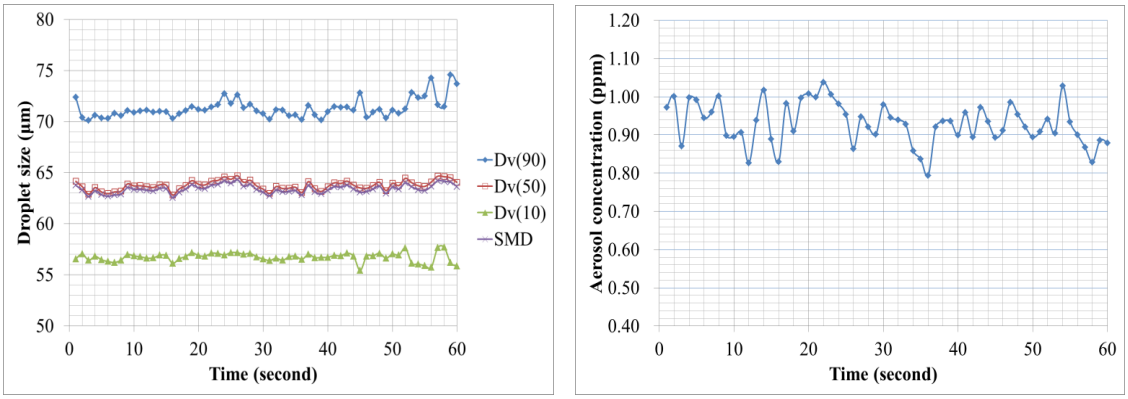

(a) Droplet size over time (b) Aerosol concentration over time

Figure 26. Stability of aerosol generated by the modified electrospray device

Table 9. Comparison of electrospray performance of the previous and current devices

	Size distribution	Dispersion in space	Stability	Concentration	Droplet size
Previous design	Wide	Not even	Not stable	Low	Big
Current design	Narrow	Even	Stable	High	Small

3.5.2. Test of aerosol flame speed

To appropriately assess aerosol hazards with regard to fire and explosion, several factors should be considered, such as aerosol flame speed, minimum ignition energy and aerosol dispersion behavior. However, because of the complexity of aerosol formation and ignition process, the information is limited. This work aims to improve the electrospray

design to produce aerosols with higher quality so more reliable aerosol flammability data can be obtained to help establish appropriate aerosol hazard mitigation measures.

The image processing procedure has been described in Chapter 3.4.3. Flame propagation of a D-600 aerosol with a mean diameter of 109 μm and a concentration of 0.55 ppm is presented in Figure 27. In Figure 27(a), the flame propagated upwardly and the characterization of propagation was unlike a vapor flame. The three-stage flame propagation process was also found and similar to that in the previous study [9]. At first, a small individual flame burned with a small cluster of droplets. As the flame propagated, the heat from radiation and resulting convection evaporated droplets, causing small flames to combine into a larger global flame. Later, the global flame split into smaller flames and was quenched at the top section of the aerosol zone.

The y-axis pixel number of the flame center was converted into real scale and it represented the vertical position of the flame. The position of the flame was plotted versus time, as shown in Figure 27(b), and the slope of the linear best fitting line represents the flame propagation speed under the test condition. It demonstrated good linearity of flame trajectory, which is indicative of stable flame propagation. It can be seen that the linearity of the flame trajectory was improved as compared to the previous study [9].

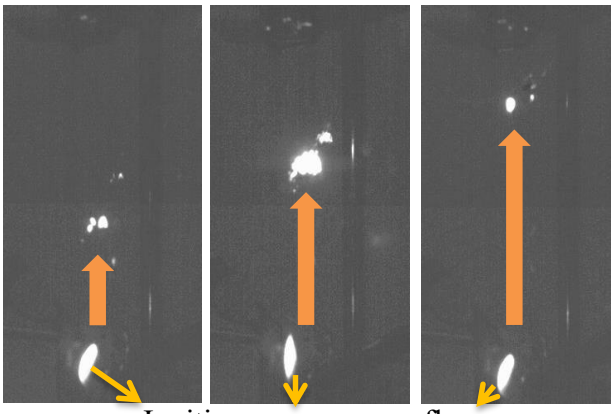

Ignition source: open flame

(a) Flame development

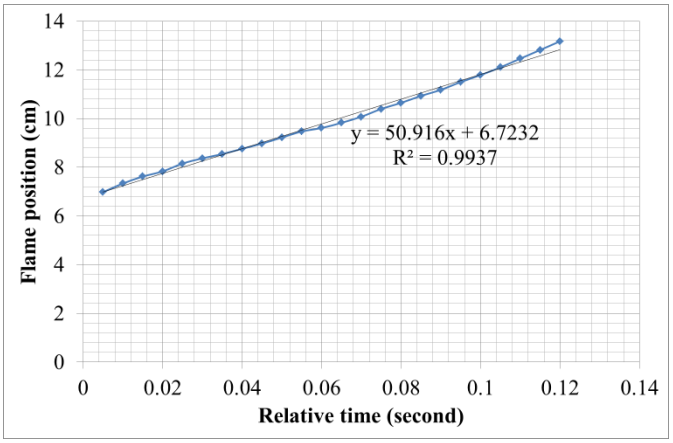

(b) Flame position versus time

Figure 27. Flame propagation of D-600 aerosol with SMD = 109 μm and C_v = 0.55 ppm

The HTF, D-600, was also tested in the previous study [51]. Due to extremely low electrical conductivity and limitation of the apparatus, only two droplet sizes of D-600 aerosol were tested (111 and 119 μm) in his dissertation. For comparison, D-600 aerosol was studied again to show the capability of the new electrospray apparatus and the results has shown in Figure 28. It was observed that as droplet size decreased, the flame

propagation speed increased. This is in good agreement with general concept. As droplet size approaches zero (*i.e.*, vapor form), the flame speed increases and approaches the vapor flame speed, which is higher than that of large droplets. Current results are slightly lower than the previous study [51], but with much smaller deviation which implied this is more reliable data.

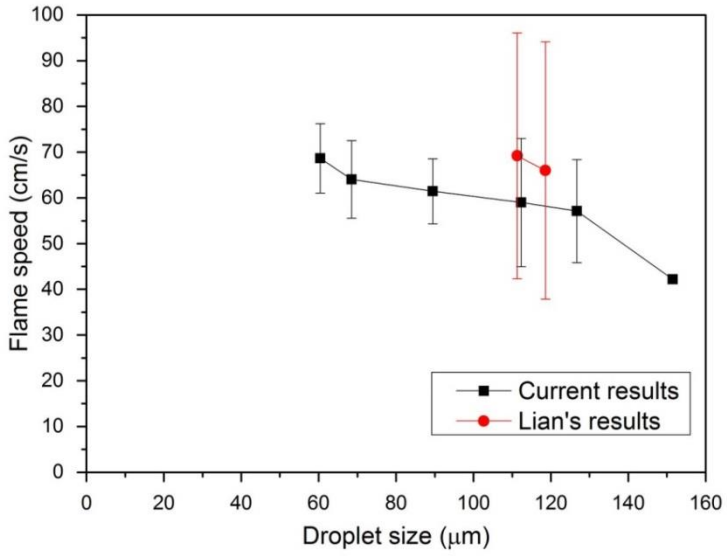

Figure 28. Flame speed vs. droplet size of D-600 aerosols in previous and current results

However, Figure 28 only shows aerosol flame speed of droplet size from around 60 to 150 μm. Further investigation on aerosols with smaller size was not successful because ignition of the aerosols smaller than 60 μm failed. This phenomenon contradicts conventional concept that smaller droplets should be easier to ignite compared to the larger droplets in the same concentration level. The possible reason for such deviation could be turbulence.

Aerosols are confined by the electric field in an open chamber. When a pilot flame is used as an ignition source, it creates strong turbulence and then may blow droplets and vapor away, resulting in a sudden drop in the fuel concentration. Since the perceived fuel concentration is lower, the ignition is not successful.

3.5.3. Ignition sources

In order to ignite the smaller droplet size aerosols, several ignition sources were examined. First, an exploding wire with 10 J of energy was tested as an alternative ignition source. The wire is a tinned copper wire with 10 mm (AWG 40) diameter [50]. However, the exploding wire with 10 J of energy also failed to ignite the aerosols with droplets smaller than 60 μm. It is possible that 10 J is not sufficient to ignite the low concentration aerosols and the wire "explosion" also creates strong turbulence. Another important factor is ignition time duration. The time duration of the exploding wire is only about 8 ms. For lean aerosols, the distance between droplets is large, and the high power of the exploding wire releases its energy in a very short period. Most of the released energy may not have been absorbed by droplets and instead dissipates into the atmosphere. Since few droplets are vaporized and thus result in low vapor concentration, there was no ignition and no flame propagation.

In the mist/spray combustion studies, sparks are usually used as ignition sources but the spark energy is not quantified in many cases. The tested liquids are usually low flash point

fuels, and the generated aerosols usually have higher concentrations and smaller droplets with saturated fuel vapor in a closed chamber [17, 38, 39]. Both the spark and exploding wire release very high energy in a very short time period. Miesse [35] noticed that dibutyl phthalate (DBP) failed to be ignited by a spark and an exploding wire with 786 J and 468 J, respectively. The flash point of DBP is 171 ^{o}C which is much higher than most tested fuels. However, the DBP aerosols can be ignited by open flame, which indicated that the DBP aerosols were within the "flammability limit". Furthermore, the DBP aerosols can also be ignited by hot wire, a device similar to exploding wire but with longer duration time. He suggested that the main reason for failure of ignition by spark and exploding wire was short duration time [35].

This suggestion agreed with the observation in this work. For a high flash point liquid, its vapor pressure is low and it requires more energy to generate enough vapor for ignition. For low concentration aerosols, the distance between droplets is far. If the time duration is short, most of the energy will dissipate into the surroundings and will not evaporate sufficient vapor for ignition and flame propagation. In contrast, vapor always surrounds the electrodes or fuse wire. Therefore, spark and exploding wire work successfully in vapor flammability.

As a result, a simple hot NiCr C wire ignitor was tested. The melting point of NiCr C wire is around 1400 ^{o}C. The wire is AWG 34 (0.16 mm in diameter) and 20 cm long. In a test, the electric current was set at 2.2 A. It was observed that the fire started on the wire, and

the wire consequently melted. The high temperature wire further contacted with the flat ground mesh, which contained collected liquid fuel. Thus the fuel was ignited and burned down the cylindrical ground mesh. Therefore, the hot wire was halted, and the ignition source switched back to propane flame.

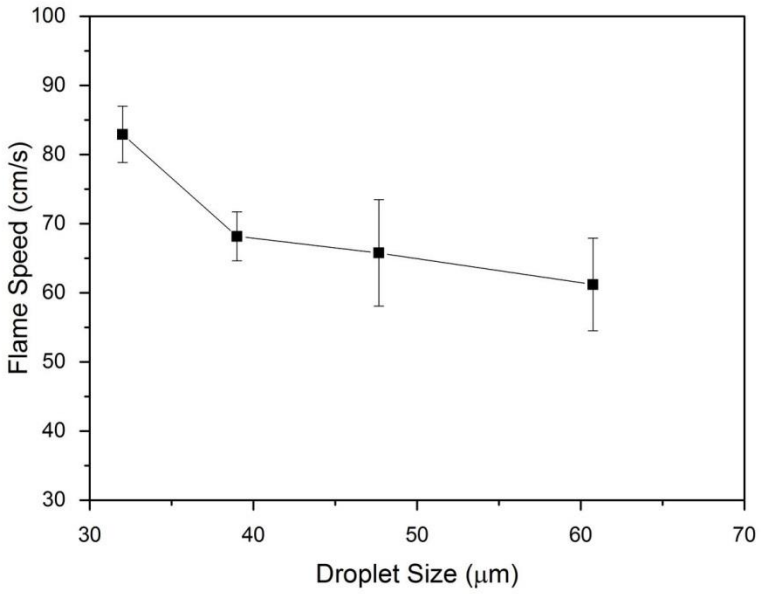

Figure 29. Flame speed of dodecane aerosols smaller than 60 μm

The reason for failed ignition of the normal propane flame and exploding wire could be generation of strong turbulence. The new (small) propane flame ignitor was set at 0.5 cm in length, which may be easily quenched and has a small yellow color cap on the blue color flame tip, as shown in Figure 20. As expected, the turbulence was greatly reduced and successful ignition of aerosols with droplets smaller than 60 μm was observed. An

example of dodecane aerosol flame speed is shown in Figure 29 which demonstrates the successful ignition.

3.6. Summary

In conclusion, the electrospray device is improved and becomes a more suitable instrument for aerosol flammability study. The generated aerosols are more uniform, evenly dispersed, and more stable over time. It can also generate smaller size droplets for flame speed study and higher aerosol concentrations for other hydrocarbons. These are accomplished by aligning nozzles and mesh holes, increasing nozzle packing density and adding ground meshes.

A flat ground mesh and a cylindrical ground mesh were required for effective aerosol confinement while the liquid pumping flow rate was increased in order to promote the aerosol concentration. For both flat and cylindrical ground meshes, three sizes of each were examined. It was concluded that medium sizes of flat and cylindrical ground meshes (4 cm × 4 cm and 10 cm × 4 cm, respectively) produced the most uniform aerosol profile in the test chamber. Since the aerosol quality was greatly improved, the results of D-600 aerosol flammability were more reliable and covered a wider range of droplet sizes.

However, aerosols smaller than 60 μm were not ignitable with the original 1.5 cm pilot flame and an exploding wire. The possible reason for failure of the pilot flame was strong

turbulence. Since the aerosols were confined by the electric field in the open chamber, small droplets would be blown away if the turbulence was too strong. For exploding wire, it was possible that 10 J of the ignition energy was still not sufficient to ignite the lean aerosol, and the wire explosion also created turbulence thereby reducing the effective concentration. Most importantly, the time duration of exploding wire was too short. Since the majority of energy would dissipate into the atmosphere and not be absorbed by droplets, the resulting vapor concentration is too low to ignite. Finally, the length of propane flame was reduced from 1.5 cm to 0.5 cm to reduce the turbulence, and droplets smaller than 60 μm can be ignited and aerosol flammability can be investigated.

This study fully demonstrated that a heat transfer fluid can be ignited easily upon being aerosolized, even though the flash point is much higher than surrounding temperature. In the researched droplet size range, the aerosol flame speed increases significantly as the droplet size decreases. Under certain conditions, the aerosol cloud with fine droplets may behave as devastating as a vapor cloud. Therefore, the risks associated with high flash point liquids should not be overlooked, especially under conditions which are favorable for the formation of fine droplets. Corresponding preventive and mitigative measures should be developed according to the characteristics of the targeted liquids.

With the modification of the electrospray device, addition of ground meshes and adjustment of propane flame, aerosol flammability can be researched more reliably and

extensively. Based on this more reliable, repeatable and extensive data, better mitigation strategies may be developed.

CHAPTER IV

EFFECT OF ADDITIVES AND OPERATING CONDITIONS ON THE FLAMMABILITY TEST OF AEROSOLS GENERATED BY ELECTROSPRAY

4.1. Introduction

As discussed in Chapter 3, improvement of electrospray device has been demonstrated to generate high quality aerosols. In addition to configuration of apparatus; however, the electrospray should be operated in the cone-jet mode in order to have a stable aerosol. To explore the applicability of electrospray, the three major parameters, including the effect of additive, the liquid flow rate and the applied voltage, were studied.

Tang and Gomes [45] studied the effect of these parameters on the droplet size and cone-jet mode of *n*-heptane with different amounts of an additive. It was found that the droplet size was dominated by the liquid flow rate. The applied voltage also had clear influence on the droplet size provided that the flow rate was high. And electrical conductivity had smallest effect on the droplet size once the liquid electrical conductivity is suitable for electrospray application. On the other hand, the stable and monodispersed aerosols can only be obtained in a certain combination of liquid flow rates and voltages for a specific liquid. This cone-jet domain became smaller with increasing electrical conductivity, which would limit the applicability of electrospray since the controllable droplet size is limited.

To explore the applicability of current electrospray system, the three major parameters, including liquid flow rate, additive effect and applied voltage were studied. In order to produce small droplets, several additives were investigated to determine which one can better facilitate the droplet breakup to generate the finest aerosols. Also, the size distribution of aerosol was also affected by additive amounts. The selection of additives was introduced in Chapter 4.2.1. The effects of the applied voltage and the liquid flow rate on droplet size and monodispersity were also discussed. A quantitative approach was used to define the "stable region" of aerosol generation. Flame speed of *n*-octane aerosols was used to demonstrate the importance of the "stable region." In this region, aerosols can be considered as near-monodispersed and suitable for fundamental study of aerosol flammability, which will contribute to aerosol safety.

4.2. Materials and methods

4.2.1. Selection of additives

Stadis 450 is widely used as an antistatic agent to avoid buildup of static charge in aviation fuel and ultralow sulfur diesel. In addition it is often used to increase the electrical conductivity of paraffin for electrospray application [9, 11, 45, 52]. Other than Stadis 450, there are other chemicals can be used for this purpose.

Surfactants can reduce surface tension drastically, which would facilitate droplet breakup process. It can also increase electrical conductivity for electrospray [53]. Therefore, it might have great potential to generate small droplet aerosol. Surfactants are composed of both hydrophilic and hydrophobic groups, and the Hydrophile-Lipophile Balance (HLB) number is used to assess the polarity.

High HLB value (above 11.0) indicates hydrophilic while low HLB value (less than 9.0) is lipophilic. HLB values ranging between 9.0 and 11.0 are intermediate. For surfactants with similar HLB value, their solubility in paraffin and alcohol may be affected by different functional groups [54]. To mix well with tested hydrocarbons, the HLB value should be low as they are lipophilic. However, high HLB value is desirable since electrical conductivity generally increases with HLB value. Three surfactants (Span 20, Tween 85 and Tween 21) were selected in this work to study their solubility in *n*-alkanes.

Ionic liquids are molten salts at room temperature. They are typically composed of organic cations and organic/inorganic anions. Ionic liquids have great research potential as their physical and chemical properties can be adjusted by alkyl chain length and additional alkyl substitution on cations, and the selection of anions [55]. Ionic liquids have extremely high electrical conductivity around the magnitude of 1 S/m, so they might be a powerful additive for electrospray application [56, 57].

However, their solubility in *n*-alkane is very low [58-60]. The cation and anion should be designed to allow ionic liquids dissolve in alkanes. Crosthwaite *et al.* reported that increasing the length of the alkyl chain on the cation can increase mutual solubility of the ionic liquid and alcohol mixtures [55]. Here, 1-Butyl-3-methylimidazolium Octyl Sulfate (or [BMIM][OcSO4]) was selected in this work because the alkyl chains are relatively long on both cation and anion, which enhances packing effect with alkane so the interaction with alkane is stronger. Therefore, its activity coefficients at infinite dilution in alkane and alcohol are relatively low, and its solubility is relatively high [61-63].

In our previous study, a heat transfer fluid, a highly hydrotreated and high molecule weight paraffin (D-600), and dodecane were used to generate aerosols [52]. The polarity of these fluids is smaller than those typically presented in the ionic liquid literature. As a result, [BMIM][OcSO4] may not be miscible with the heat transfer fluid and dodecane. To overcome this problem, three alcohols (ethanol, 1-propanol and 1-butanol) were used as a co-solvent to dissolve the mixture of [BMIM][OcSO4] and dodecane. In addition, alcohol can also be used as an additive for electrospray. However, the required amount is usually high, typically ranging from 10% to 30% [64, 65]. Additives tested in this work are summarized in Table 10.

Table 10. Additive selection based on group

Antistatic Agent	Surfactant	Ionic Liquid	Alcohol
Stadis 450	Span 20	1-Butyl-3-methylimidazolium Octyl Sulfate	Ethanol
	Tween 85		1-Propanol
	Tween 21		1-Butanol

4.2.2. Aerosol generation

Dodecane was used as the main fuel in this chapter to examine the effect of additives and electrospray operating parameters. Since dodecane is a non-conductive liquid, it was mixed with various amounts of additives to increase its electrical conductivity for electrospray operation. The mixtures were well stirred and left still for at least half day to allow complete mixing. The electrospray setup details are illustrated in the previous chapter. Ten 2.5×10^{-6} m^3 syringes were filled with the fuel mixture, and then pumped through plastic capillaries by an infusion syringe pump (KDS 220). The capillaries connected to an array of ten nozzles (2.54×10^{-4} m i.d. and 5.08×10^{-4} m o.d.) on a stainless steel disk. The nozzles and the disk were maintained at high voltage (HV1) with a high voltage amplifier (Trek Inc. 610E) and a function generator (Stanford Research System, DS-345). A metal mesh was positioned below the metal disk, with nozzles centered in the mesh holes in order to create a uniform electrical force. A second high voltage system

(HV2) and the metal mesh formed a relative ground plane. The liquid stream was energized by the voltage difference between HV1 and HV2 and was broken into fine droplets. Those charged particles were further guided and collected by a flat grounded mesh (0.04 m × 0.04 m) and a cylindrical grounded mesh (0.04 m in height and 0.1 m in diameter) 0.15 m below the metal mesh (HV2).

4.2.3. Aerosol characterization

The fine droplets were continuously monitored by Laser Diffraction Particle Analyzer (Spraytec, Malvern Inc.). It consists of a 2 mW Helium-Neon laser with 632.8 nm wavelength. The diffraction angle of laser scattering decreases logarithmically as the particle size increases so the size can be calculated. The average size is based on Surface Area Moment Mean Diameter ($D_{[3][2]}$), so-called Sauter Mean Diameter (SMD), which is widely used in aerosol field [8]. The concentration was also obtained simultaneously based on the Beer-Lambert Law and Mie Theory, which requires the liquid refractive index to perform the calculation. The refractive index of dodecane is $1.42 + i0$, and its dispersant (*i.e.*, air) is $1 + i0$.

After aerosol droplet size and concentration were recorded and deemed stable, the aerosol cloud was ignited by a 0.5 cm propane pilot flame. The flame propagated upwardly and was recorded by a high speed camera (Phantom 4.2, Vision Research Inc.). The short video was converted into images and further analyzed by ImageJ software (v1.47, National

Institutes of Health). The process to obtain flame speed was similar to that used in previous work [9, 52]. The sequential locations of the flame center were plotted versus time, and the aerosol flame speed under this condition was obtained from the slope of the plotted line.

4.3. Results and discussion

4.3.1. Additive solubility in hydrocarbons and additive selection

As shown in Table 10 and Chapter 4.2, several potential additives can be used to increase the electrical conductivity of fuels for electrospray application. In literature many of them have not been tested with paraffin so their solubility needs to be examined first, and the additives should be soluble with a wide range of hydrocarbons for electrospray study. In previous work [52], a high flash point heat transfer fluid (D-600) was studied, and it should be extended to other lower flash and lower molecular weight hydrocarbons to provide useful data for aerosol hazard assessment.

Table 11 shows the solubility tests for surfactants with paraffin. Span 20 is quite soluble with long chain hydrocarbons since its HLB value is less than 9.0 and is regarded as lipophilic so it should be also soluble in other paraffin, such as decane. In addition, surfactants in the “span” group are lipophilic and those in the “tween” group are hydrophilic in nature [54]. Although some reported that Tween 85 and Tween 21 are

soluble in mineral oil, they are not miscible in the tested hydrocarbons here. As a result, only Span 20 was used for electrospray in the surfactant group.

Table 11. Surfactants and paraffin solubility tests*

	Flash point	**Molecular weight**	**Span 20**	**Tween 85**	**Tween 21**
HLB value	—	—	8.6	11.0	13.3
D-600	224	372	Miscible	Immiscible	Immiscible
Hexadecane	135	226	Miscible	Immiscible	Immiscible
Dodecane	82	170	—	—	Immiscible
Decane	46	142	—	Immiscible	—
Octane	13	114	—	—	Miscible but opaque

*The solubility test is based on 5.0 wt% of surfactant in hydrocarbon.

For a solute to be dissolved in a solvent, the molecules of the solute and solvent should sufficiently interact with each other. For the ionic liquid and dodecane, the solute (ionic liquid) will need a very polar solvent to provide sufficient interaction to dissolve. The solvent (dodecane) is a non-polar liquid so they may not be miscible, although the alkyl chains on both cation and anion of the ionic liquid have been designed carefully.

Table 12. Solubility test with alcohols and paraffin*

	Ethanol	**1-Propanol**	**1-Butanol**
Dielectric constant	25	20	18
D-600	Opaque	Opaque	Miscible
Dodecane	—	—	Miscible

*The solubility test is based on 5.0 wt% of alcohol in hydrocarbon.

An alcohol is a polar protic solvent. The medium polarity makes it a suitable solvent for many polar and nonpolar liquids. The hydrogen bonding and polarity allow it to provide certain solubility with ionic chemicals. Domanska *et al.* reported that alcohols (C1 to C10) were completely miscible with [BMIM][OcSO4] at 310 K [63]. Therefore, the three alcohols were examined with D-600 and dodecane, as presented in Table 12. Amongst the three alcohols tested, only 1-butanol was miscible with all hydrocarbons, and it was used as a co-solvent to dissolve the ionic liquid and hydrocarbons together. 1-Butanol alone was also tested to increase the electrical conductivity for electrospray.

Table 13 indicates the solubility results of the ionic liquid and *n*-alkane. It was found that [BMIM][OcSO4] itself is not miscible (or has very low solubility) with dodecane and octane at room temperature, although its activity coefficients at infinite dilution in alkane and alcohol are relatively low. With assistance from 1-butanol, these three chemicals ([BMIM][OcSO4], 1-butanol and dodecane/octane) were made miscible. It can be noted

that the amount of 1-butanol required to make them miscible decreased when the alkyl chain length of *n*-alkane decreased (*i.e.*, for dodecane, it is 4.3 wt%; for octane, it is 2.8 wt%). The results were expected since reducing the length of the alkyl chain of an alkane will increase the solubility of the ionic liquid [62].

Table 13. Solubility test with ionic liquid and paraffin*

	Dodecane	**Octane**
0.5 wt% [BMIM][$OcSO_4$]	4.3 wt% butanol**	2.8 wt% butanol**

*The solubility test is based on 0.5 wt% of ionic liquid in hydrocarbon.
** This is approximate butanol amount to dissolve them together.

4.3.2. Effect of additives on droplet size

In previous study, the heat transfer fluid, D-600, was used to examine the capability of our electrospray device and to study the aerosol flame speed [52]. The amount of additive (Stadis 450) was one of the parameters manipulated to control droplet size, as shown in Figure 30. In the test, the high voltages applied (HV1 and HV2) were fixed at 6 kV and 3 kV, respectively (so the electric field, E, to break the liquid stream was 1.2×10^6 V/m). For D-600 with a flow rate of 4.8 ml/h, the droplet size changed sharply from 151 μm to 124 μm when Stadis 450 was increased from 1.0 to 2.0 wt%. For a flow rate of 2.4 ml/h, the effect of Stadis 450 was less significant. For flow rates of 1.7 and 1.2 ml/h, the

influence of this additive was marginal. In general it can be concluded that increasing the amount of Stadis 450 from 1.0 to 5.0 wt% can reduce the droplet size of D-600 aerosols.

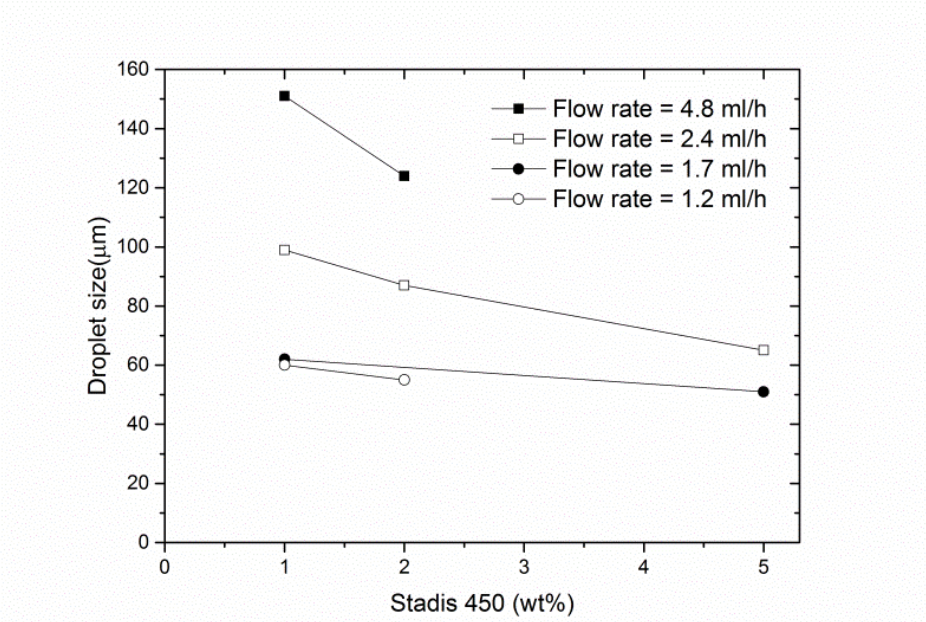

Figure 30. Droplet size vs. additive amount (Stadis 450) for the heat transfer fluid (D-600) aerosols generated under HV1 = 6 kV and HV2 = 3 kV (E = 1.2×10^6 V/m)

To study a broader scope of aerosol flame speed, dodecane was also examined as shown in Figure 31. The high voltages applied (HV1 and HV2) were set with a 2 kV potential (either HV1 = 5 kV and HV2 = 3 kV, or HV1 = 7 kV and HV2 = 5 kV. E = 8.0×10^5 V/m). Unlike D-600, amount of Stadis 450 mixed in dodecane has a negligible effect on reducing aerosol droplet size. For dodecane with a flow rate of 4.8 ml/h and HV1 = 7 kV and HV2 = 5 kV, the dodecane droplet sizes did not change appreciably when Stadis 450 was increased from 1.0 to 5.0 wt%. Similar phenomenon was also observed for the experiments conducted with dodecane at a flow rate of 3.6 ml/h.

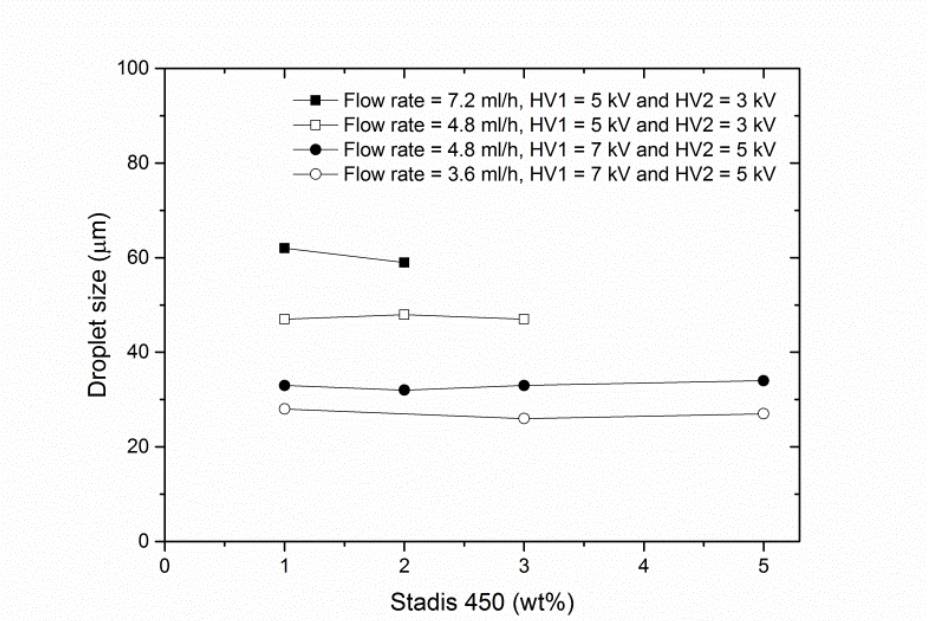

Figure 31. Droplet size vs. additive amount (Stadis 450) for dodecane aerosols at E = 8.0×10^5 V/m

The addition of Stadis 450 from 1.0 to 5.0 wt% can reduce droplet size of D-600 aerosols but failed with dodecane aerosols. There was also some conflicting behavior presented in literature [45, 66]. Hayati *et al.* used isoparaffinic oil blended with 15.0% to 50.0% *n*-butanol in electrospray application. The droplet size initially reduced when the electrical conductivity increased. It reached a minimum, and then increased with increasing electrical conductivity. The variation of droplet size with different additive amount was relatively large [66]. Tang and Gomes investigated heptane with 0.1% to 3.0% Stadis 450 as a fuel for electrospray study. Although the droplet size variation was relatively small, the trend was clear that the droplet size of heptane aerosols reduced when the electrical conductivity increased [45].

One major difference in the above studies is the type and amount of additives, which may be the cause of differing observations on the effect of additives. Hayati *et al.* used large amounts of *n*-butanol as an additive to increase the electrical conductivity. Although Hayati *et al.* indicated viscosity did not change significantly, the dielectric constant did change [67]. The dielectric constant and electrical conductivity increased significantly with the increase of butanol. This has an effect on the relaxation time of isoparaffinic oil mixtures and the resulting electrical force acting on the liquid. Tang and Gomes used small amounts of Stadis 450 to increase the electrical conductivity and only electrical conductivity was changed significantly. In this study, Stadis 450 was added from 1.0 wt% to 5.0 wt%, and the droplet size of D-600 aerosols reduced with increasing electrical conductivity. The results were expected and were similar to Tang and Gomes's experiment, although the effect attenuated at higher additive amounts and lower liquid flow rate. However, this observation was not obvious for dodecane aerosols. The possible explanation is that the applied voltage and the additive amount were high, and the liquid flow rate was low as compared to Tang and Gomes's experiment. It is known that the effect of reducing droplet size will attenuate under high applied voltage, high additive amount and low liquid flow rate.

In order to reduce aerosol droplet size under the same voltage and liquid flow rate, multiple additives, including Stadis 450, butanol, ionic liquid ([BMIM][OcSO4]) and Span 20, were examined in dodecane aerosols. At first, Stadis 450 was tested with various concentrations and different liquid flow rates. In addition, 4.3 wt% butanol was also

blended in the mixture of dodecane and Stadis 450 so it can be a direct comparison with dodecane/[BMIM][OcSO4]/butanol mixture (because [BMIM][OcSO4] requires 4.3 wt% butanol to be dissolved in dodecane).

The results are presented in Figure 32. The applied high voltages were fixed at 7 kV and 5 kV. It can be seen that the use of 0.1 wt% Stadis 450 generated a relatively large droplet size in this group. Adding extra 4.3 wt% butanol had little effect in reducing the droplet size. Other amounts of Stadis 450 created comparable droplet sizes over a wide range of liquid flow rates. When the liquid flow rate was less than 1.2 ml/h, the amount of Stadis 450 had no significant influence on the droplet size.

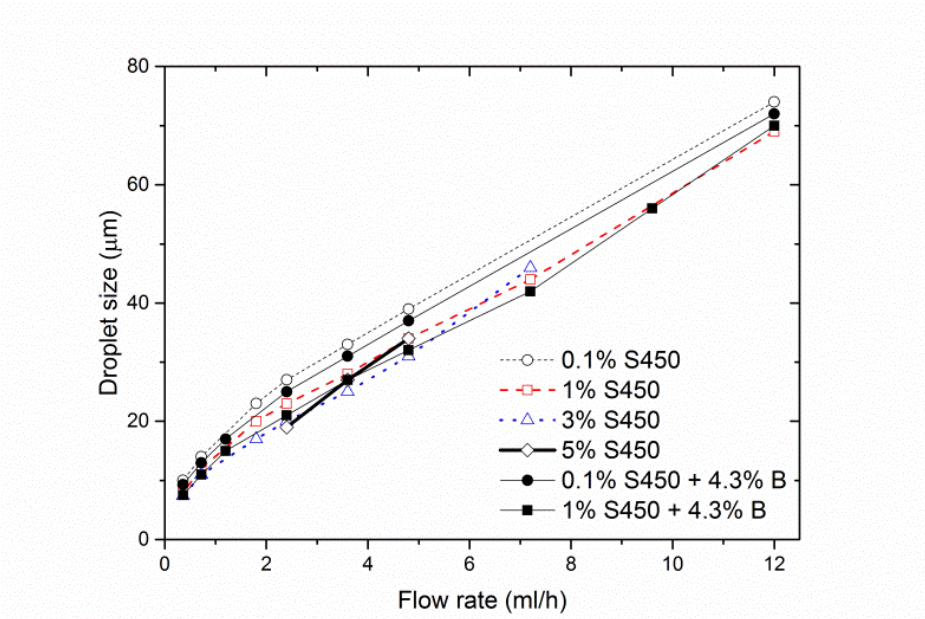

Figure 32. Droplet size vs. liquid flow rate for dodecane aerosols generated under HV1 = 7 kV and HV2 = 5 kV (E = 8.0 × 10^5 V/m) (1). S450 = Stadis 450, B = butanol

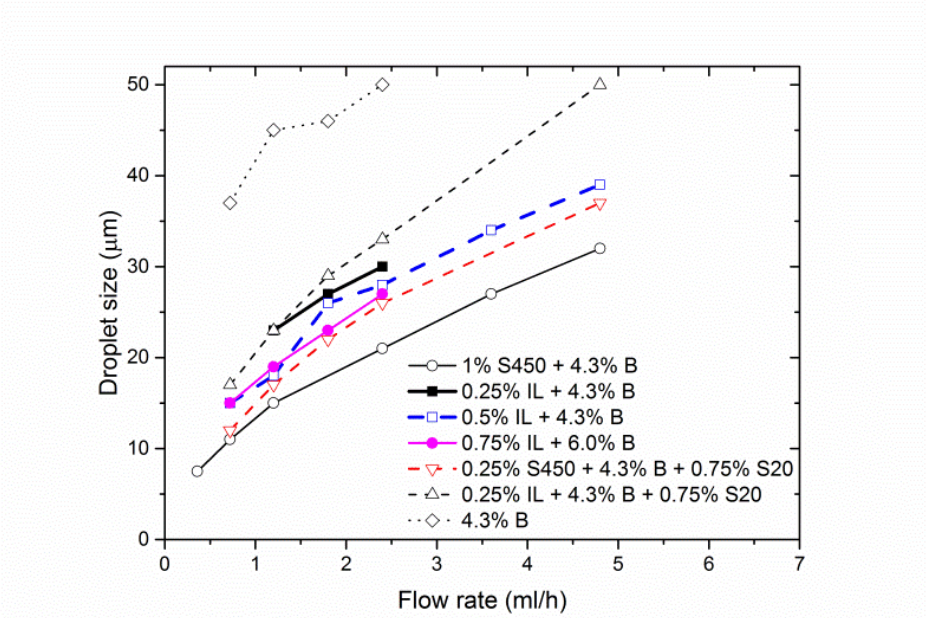

Figure 33. Droplet size vs. liquid flow rate for dodecane aerosols generated under HV1 = 7 kV and HV2 = 5 kV (E = 8.0 × 10^5 V/m) (2). S450 = Stadis 450, B = butanol, IL = [BMIM][OcSO4], S20 = Span 20

The mixture of dodecane/1.0 wt% Stadis 450/4.3 wt% butanol was taken as a benchmark to compare with other combinations of additives, as shown in Figure 33. The quantity of [BMIM][OcSO4] was increased from 0.25 wt% to 0.75 wt%. In order to dissolve 0.75 wt% [BMIM][OcSO4], the amount of butanol was also increased from 4.3 wt% to 6.0 wt%. The mixture with 0.75 wt% [BMIM][OcSO4] exhibited smaller droplet sizes than the mixture with 0.25 wt% [BMIM][OcSO4], but it was not significantly smaller than the mixture with 0.5 wt% [BMIM][OcSO4]. Higher amounts of [BMIM][OcSO4] was not tested since it requires a lot of butanol to be dissolved in hydrocarbon.

Extra 0.75 wt% Span 20 was blended in dodecane/0.25 wt% [BMIM][OcSO4]/4.3 wt% butanol mixture. However, the additional 0.75 wt% Span 20 did not help reduce the aerosol droplet size; rather, it increased the droplet size of this mixture. The phenomenon was also observed with the dodecane/0.25 wt% Stadis 450/4.3 wt% butanol mixture. Span 20 is not an effective agent in reducing droplet size compared to Stadis 450 and [BMIM][OcSO4].

By comparing dodecane/0.25 wt% Stadis 450/4.3 wt% butanol/0.75 wt% Span 20 mixture and dodecane/0.25 wt% [BMIM][OcSO4]/4.3 wt% butanol/0.75 wt% Span 20 mixture, it can be found that Stadis 450 was more effective than [BMIM][OcSO4]. From Figure 33, it can be concluded that Stadis 450 was the most powerful additive to reduce droplet size. Other combinations of additives were also tested; however, they were not plotted here in order to simplify Figure 33 and those data did not reveal more information. The use of 4.3 wt% butanol alone can barely facilitate the electrospray atomization process. The droplet sizes were large and the size distribution was very wide. The spray generated with the addition of 4.3 wt% butanol was not stable. This is consistent with the fact that 10% to 15% alcohol is usually needed with alkanes to increase the electrical conductivity for electrospray to be feasible [65, 66].

4.3.3. Effect of liquid flow rate and applied voltage on droplet size and monodispersity

The effect of liquid flow rate on the droplet size was the most significant amongst all controlling factors [45]. As indicated in Figure 32 and Figure 33, the droplet size changed almost linearly with the liquid flow rate. In order to generate small droplets, the liquid flow rate should be small. However, this directly affects aerosol concentration and it is not always a desirable test condition. Therefore, a multiple nozzle system is necessary to overcome this issue [10, 52]. A similar trend was also reported in literature [45, 66].

On the other hand, the liquid flow rate had a non-linear influence on the monodispersity or droplet size distribution when the applied voltages were set at 7 kV and 5 kV, respectively. The experimental results are presented in Figure 34. Span ratio was used to evaluate monodispersity of aerosols as defined in eq. (4):

$$\text{Span ratio} = \frac{D_v(90) - D_v(10)}{D_v(50)} \quad (4)$$

$D_v(10)$, $D_v(50)$ and $D_v(90)$ represent 10^{th}, 50^{th} and 90^{th} percentile of droplets by volume respectively. Span ratio of a perfectly monodispersed aerosol is zero. If droplet size distribution is wide, then its span ratio is large. As shown in Figure 34, the relationship between the span ratio and flow rate for four different additives were studied. The general trend was that span ratio at first decreased when liquid flow rate was increased. After a minimum span ratio was reached, it increased with increasing liquid flow rate. The results

of dodecane aerosol mixed with 0.1 wt% Stadis 450 and 1.0 wt% Stadis 450 were quite comparable. For dodecane aerosol mixed with 3.0 wt% Stadis 450, its span ratio was compatible to that of 0.1 or 1.0 wt% Stadis 450 when the liquid flow rate was less than 4 ml/h. However, its span ratio increased rapidly when the liquid flow rate was further increased. The trend of dodecane aerosol mixed with 1.0 wt% Stadis 450 + 4.3 wt% butanol was similar to that of 3.0 wt% Stadis 450. The major difference was the rapid increase of the span ratio occurred after the liquid flow rate was higher than 7.2 ml/h.

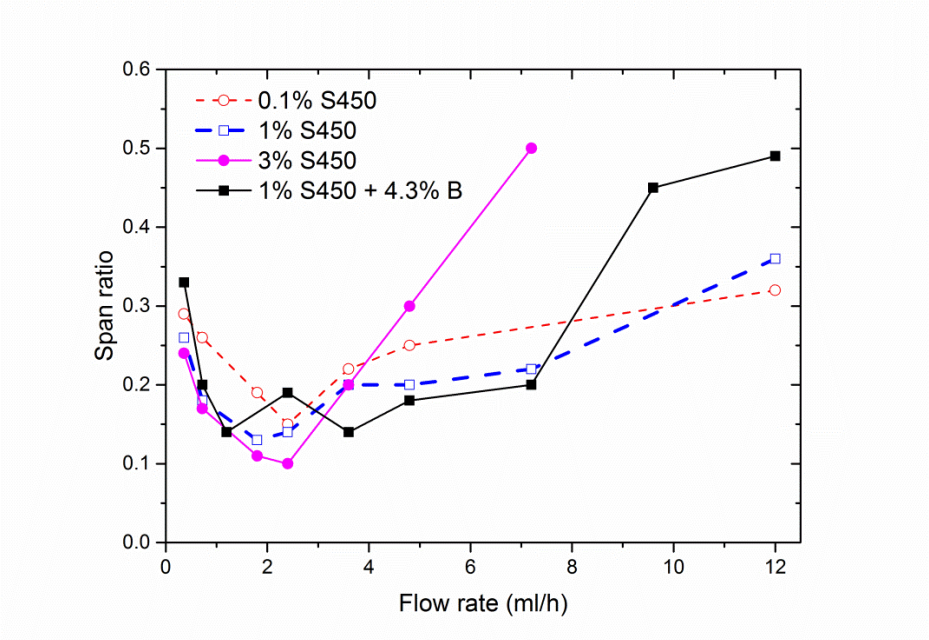

Figure 34. Span ratio vs. liquid flow rate for dodecane aerosols generated under HV1 = 7 kV and HV2 = 5 kV (E = 8.0 × 10^5 V/m). S450 = Stadis 450, B = butanol

Experiments with different voltages were also conducted and the overall conclusion was similar. From Figure 34 it can be observed that the higher amount of additive tends to destabilize the spray (*i.e.*, wide distribution and high span ratio) when the liquid flow rate

is high. Since the total amount of additive with 1.0 wt% Stadis 450 + 4.3 wt% butanol is more than that of 3.0 wt% Stadis 450, and the effect of increasing span ratio is less obvious, the effect of destabilization of Stadis 450 is more prominent than butanol.

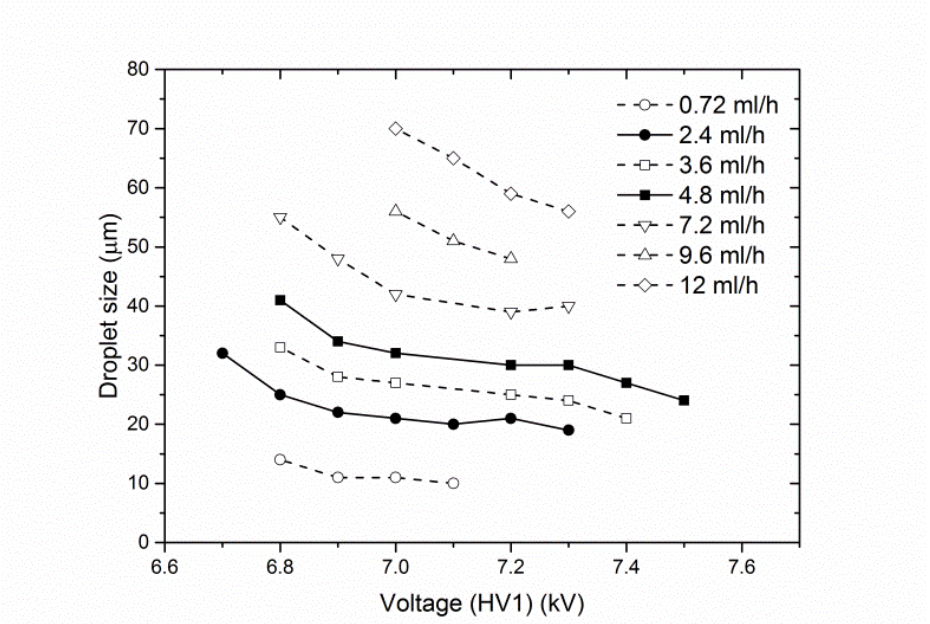

Figure 35. Droplet size vs. applied voltage (HV1) for dodecane aerosols generated under HV2 = 5 kV. The additive was 1.0 wt% Stadis 450 + 4.3 wt% butanol

The effect of the applied voltage on droplet size was also studied, as presented in Figure 35. Dodecane was blended with 1.0 wt% Stadis 450 + 4.3 wt% butanol and the flow rate was varied from 0.72 ml/h to 12.0 ml/h. The relative ground level (HV2) was set at 5 kV and the applied high voltage (HV1) was increased from 6.7 kV to 7.5 kV. The effect of the applied voltage is less significant than the liquid flow rate. When the liquid flow rate was low, the applied voltage can reduce droplet size at the lower voltages. But the

influence was attenuated when the voltage was further increased. Similar phenomenon was also reported in literature [10, 11, 45].

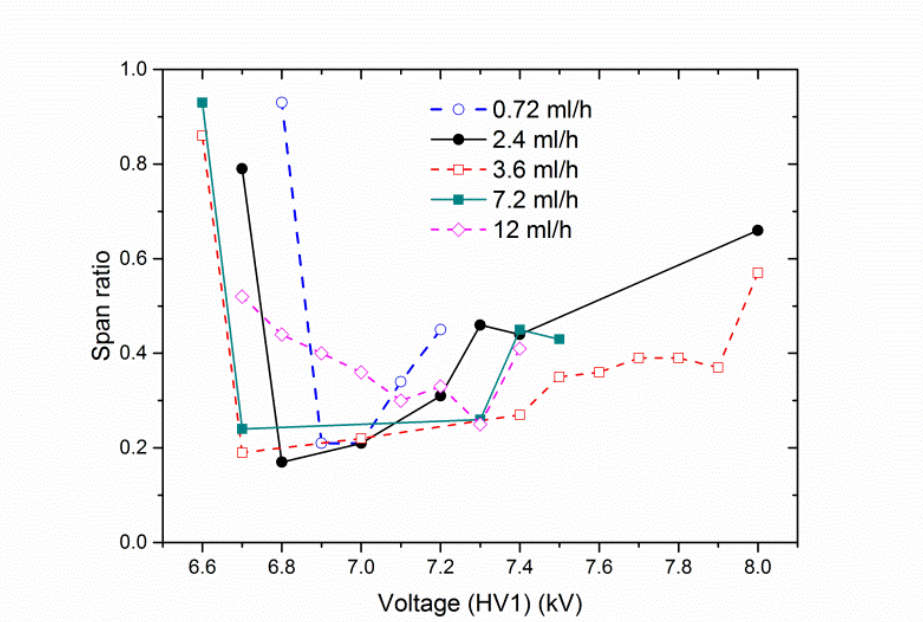

Figure 36. Span ratio vs. applied voltage (HV1) for dodecane aerosols generated under HV2 = 5 kV. The additive was 0.1 wt% Stadis 450 + 4.3 wt% butanol

Similar to changing liquid flow rate, there was also a minimum in span ratio when varying the applied voltage. Figure 36 demonstrates the experimental results of dodecane aerosols with 0.1 wt% Stadis 450 + 4.3 wt% butanol. The relative ground (HV2) was fixed at 5 kV and the liquid flow rate was increased from 0.72 ml/h to 12.0 ml/h. The applied high voltage (HV1) was varied from 6.6 kV to 8 kV. It is interesting to note that the minimum span ratio and the window of low span ratio (defined as span ratio less than 0.4, see Chapter 4.3.4) for the applied voltage shifted when the liquid flow rate was increased.

When the liquid flow rate was 0.72 ml/h, the minimum span ratio happened at HV1 = 6.9 kV, and the window of low span ratio was only about 0.3 kV (around 7.15−6.85). When the liquid flow rate increased to 2.4 ml/h, the minimum span ratio occurred at 6.8 kV, and window increased to 0.5 kV. When the liquid flow rate increased to 3.6 ml/h, the minimum span ratio shifted further to 6.7 kV, and window expanded to 1.3 kV. However, when the liquid flow rate further increased to 12 ml/h, the minimum span ratio shifted toward higher voltage (7.3 kV), and window of low span ratio shrunk to 0.5 kV.

The voltage has another effect on average droplet size and span ratio. Usually the force to break liquid stream is the electrical force created by high voltage difference between HV1 and HV2. In Figure 36 the voltage difference is between 1.6 kV and 3 kV. However, the electrical force between relative ground (HV2) and absolute ground level (grounded meshes) also plays a role. As shown in Figure 37, the high voltage difference between HV1 and HV2 was fixed at 2 kV, whereas HV2 was set either at 3 kV or 5 kV, and the liquid flow rate was fixed at 4.8 ml/h.

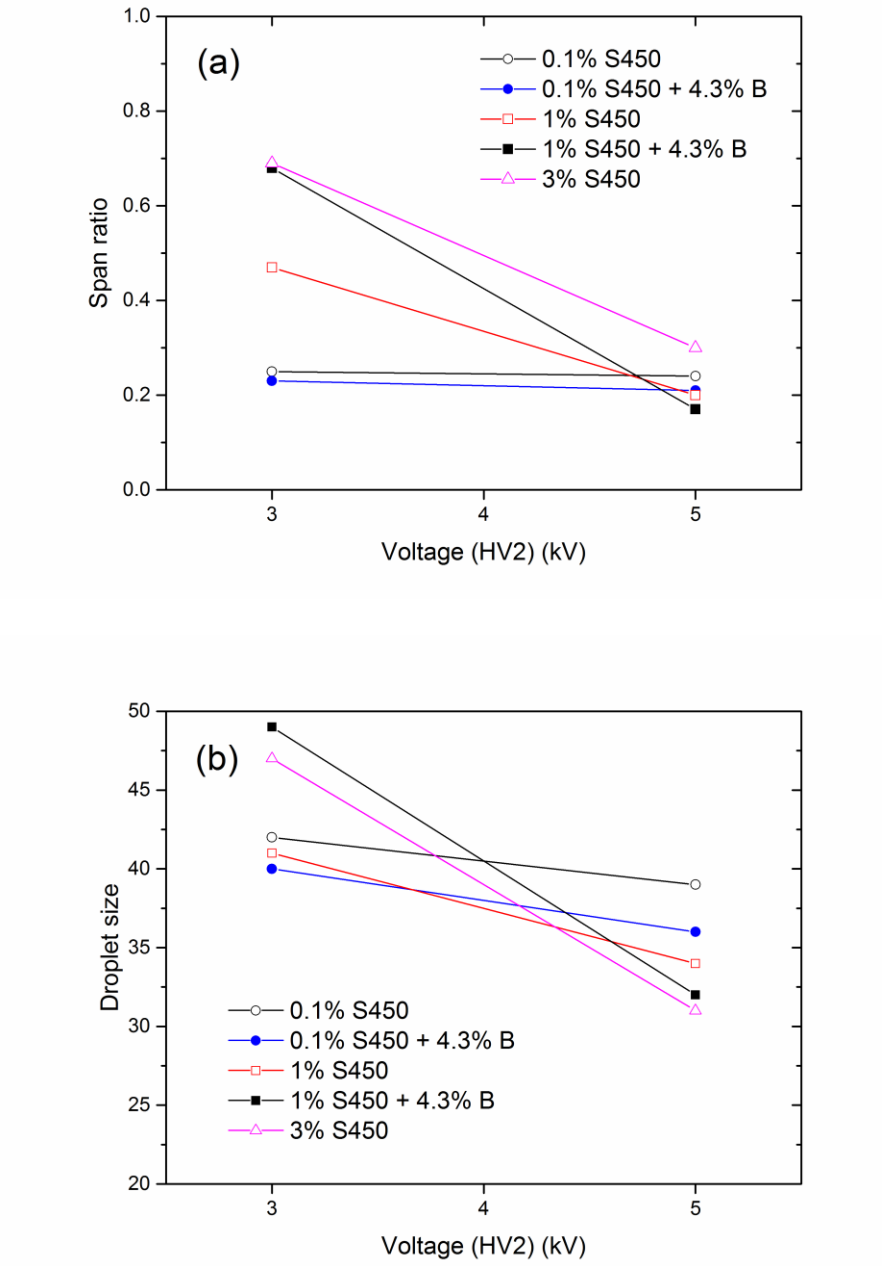

Figure 37. Effect of relative ground (HV2) on dodecane aerosols in terms of (a) span ratio and (b) droplet size at fixed voltage difference (HV1−HV2 = 2 kV, E = 8.0 × 10^5 V/m), liquid flow rate = 4.8 ml/h. S450 = Stadis 450, B = butanol

The Figure 37(a) represents span ratio data and Figure 37(b) indicates droplet size data. The results clearly demonstrates that aerosols generated under high HV2 exhibited smaller span ratio and droplet size, regardless of what additive amounts were used. As a result, the data in this work were all obtained under HV2 = 5 kV unless otherwise noted. It is also noted that the effect of relative ground was more obvious on mixtures with more additives (3.0 wt% Stadis 450 and 1.0 wt% Stadis 450 + 4.3 wt% butanol).

4.3.4. Stable aerosol generation region

The ultimate goal of this research is to study aerosol flammability, and aerosol flame speed is the first characteristic to be examined. Octane aerosol was tested in this study by using the improved electrospray device described in the previous work [52]. The initial results are displayed in Figure 38. The data points were quite scattered (adjusted R-square = 0.25), although there seemed to be a weak linear relationship ($y = 94.42 - 1.09x$) between aerosol flame speed and droplet size in the examined droplet size range.

It is intriguing why there is a large variation in the individual flame speed measurements. Upon reviewing their span ratios, it was found that all of the span ratios were about 1, which meant the droplet size distribution was very wide. Since the spray is polydispersed, a range of aerosol droplet size may dominate the flame propagation behavior at the point of ignition, which could lead to data deviation. This may explain the scattered flame speed with a weak linear relationship. Figure 39 shows the flame speed results of octane aerosols

with span ratio less than 0.5. The linear relationship ($y = 149.75 - 2.76x$) in Figure 39 is stronger than that in Figure 38. The adjusted R-square value was increased from 0.25 to 0.67.

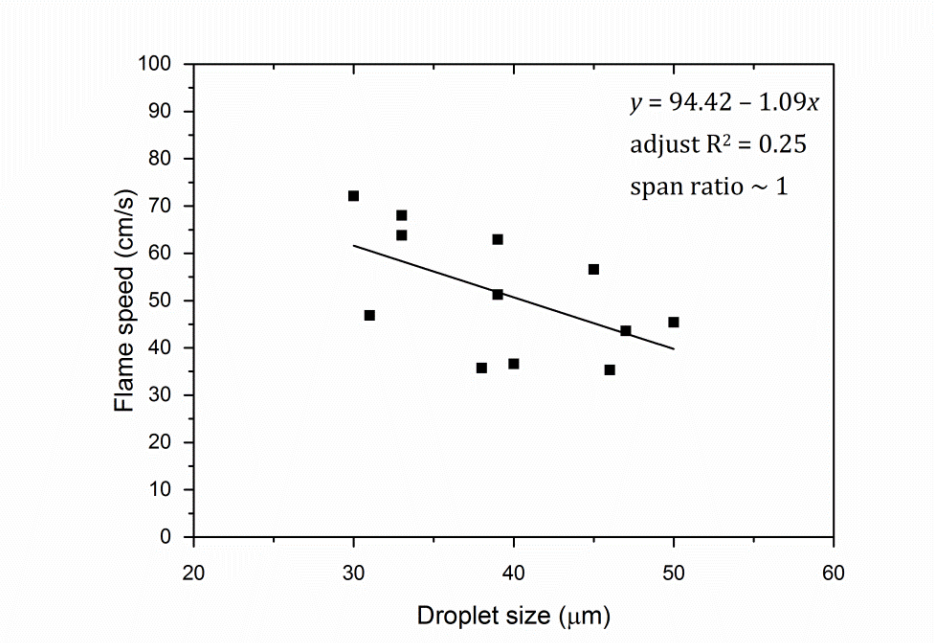

Figure 38. Flame speed of octane aerosols generated under HV2 = 5 kV with large span ratio (~1)

Such linear relationship was also observed in Greenberg's work in this droplet size range [68]. Two simulation models were applied to predict the trend of aerosol flame propagation. Zhu and Rogg described gas phase and liquid phase separately by Eulerian form and Lagrangian form respectively [69]. The trend of flame speed didn't fit well at smaller droplet sizes. Polymeropoulos solved energy balance and mass balance of controlled volume (containing both vapor and liquid fuel) simultaneously [16]. The simulated aerosol flame speed was lower than the experimental data. The reason could be

quiescent mixture condition was assumed in Polymeropoulos's work. Therefore, better predicting model and more experimental data are necessary to move the aerosol safety forward.

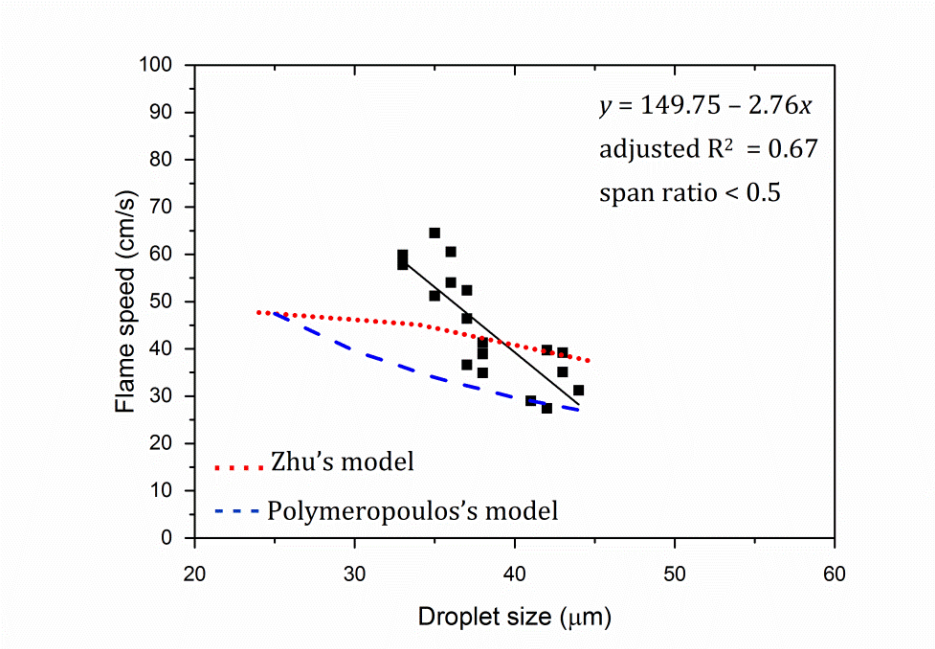

Figure 39. Flame speed of octane aerosols generated under HV2 = 5 kV with small span ratio (<0.5)

As a result, it is imperative to have a fundamentally understood electrospray device to generate high quality and repeatable aerosols. Attention should also be paid to the type of additive, amount of additive and operating parameters to create aerosols with small span ratios. From Figure 38 and Figure 39, we can define a stable aerosol as those with a span ratio less than 0.4. The stable region can be associated with the liquid flow rate and applied voltage (HV1) for a specific additive as shown in Figure 34 and Figure 36. The stable region for dodecane aerosol generated under HV2 = 5kV is indicated in Figure 40. The

stable region is bounded by the lower and upper applied voltage HV1, with a boundary span ratio around 0.4. The span ratio of aerosol in the middle of stable region could be as low as 0.1. Flame speed of those near-monodispersed aerosols demonstrated a fair linear increasing trend when the droplet size decreased as shown in Figure 39.

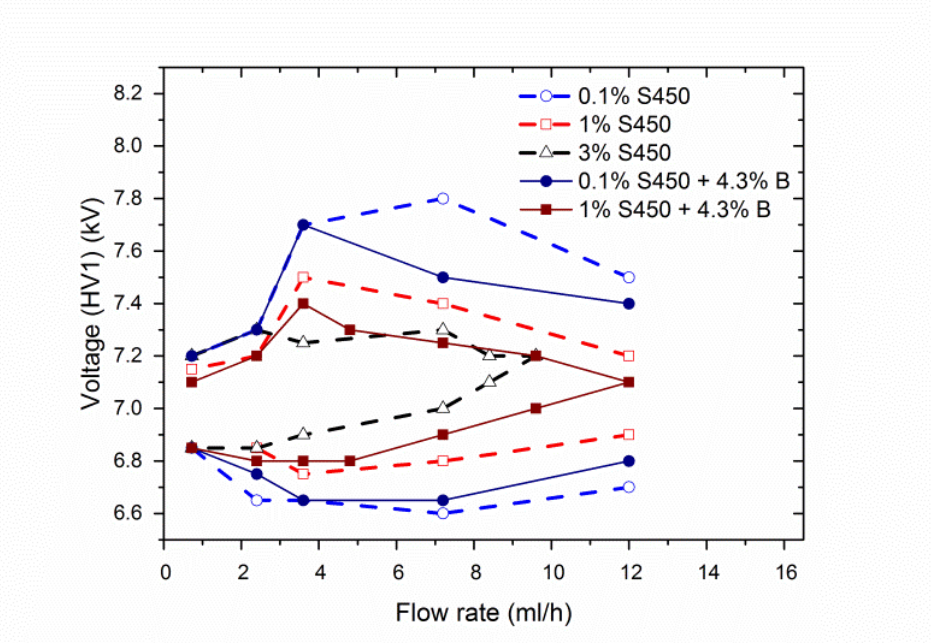

Figure 40. Stable region in terms of applied voltage (HV1) and liquid flow rate for dodecane aerosols generated under HV2 = 5 kV. S450 = Stadis 450, B = butanol

The overall trend of the stable region was that the window of the applied voltage (upper bound minus lower bound) expanded to a maximum when the liquid flow rate increased, and then the window reduced when the flow rate further increased. The stable region shrunk as the additive amount increased, and the effect of Stadis 450 was more influential than 1-butanol. When the additive amount was 1.0 wt% Stadis 450 + 4.3 wt% butanol or 3 wt% Stadis 450, the stable region shrunk to a single point at high liquid flow rate. Tang

and Gomes also demonstrated the cone-jet domain for heptane aerosols with a similar pattern [45]. However, the cone-jet domain was a qualitative concept and relies on photo evidence. It was time consuming and not precise with respect to droplet size distribution. On the other hand, span ratio is a quantitative indicator and represents monodispersity of aerosol, which is highly connected to data consistency as mentioned in the above discussions. Aerosols should be produced within this region to provide consistent results for fundamental research.

4.4. Summary

In order to study the flammability of aerosols, the generation method should be designed carefully, and consider additives effect and operating parameters. In this work, four groups of potential additives were investigated, including antistatic agents, surfactants, ionic liquids and alcohols. In each group, candidates were selected based on their potential to facilitate droplet breakup and solubility in alkanes. Furthermore, experimental results were obtained to indicate whether the additives were miscible with alkanes, and only one additive in each group was studied. Amongst these four candidates, the antistatic agent, Stadis 450, was still the most powerful additive to reduce droplet size.

The liquid flow rate had a near linear relationship with aerosol droplet size, and was the most influential parameter to control droplet size. It also affected droplet size distribution.

As flow rate increased, aerosols became nearly monodispersed initially. However, further increase in the flow rate will destabilize the spray. Similar behavior was also found for the application of voltage. There was a minimum span ratio which occurred at a median applied voltage. The window of low span ratio changed with the liquid flow rate. The window of low span ratio reached a maximum at the flow rate equaled to 3.6 ml/h for the dodecane/0.1 wt% Stadis 450/4.3 wt% butanol aerosol. On the other hand, increasing voltage can also reduce droplet size, though it was not as effective as the liquid flow rate, especially when the flow rate was low and the applied voltage was high. Besides the applied high voltage (HV1), the relative ground (HV2) also helped reduce droplet size and span ratio. When the electrical force between HV2 and ground level was stronger, droplets were further broken into smaller and more stable droplets.

The droplet size distribution or monodispersity will affect the reproducibility of aerosol flame speed study. Therefore, the aerosol span ratio (a parameter that describes monodispersity of aerosol droplets) should be maintained below 0.4 to obtain consistent results. A stable region was obtained based on the lower and upper bound of voltage where the span ratio was around 0.4. This stable region was also influenced by the amount of additive. As the amount increased, the region shrunk to a smaller area, which could limit the application of electrospray to generate high quality aerosol.

In summary, it is extremely important to carefully design and understand the fundamental workings of the electrospray device. The understanding includes the proper selection of suitable additives, their amounts, liquid flow rates, and applied voltages to achieve appropriate droplet size, span ratio and concentration for fundamental flammability study. The flame speed of *n*-octane aerosols was measured and simulated works were compared. This study clearly underlines the importance of monodispersed aerosols, the concern of aerosol hazards, the need of experimental results and well-prediction models to provide insight into preventative and mitigative strategies.

CHAPTER V

ANALYSIS AND OBSERVATION OF ENHANCED FLAME SPEED IN TRANSITION DROPLET SIZE RANGES FOR N-ALKANE AEROSOLS GENERATED BY ELECTROSPRAY

5.1. Introduction

Aerosols are suspensions of minute droplets or particles in a gas. The droplets may be formed via condensation of vapor or mechanical breakup of a liquid stream from high pressure container. In the process industries, there are numerous containers full of flammable or combustible materials stored at elevated temperature and pressure. Once the materials release accidentally, they are capable of forming aerosol clouds and pose unexpected threats to personnel, plant and public.

In 1974, Flixborough, UK, a large quantity of superheated cyclohexane flashed and condensed in the ambient condition. The aerosol cloud found an ignition source and the resulting explosion demolished the plant, killing 28 personnel and injuring 36 others [13]. In 1995, a severe fire and explosion occurred in Milliken & Company's Live Oak/Milstar Complex and Carpet Service Center, causing a total loss of more than $400 million. The direct cause was aerosol cloud from the leakage of hot oil with a 350 ^{o}F flash point [4].

It can be seen that a variety of hydrocarbons have the potential to form aerosol clouds and create huge losses, regardless of low or high flash point. However, there is a misconception that liquids are safe when they are stored below their flash points, and standards often classify their hazardous degree according to their flash points [11, 52]. Unfortunately, incidents described above have proven it is not proper to do so. Therefore, more efforts should be conducted to resolve this issue.

Flammability of aerosols has been researched for a long time, but no conclusive results can be determined. Furthermore, the trend of aerosol flame speed is not clear and is even contradictory in literature. Flame speed is the important factor to evaluate the hazardous consequences of materials. It is believed that the flame speed changes as droplet size shifts. However, there is no systematic approach to investigate aerosol flame speed and no definitive conclusions because of the difficulty of aerosol generation by a well-controlled manner.

Some literature showed aerosol flame speed would only increase as droplet size decreases [39, 70]. The maximum flame speed of such aerosols is flame speed of vapor, which can be achieved at very small droplet sizes, typically smaller than 10 μm. Interestingly, others demonstrate that there is a transition droplet size range. When droplet size is in this range, the corresponding aerosol flame speed would be even faster than that of smaller droplet sizes and vapor [17, 18, 38, 71]. Moreover, some unclear patterns are also found [34, 72].

As discussed above, there is contradictory observation regarding aerosol flame speed. If there is a transition range in which aerosol flame speed would be enhanced, then this range should be avoided to reduce the consequences if aerosol is likely to form. Hence, it is necessary to prove the concept of transition range study on aerosol flame speed, both in experimental study and fundamental understanding.

In this research, three alkanes (*n*-octane, *n*-decane and *n*-dodecane) were made into aerosols by using electrospray technique. The selection of fluids was based on their flash point, ranging from 286 K to 347 K. The generated aerosols were further characterized to evaluate their droplet sizes and associated flame speeds by Malvern Laser Diffraction Particle Analyzer and a high speed camera. Both theoretical calculation and empirical analysis were applied to explain the observed phenomenon.

5.2. Materials and methods

5.2.1. Materials

In this study, three alkanes, *n*-octane, *n*-decane and *n*-dodecane, were examined for their aerosol flame propagation behavior by using electrospray to produce aerosols. Their relevant properties are listed in Table 14. Since they are saturated hydrocarbons, their dipole moment and electrical conductivity are too low to create aerosols by using

electrospray. Therefore, a suitable additive is necessary to promote their electrical conductivity significantly without altering other properties obviously.

Table 14. Relevant properties of alkanes

	n-Octane	*n*-Decane	*n*-Dodecane
Molecular weight	114.23	142.29	170.34
Flash point (K)	286	319	347
Boiling point (K)	399	447	489
Density (kg/m^3)	703	730	749
Thermal conductivity (W/(m·K))	0.128	0.132	0.152
Isobaric specific heat (J/(kg·K))	2228.8	2209.7	2207.4
Heat of evaporation (J/kg)	301147	272683	261242
Heat of combustion (J/kg)	47726096	47635111	47475637
n[a]	1.40	1.41	1.42
k[a]	0	0	0

[a] Refractive index is required for Malvern laser analysis, where n and k are the real part and imaginary part of refractive index, respectively.

Several additives have the potential to increase electrical conductivity, such as Stadis 450, surfactants, ionic liquids and alcohols as demonstrated in Chapter IV. Stadis 450 was chosen because it demonstrated excellent ability to increase electrical conductivity while other liquid properties remained consistent [45]. The amount of Stadis 450 was fixed at 0.1 wt%. The liquid mixtures were stirred for 3 minutes and stood still overnight to make sure they mixed homogeneously.

5.2.2. Aerosol generation

After samples were mixed well, they were aerosolized by a homemade electrospray system same as the previous publication [52]. The schematic setup of electrospray device and overall system is shown in Figure 41. The samples were put into 10 syringes of 2.5 mL capacity. The syringes were pumped by a syringe propeller (KDS 220) and connected by plastic tubing (508 μm i.d.) to the respective nozzles. The stainless steel nozzles (254 μm i.d. and 508 μm o.d.) were assembled on a compact disc and associated with a high voltage (HV1). A metal mesh connected to second high voltage (HV2) was aligned with the nozzles to create a uniform electric field. The voltage was generated by a function generator (SRS, DS-345) and amplified to desired magnitude by an amplifier (Trek Inc. 610E).

The stable operating parameters for aerosol generation had been discussed in Chapter IV. Here the aerosols were generated with the suitable parameters for consistent results. HV1 was set around 7 kV and HV2 was maintained at 5 kV (served as relative ground level). A flat grounded mesh (4 cm × 4 cm) and a cylindrical grounded mesh (4 cm in height and 10 cm in diameter) were positioned 15 cm beneath the HV2 mesh to collect the charged droplets. When the liquid streams with appropriate properties flow through the steel nozzles, a conical shape of liquid stream can be observed and minute droplets are produced from the cone tips [10, 45].

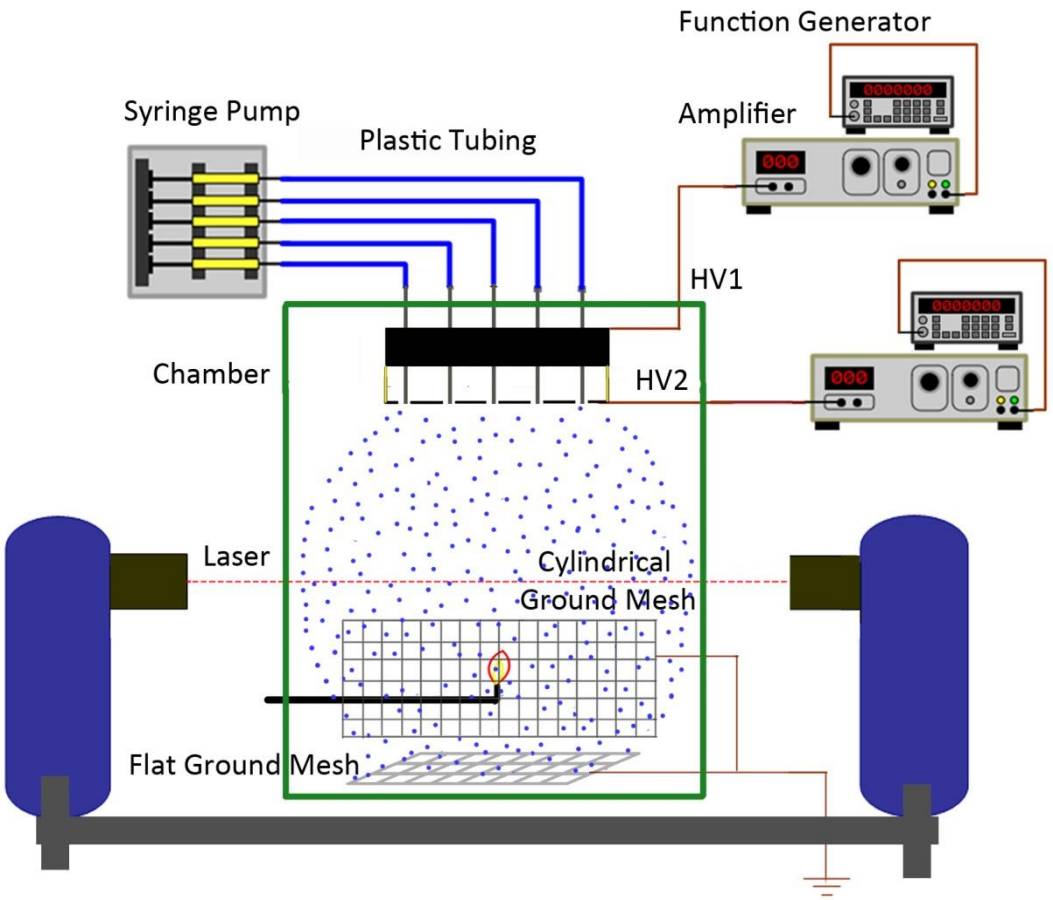

Figure 41. Schematic setup of electrospray device and overall system

5.2.3. Aerosol characterization

To monitor the aerosol continuously without interrupting the generation process, a Laser Diffraction Particle Analyzer (SprayTec, Malvern Inc.) was used to obtain droplet size and aerosol concentration. The He-Ne laser has energy of 2 mW and is classified as 3R laser. All personnel in the lab should wear proper laser goggles while the laser is in operation.

The technique relies on Mie Theory and requires accurate refractive index ($n + ik$) to calculate the respective droplet size and concentration. The real part of refractive index provides information on how the light is scattered while the imaginary part describes the amount of laser energy being absorbed by droplets. The scattered angle of laser light decreases logarithmically when droplet size increases. The droplet size reported here was based on Surface Area Moment Mean Diameter ($D_{[3][2]}$) or Sauter Mean Diameter (SMD). Aerosol concentration was further obtained by the Beer-Lambert Law.

When aerosol cloud deemed stable, it was ignited by a 0.5 cm propane flame and the flame propagation was recorded by a high speed camera (Phantom 4.2, Vision Research Inc.) as described in literature [52]. The videos were further converted into a series of pictures with resolution of 512×512 pixels. The image analysis was similar to Lian's method [9]. The presence of droplet created obstacles, and the relay propagation or inhomogeneous vapor distribution may result in irregular flame propagation. Therefore, it was difficult to determine a flat flame front for flame speed calculation. Alternatively flame speed was calculated by moving center of flame bodies (*i.e.*, slope of flame position versus time).

5.2.4. Flame speed model description

Droplet evaporation plays an important role in aerosol flame propagation and minimum ignition energy [9, 73]. If all droplets evaporate completely before encountering flame, then the behavior of this aerosol is similar to vapor, which happens for very small droplets

[16]. However, if the droplets still present while contacting with the flame, the droplets will absorb combustion heat and decelerate flame propagation. On the other hand, the droplets can create turbulence and serve as obstacles to wrinkle the flame front, which can increase the reaction area and enhance the flame speed. To study the great complexity of droplet burning, a convective droplet evaporation model was utilized in the energy and mass balance equations. The equations were further converted to relate to the flame thickness and flame speed. The detailed model description and the necessary physical properties are as follow.

The convective droplet evaporation was given by Sirignano [74]:

$$\dot{m} = 2\pi \frac{kD_{32}}{C_p} \ln(1+B)\left(1+\frac{\mathrm{c}Pr^{1/3}Re^{1/2}}{2\mathrm{F}(B)}\right) \tag{5}$$

where $\dot{m}$ is the convective droplet vaporization rate (kg/s), k and C_p are the thermal conductivity (W/(m·K)) and isobaric specific heat of gas (J/(kg·K)) respectively, B is Spalding transfer number, c is a constant (0.848 from Ranz-Marshall's correlation), Pr and Re are Prandtl number and Reynolds number respectively, and F(B) is a correlation of numerical results for Falkner-Marshall solutions.

Spalding transfer number B or non-dimensional energy transfer number can be represented as eq. (6) according to Williams's work [75]:

$$B = \frac{C_p(T_{ad} - T_b) + H_c Y_{O,\infty} f}{H_v} \tag{6}$$

where T_{ad} and T_b are adiabatic flame temperature and boiling point respectively, H_c and H_v are the heat of combustion (J/kg) and heat of vaporization (J/kg) of the liquid fuel respectively, $Y_{O,\infty}$ is the oxygen concentration at the infinity, and f is the fuel to oxygen ratio.

$\mathrm{F}(B)$ can be represented as eq. (7) [76]:

$$\mathrm{F}(B) = (1 + B)^{0.7} \frac{\ln(1+B)}{B} \qquad \text{for } 0 \leq \mathrm{B} \leq 20 \text{ and } 1 \leq \mathrm{Pr} \leq 3 \tag{7}$$

However, for Re less than 10, eq. (5) should be corrected as eq. (8) [74]

$$\dot{m} = 2\pi \frac{kD_{32}}{C_p} \ln(1 + B)\left(1 + \frac{\mathrm{c}(1+2RePr)^{1/3} \max[1, (2Re)^{0.077}] - 1}{2\mathrm{F}(B)}\right) \tag{8}$$

Eqs. (6) to (8) provide how the droplet evaporation is influenced by liquid and gas properties and droplet moving velocity. The information needs to be further correlated with overall mass and energy balance to calculate laminar aerosol flame speed (S_{La}) under steady-state condition. According to Polymeropoulos's work [16], the energy balance relationship in the reaction zone can be represented that the heat release from liquid fuel

and vapor fuel combustion equals the heat loss due to conduction to the surroundings as shown in eq. (9).

$$\dot{m}_t \Delta H t_q = \dot{m}_l \Delta H t_e + \dot{m}_v \Delta H t_c \tag{9}$$

where $\dot{m}_t$, $\dot{m}_l$ and $\dot{m}_v$ are the total mixture mass flow rate (kg/s), the liquid phase flow rate and the vapor phase flow rate at the instant of droplet ignition, respectively. The characteristic heat loss time t_q and characteristic chemical reaction time for the vapor phase t_c can be shown as eq. (10) and (11) based on Ballal and Lefebvre's study [39].

$$t_q = \frac{\alpha}{S_{La}^2} \tag{10}$$

$$t_c = \frac{\alpha}{S_{Lg}^2} \tag{11}$$

where α is thermal diffusivity of gas (m^2/s), and S_{Lg} is the laminar flame speed of gas mixture.

The characteristic droplet vaporization time t_e at the instant of droplet ignition follows the relation:

$$t_e = \frac{\text{mass of a droplet at ignition}}{\text{rate of evaporation}} = \frac{\rho_l \times \frac{\pi}{6} \times D_i^3}{\dot{m}} \tag{12}$$

where ρ_l is the liquid density, and D_i is the droplet diameter at ignition. D_i can be calculated by considering ignition criterion for aerosol. To simplify the work, Polymeropoulos had shown that $D_i \cong D_{32}$ for isooctane aerosols when $D_{32} \geq 15$ μm [16]. Therefore, the simplification of $D_i \cong D_{32}$ was used in this work since the hydrocarbons tested in this research are more difficult to ignite than isooctane.

Substitute eq. (8) into eq. (12) to obtain eq. (13).

$$t_e = \frac{\rho_l D_{32}^2}{12\alpha\rho \ln(1+B)\left(1+\frac{c(1+2RePr)^{1/3}\max[1,(2Re)^{0.077}]-1}{2F(B)}\right)} \tag{13}$$

The mass balance of the fuel from upstream to the point of ignition is

$$\dot{m}_t = \dot{m}_l + \dot{m}_v \Rightarrow \frac{\dot{m}_v}{\dot{m}_t} = 1 - \frac{\dot{m}_l}{\dot{m}_t} \tag{14}$$

And the mass ratios of eq. (14) can be represented by using the upstream fuel fraction in the vapor form, Ω

$$\frac{\dot{m}_l}{\dot{m}_t} = (1-\Omega)\frac{D_i^3}{D_{32}^3} = (1-\Omega) \tag{15}$$

$$\frac{\dot{m}_v}{\dot{m}_t} = 1-(1-\Omega) = \Omega \tag{16}$$

The aerosol flame speed eq. (17) can be obtained by substituting eqs. (10), (11), (13), (15) and (16) into eq. (9)

$$S_{La} = \{ \frac{(1-\Omega)\rho_l D_{32}^2}{12\alpha^2 \rho \ln(1+B)\left(1+\frac{c(1+2RePr)^{\frac{1}{3}}\max[1,(2Re)^{0.077}]-1}{2F(B)}\right)} + \frac{\Omega}{{S_{Lg}}^2} \}^{-0.5} \quad (17)$$

5.3. Results and discussion

5.3.1. Experimental and simulation results of flame speed for n-octane aerosols

The three hydrocarbons, *n*-octane, *n*-decane and *n*-dodecane, were examined by the instruments and experimental procedure outlined above. Due to the nature of electrospray and the difficulty of aerosol generation in a well-controlled manner, it is hard to target different droplet sizes with consistent concentration. As a result, the volume concentration of large droplet aerosol is usually slightly higher than that of small droplet aerosol. However, the trend of flame propagation seems not to be changed by this variation.

In order to determine the adiabatic flame temperature, the equivalence ratio, ϕ, was taken as 0.7 after considering the kinetic concentration [36]. The adiabatic flame temperature for these hydrocarbons was therefore set at 1880 K. The physical properties of gas mixtures were calculated at the temperature of $(T_{ad} + T_u)/3 = 725$ K based on

Polymeropoulos's work [16]. T_u was the upstream temperature or room temperature for this experiment (294 K).

The upstream fuel fraction in the vapor form, Ω, was taken as zero because the aerosols were produced from electrospray method instead of condensation. In addition, the saturated vapor pressure of these hydrocarbons is relatively low.

The laminar flame speed of these gas mixtures at the room temperature, S_{Lg}, was not found in literature. In addition, the flash point of *n*-decane and *n*-dodecane is higher than room temperature, which means their saturated vapor cannot be ignited at this condition. Therefore, their S_{Lg} was calculated from elevated temperature (*n*-octane at 353 K and *n*-decane at 403 K when the equivalence ratio was 0.7 [77]). It is known that the flame speed of the same group hydrocarbons is similar, and S_{Lg} has an exponentiation relationship with base T and exponent x. A simple correlation can be obtained as shown in eq. (18). As a result, $S_{Lg}(294\ \mathrm{K}) = 0.21$ (m/s) was used throughout our calculation.

$$S_{Lg}(T_2) = S_{Lg}(T_1) \times \left(\frac{T_2}{T_1}\right)^{2.14} \tag{18}$$

The experimental results and model predictions of flame speed for *n*-octane aerosols are shown in Figure 42. It can be observed that there was a transition range where the aerosol flame speed was enhanced (*i.e.,* the flame speed first increased with decreasing droplet

size and reached a maximum. Then the flame speed reduced with further decreasing droplet size). This trend was also observed in literature and there were some models to predict the flame propagation [16, 69].

Polymeropoulos developed a model for isooctane aerosols to fit Ballal and Lefebvre's work. The properties of *n*-octane were plugged into Polymeropoulos's model [16]. For droplets larger than 27 μm, the aerosol flame speed was underestimated. Moreover, the location of transition range was not predicted accurately. Zhu and Rogg also developed a model for *n*-octane aerosol [69]. The magnitude of flame speed was around the same level. But again, no transition range was predicted here.

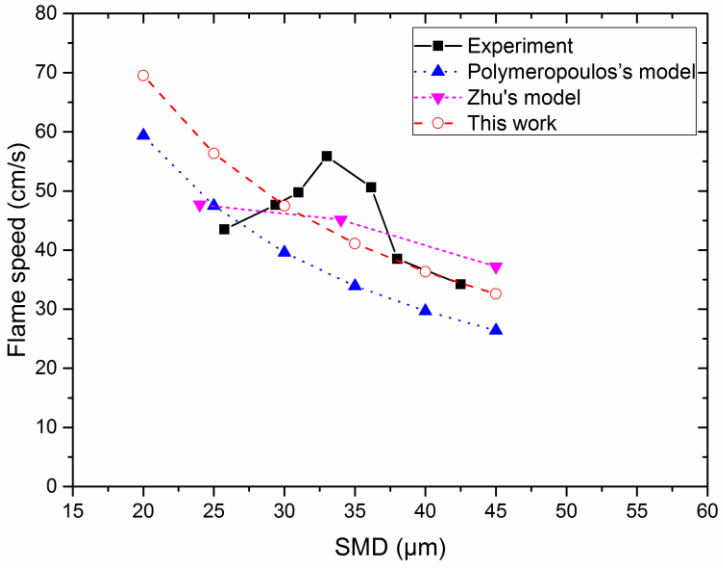

Figure 42. Flame speed of *n*-octane aerosols with experimental data, Polymeropoulos's model, Zhu's model and this work

The Reynolds number for the convective evaporation in our calculation was based with $u_d = 3$ (m/s) according to Lian's work [9]. This model provided a good fit when droplets were larger than 38 μm. However, it was unable to predict the transition range observed in the experiment.

There are few explanations why the enhanced flame speed would occur in the transition droplet size range. First, gas products released from burning droplets expanded hugely as compared to the small volume of liquid. This thermal expansion promotes mass and thermal transport, resulting in higher reaction rate and flame speed. Second, the moving droplet has an elongated burning tail once it is ignited. The larger flame area may provide excess heat source for evaporation. In addition, droplet can be ignited in a different way as vapor does. Radiation may ignite a droplet without bringing the whole volume of gas/aerosol mixtures to the required temperature [36].

There is another explanation for the relay propagation. If the flame radius of single droplet equals to the droplet spacing, the flame propagation would reach a maximum because the flame front contacts with droplet directly. Another possibility is that the vaporization of burning droplet provides the optimum range of fuel to oxygen ratio when certain droplet sizes and specific liquid properties are met. This can increase local combustion and thus promote overall reaction.

Finally, the presence of droplets serves as obstacles and can wrinkle the flame front provided that the droplets are large enough and liquid volatility is adequate. The wrinkled flame has higher surface area for combustion and therefore flame speed is enhanced under the combination of droplet size and liquid properties. Photo evidence of wrinkled flame front of large droplets has been demonstrated in literature [38, 72]. It can also be observed that the flame front of smaller droplets is much smooth, which is similar to vapor form. These factors may intertwine together so a more robust model is necessary to describe the complicated process.

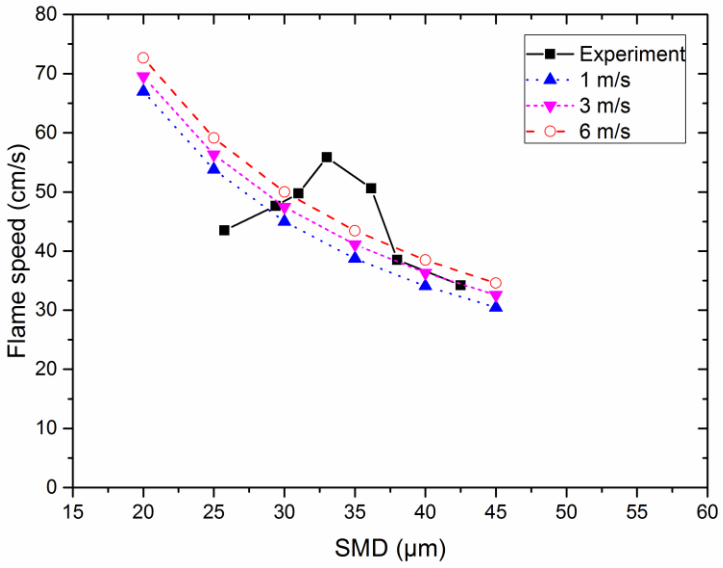

Figure 43. Sensitivity analysis of current model with droplet moving speed at 1, 3 and 6 m/s for *n*-octane aerosols

In addition to the flame speed model, sensitivity analysis was also conducted for $u_d =$ 1, 3 and 6 (m/s) as Deng's work demonstrated that droplet moving speed was around 6

m/s [78]. Figure 43 indicates that once convective droplet evaporation was considered in this model, the variation of aerosol flame speed was small as compared to Polymeropoulos's model (*i.e.*, not sensitive to droplet speed if convective evaporation has been considered). However, our calculation cannot predict the location of enhanced flame speed although the magnitude of flame speed was close. It is possible that the moving droplet also has an impact on the ignition criterion. It should be considered to improve the model for transition range prediction in the future.

5.3.2. Results of flame speed for n-decane and n-dodecane aerosols and the trend of transition droplet size range

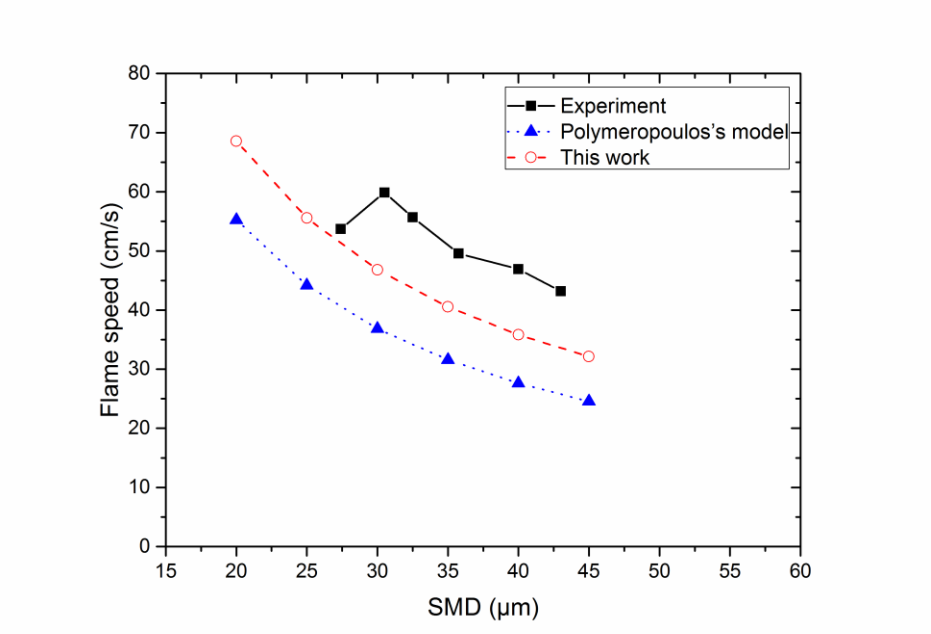

Figure 44. Flame speed of *n*-decane aerosols with experimental data, Polymeropoulos's model and this work

The results of aerosol flame speed for *n*-decane and *n*-dodecane are displayed in Figure 44 and Figure 45, respectively. Similarly, the phenomenon of enhanced flame speed was also observed for these two *n*-alkane aerosols. The transition droplet range cannot be predicted accurately. In addition, the model became less accurate when the number of carbon in the *n*-alkane increased. It was speculated that the vapor flame speed under room temperature (S_{Lg}) cannot be applied directly for *n*-decane and *n*-dodecane since the vapor from their liquid form is not flammable under this condition. Therefore, the deviation between experiment and calculation became larger as the carbon chain increased.

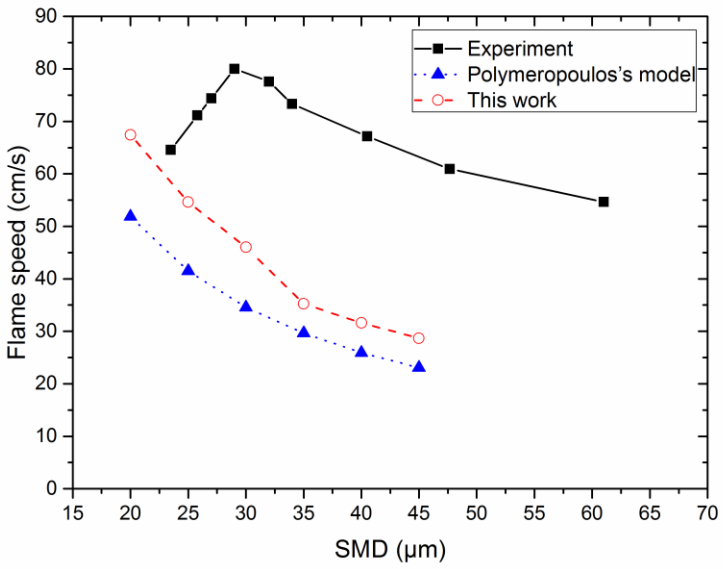

Figure 45. Flame speed of *n*-dodecane aerosols with experimental data, Polymeropoulos's model and this work

Although the phenomenon of enhanced aerosol flame speed was seen on all three hydrocarbons here, the location of transition droplet size range was not a fixed value. This

behavior may change with liquid properties and aerosol concentration. The maximum flame speed was found when the aerosol diameter was between 10 and 20 μm for tetralin aerosols in Chan and Jou's test [17], which agreed with Polymeropoulos's prediction [16]. However, in Niioka's experiment [18], the maximum peak for *n*-decane aerosol was around 100 μm instead of 10 to 30 μm. Besides equipment and test differences, different volatilities/flash points and other properties of the tested fuels may contribute to this discrepancy. The maximum peak of aerosol flame speed for *n*-octane, *n*-decane and *n*-dodecane in this study occurred around 33, 30.5 and 29 μm respectively, and their corresponding flash points are 286, 319 and 347 K.

It is reasonable to assume that the transition droplet size should be smaller for high flash point liquid (or lower volatility liquid) since it is not easy to evaporate or not easy to burn. Hence, the droplet size must be smaller to provide higher surface area for quick evaporation and subsequent combustion. On the other hand, for low flash point liquid (or higher volatility liquid) which is easy to evaporate or easy to burn, the droplet size may be larger and still able to provide enough vapor for combustion. Since flame speed of aerosol is higher than that of vapor under certain conditions, aerosol hazards may be more devastating than vapor. In addition, people are relatively unaware of aerosol hazards. This clearly raises the need to investigate the flammability of aerosol and provide a thorough understanding. Then the preventative and mitigative measures can be made to avoid or reduce the associated risks.

5.3.3. Normalization and empirical analysis of flame speed for n-alkane aerosols

The complication of flame propagation and transition droplet size range has been described above. In order to simplify the hassle and provide a quick and adequate analysis, empirical analysis was used to fit the trend of flame propagation based on the normalized data. The aerosol flame speed and droplet size were normalized by its maximum aerosol flame speed and corresponding droplet size for each hydrocarbon. As a result, the three flame propagation curves can be plotted and compared on the same graph despite different properties, as shown in Figure 46.

As they were normalized by their maximum aerosol flame speeds and corresponding droplet sizes, the three normalized flame curves intercepted at (1.0, 1.0). It can be seen that the normalized aerosol flame speed curves for different *n*-alkanes were consistent when the normalized droplet sizes were less than 1.0. It was possible that as the flame speeds reached maximum under such small diameters, the droplet behavior began acting similar to vapor. In addition, once the flame speeds were normalized by their maximum aerosol flame speeds, the discrepancy between the *n*-alkanes would be eliminated and resulted in the curves being quite matched.

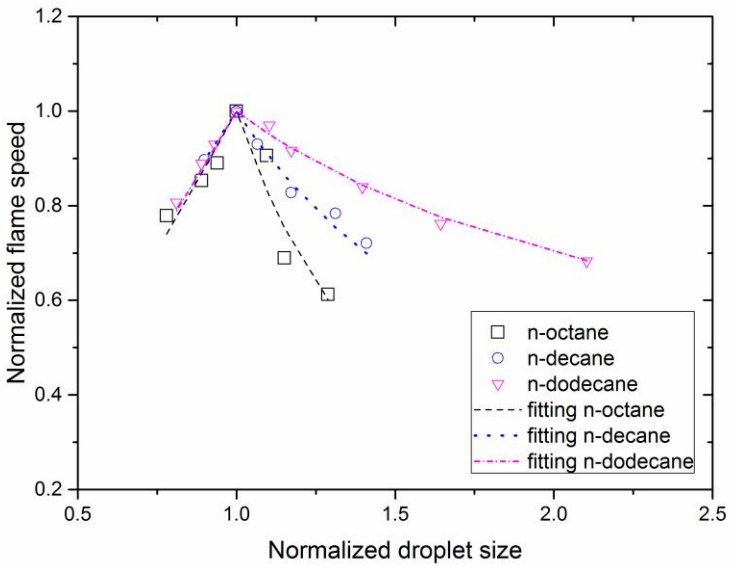

Figure 46. Normalized aerosol flame speed and corresponding empirical fitting for *n*-alkane aerosols

On the other hand, there was a clear distinction between the normalized aerosol flame speeds for the normalized droplet sizes larger than 1.0. It is possible that the droplets were burned under the individual flame envelopes in these situations. Therefore, their liquid properties would determine how it behaves. From Table 14 in Chapter 5.2.1, it can be found that the heat of evaporation increases appreciably when the number of carbon in the alkane decreases. However, the isobaric specific heat and heat of combustion are almost the same for these alkanes. As a result, the larger the droplet, the higher amount of heat is required to vaporize *n*-octane droplets during combustion as compared to *n*-decane and *n*-dodecane. This may explain why the normalized aerosol flame speed of *n*-octane is the

smallest one. It also explains why the difference becomes more obvious while the normalized droplet size is larger.

In order to understand how the liquid properties affect the trend of aerosol flame propagation, a set of empirical equation was developed to predict the normalized flame speed based on the normalized droplet size. The liquid properties include density (ρ_l), thermal conductivity (k_l), isobaric specific heat (C_{pl}), heat of evaporation (ΔH_v), heat of combustion (ΔH_c), flash point (T_{flash}), boiling point (T_b) and mass diffusivity (D_{AB}). The flash point provides information at which temperature the vapor from droplet can sustain a flash fire, and the boiling point determines how much heat ($C_{pl} \times \Delta T,\ \Delta T = (T_b - T_u)$) is needed to bring the liquid droplet to the point of evaporation. Because the three hydrocarbons are in the same group and the flash point has a strong relationship with their boiling points, ΔT would be used to represent the effect of T_b and T_{flash} in the equation.

The mass diffusivity was calculated at 725 K as mentioned in Chapter 5.3.1, and it was obtained from MD simulation based on experimental data from nitrogen atmosphere at 1 atm [79]. The functions of mass diffusivity (cm^2/s) as temperature (K) are given in eq. (19).

$$C_8H_{18}/N_2: D_{AB} = 4.993 \times 10^{-6} T^{1.671}$$
$$C_{10}H_{22}/N_2: D_{AB} = 4.006 \times 10^{-6} T^{1.681}$$
$$C_{12}H_{26}/N_2: D_{AB} = 3.508 \times 10^{-6} T^{1.679} \quad (19)$$

With the information provided, the empirical equation to predict the normalized flame speed ($\bar{S}$) based on the normalized droplet size ($\bar{d}$) is demonstrated in eq. (20).

$$\bar{S} = \bar{d}^{m}$$

$$\text{for } \bar{d} \leq 1,\ m = \frac{{\rho_l}^{1.78} \times {k_l}^{1.78} \times \Delta H_c \times {D_{AB}}^{0.05}}{C_{pl} \times \Delta H_v \times \Delta T}$$

$$\text{for } \bar{d} > 1,\ m = \ln\left(\frac{\rho_l \times k_l \times \Delta {H_c}^{6.495} \times {D_{AB}}^{0.01}}{C_{pl} \times \Delta {H_v}^{9}}\right) \quad (20)$$

The results of m for the three *n*-alkanes are shown in Table 15, and the fittings of empirical equation are plotted in Figure 46. It can be found that the value of m for different alkanes is very close for $\bar{d} \leq 1$, and the value of m was doubled when the number of carbon was decreased by 2 for $\bar{d} > 1$. In addition, the empirical curves fitted well with experimental data for all three hydrocarbons here. Therefore, the trend of normalized aerosol flame speed can be reasonably represented by the normalized droplet size and liquid properties.

Table 15. Values of m for the three *n*-alkanes

	n-Octane	*n*-Decane	*n*-Dodecane
$\bar{d} \leq 1$	1.21	1.03	1.13
$\bar{d} > 1$	-2.01	-1.04	-0.51

There was a qualitative scheme for the selection of heat transfer fluids in the process industries. This selection mainly based on operating pressure and potential droplet size

once leaked [22]. The smaller size the aerosol may be generated, the higher hazards the liquid may possess. However, it didn't consider that the aerosol flame speed can be enhanced once the droplet size falls into the transition range. In addition, the location of transition range may change with liquid properties. Therefore, it is extremely important to understand the behavior of aerosols in order to make the proper judgement.

5.4. Summary

The three *n*-alkane aerosols were produced by electrospray to examine their flame speed. It was found that the aerosol flame speeds for the three hydrocarbons were increased in a certain range of droplet sizes, termed transition droplet size range. A theoretical calculation based on convective droplet evaporation, mass and energy balance was used to predict the trend of flame propagation. Although the magnitude of flame speed was acceptable for *n*-octane aerosols, the transition range was failed to predict. Moreover, the deviation between experimental data and calculation became more obvious when the carbon chain increased. This may be due to the fact that the vapor flame speed under room temperature cannot be applied to liquids with higher flash points. Sensitivity analysis of droplet moving speed was conducted. The results concluded that the effect of droplet speed was not significant once it had been considered in the model.

An empirical equation was performed to describe the behavior of flame propagation. The equation relied on the normalized flame speed, normalized droplet size and liquid

properties. Since the three flame speeds were normalized, they can be compared on the same graph. The trend of normalized flame speeds for the normalized droplet size less than one was similar. This may be explained that their behavior were similar to vapor under this condition. Nevertheless, the distinction between the normalized flame speeds became significant when the normalized droplet size became larger. This may stem from the fact that more and more energy was required to vaporize the droplets.

It is proved that the aerosol flame speed can be enhanced under certain conditions, which poses higher hazardous situations. Besides, the complexity of flame propagation and the scarcity of flammability data all hinder the understanding of aerosol flammability. In addition, the transition range may shift with liquid properties. It is therefore necessary to research other fluids under the same or different conditions with regard to aerosol formation, flame speed, flammability limit and ignition energy. Then the use of such information can help the selection of appropriate fluids and change of process parameters to make the process inherently safer. At least, when the potential of aerosol generation and transition range are identified, appropriate countermeasures must be employed to reduce the consequences.

CHAPTER VI

CONCLUSIONS AND FUTURE WORK

This chapter summarizes the major findings of the aerosol research presented in this dissertation. In addition, potential future work and opportunities to improve aerosol safety are also outlined in this chapter.

6.1. Conclusions

In this dissertation the study of aerosol flame speed has been realized by using electrospray technique. The electrospray system was modified in order to generate higher quality aerosols, and the major parameters to control the generation of aerosol had been discussed. The field of aerosol research has been studied for decades and the use of electrospray to produce aerosol are also not brand new. However, the design of electrospray and discussion of ignition sources may put some new thought to this field. In addition, the major controlling parameters were explored more extensively and the "stable region" was defined for the consistent results. Finally, the special flame propagation phenomenon was identified and the theoretical calculation was improved to better describe its behavior. An empirical analysis was demonstrated to fit the trend of aerosol flame propagation of different hydrocarbons successfully, which may provide insight on the fundamentals of aerosol properties.

In Chapter III, the physical improvement of electrospray device was achieved by redesigning the electrospray configuration completely. The distance between nozzles was reduced, which resulted in the nozzle packing density increased by five folds. The denser packing of nozzles can increase the aerosol concentration although it was not linear. This is due to the fact that the highly charged droplets will repulse each other and expand the aerosol plume. These nozzles were aligned with the center of the mesh holes to create uniform electric field. If the electric field is not uniform, the resulting electrical force on each nozzle is not even. This can cause the droplets to be poly-dispersed, which will degrade the quality of aerosol flame speed data since we cannot determine which part of aerosols contributes to the observed phenomenon.

As mentioned earlier, the droplets are highly charged. On the positive side, they would not be agglomerated easily. However, on the negative side, they will be attracted back to the electrospray device unless there is another guiding force. This had caused the low concentration problem in previous studies. Therefore, three flat grounded meshes were first introduced to resolve or mitigate this issue. And the medium-size flat grounded mesh can provide the best results. Nevertheless, when liquid flow was high, the flat grounded mesh alone was unable to confine the aerosol plume appropriately. The escaped droplets stained the laser lens and impeded the measurement of droplet size and aerosol concentration. As a result, the other three grounded meshes in cylindrical shape were provided to confine the aerosols. Again, the medium-size cylindrical grounded mesh is the

best one. The results of aerosol generation from the improved electrospray system and the previous device were compared to depict the capability of the new device.

In addition to electrospray, ignition sources were also examined. It was found that the 1.5 cm pilot flame failed to ignite small droplet size aerosols. It is speculated that the turbulence created by the pilot flame is too strong. Therefore, a simple hot NiCr wire was designed and tested. However, the hot wire melted down while igniting the aerosol and it is not safe to use hot wire as an ignition source here. Exploding wire with 10 J of energy was also tested, but it failed either. Finally, the small droplet aerosols were ignited with 0.5 cm pilot flame successfully.

In Chapter IV, the three major parameters (additive effect, liquid flow rate and applied voltage) were explored in order to generate stable and small droplet size aerosols. The goal was to research transitional flame speed which may occur at small droplet size range. First of all, four types of additives (antistatic agent — Stadis 450, ionic liquid — [BMIM][OcSO4], surfactant — Span 20 and alcohol — butanol) were selected based on their potential to facilitate the breakup of liquid droplets by increasing liquid electrical conductivity and lowering surface tension. It is concluded that Stadis 450 is the most effective one to reduce droplet size. However, this is the least influential factor to change droplet size amongst these three parameters once the liquid electrical conductivity is increased and suitable for electrospray application. In addition, the amount of additive also plays a major role in affecting droplet size distribution. When the amount of additive is

high, the size distribution tends to be wide. Therefore, the type and amount of additive should be designed carefully in order to produce an aerosol with small and uniform size distribution.

The liquid flow rate is the most influential parameter to change droplet size. It has almost linear relationship with droplet size. Nevertheless, in many cases, reducing flow rate to obtain small droplet is not a viable solution. The applied voltage or electrical force also can adjust droplet size, especially for high liquid flow rate. Unlike additive effect, the liquid flow rate and applied voltage showed different behavior in affecting droplet size distribution. There is a certain range of liquid flow rate and applied voltage where the size distribution is much uniform than smaller or larger values of liquid flow rate or applied voltage. Besides, the second electric field between relative ground meshes and absolute ground also played a role in reducing droplet size and size distribution. Based on the information, a "stable aerosol generation region" was defined. Example of *n*-octane aerosol flame speed was presented to highlight the importance of this region with regard to obtaining consistent flame speed data.

In Chapter V, the three *n*-alkanes, *n*-octane, *n*-decane and *n*-dodecane, were studied using the improvement of electrospray and optimal operating parameters. A "transition droplet size range" where the aerosol flame speed is enhanced is identified for these hydrocarbons. If an aerosol has the potential to form with such droplet sizes, its hazards may be more devastating than vapor or other smaller droplet size aerosols. Therefore, appropriate

countermeasures should be applied to avoid or mitigate the hazards, such as use of other fluids and change of process conditions, if possible.

Theoretical calculation based on mass and energy balance and convective droplet evaporation was used to predict the aerosol flame speed. Although it has been improved and provide adequate estimate on the magnitude of flame speed, it failed to predict the transition range. Moreover, the model was less accurate for longer chain hydrocarbons. Sensitivity analysis on droplet moving speed was also performed and it is concluded that the droplet moving speed had marginal influence in the theoretical calculation. It must be noted that the transition range is not a fixed value and it shifts with liquid properties. Therefore, this factor should also be incorporated when selecting a working fluid or designing the process operating conditions. Finally, an empirical analysis was provided to correlate the aerosol flame speed with droplet size and liquid properties. This provides us insight into how the liquid properties may affect the aerosol flammability and the possibility to improve the theoretical model.

6.2. Future work

The possible areas where improvements in aerosol flammability research and the new directions which can help us advance the understanding of aerosols and reduce aerosol hazards are suggested in this chapter.

6.2.1. Recommendations on the instrumental setup

In this work, the electrospray device was modified and the three major controlling parameters were explored to generate high quality aerosols. However, the aerosol concentration was still not high enough to research even smaller droplet size aerosols. This caused the inability to map out the complete flammable zone of aerosols. Therefore, further improvement to the electrospray device is needed. One possible way is to apply microfabrication [46] or CNC fabrication [80] to create extremely high nozzle packing density. It should be noted that the ground level or guiding force needs to be designed carefully. In addition, this electrospray device should have the ability to turn on/off the working nozzles, as demonstrated in literature [81]. It can make sure the aerosol concentration is consistent throughout various aerosol droplet sizes.

The current aerosol system is in an open chamber. Although it is easy to construct and operate, the test atmosphere cannot be changed. As a result, it is recommended to redesigning and building a new closed chamber with the ability to change temperature, pressure, humidity and gas composition (*e.g.*, oxygen concentration, addition of other flammable gases). This will allow us to research the aerosol properties extensively under different conditions and provide valuable data for theoretical modeling and managing aerosol hazards.

An electrical spark ignition (ESI) system is proposed to replace the current pilot light ignitor. The ESI has several advantages over a pilot light or a laser spark ignition (LSI). Advantages include rapid energy delivery without disruption of the aerosol generated by the electrospray as is possible by the moving pilot light. An advantage of ESI is the more realistic (lower) ignition energy values as compared to LSI, resulting in values more quantifiable to ignition sources in the field for hazard mitigation. The ESI system has been reported and deployed successfully in numerous studies of aerosols [17, 30].

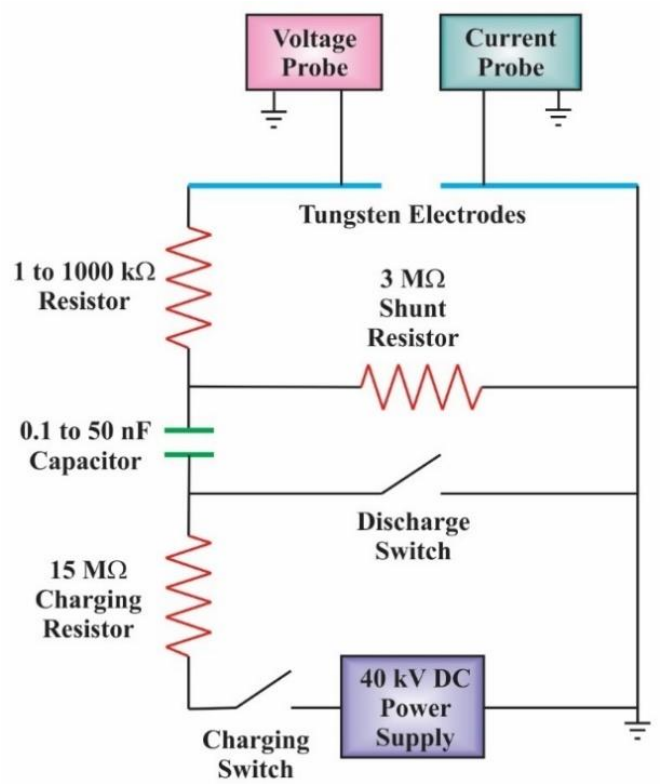

Figure 47. Electronic Spark Ignition (ESI) system

The ESI circuit is shown in Figure 47. It consists of 2.4 mm diameter tungsten electrodes placed with an adjustable gap with a standard position of 2 mm of separation. The system will allow the control of the energy and duration of sparks. The modified RC circuit in Figure 47 will have a range of capacitors from 0.5 to 50 nF. A high voltage charging supply will provide 20 kV to the capacitors. Discharge will occur through a resistor ranging from 1 to 1000 Ω. Precise control of the charging and discharging switching will be performed automatically permitting duration of 60 μs. A high voltage probe will be used to capture current and voltage traces during spark discharge to determine the energy delivery and duration. With the range of capacitors, the ignition energies vary from 0.35 to 50 mJ. If expansion of the energy is required for specific hydrocarbon lean limits, larger capacitors can be added.

OH Planar Laser-Induced Fluorescence (PLIF) and simultaneous OH/CH_2O (formaldehyde) PLIF are also recommended to expand the capability of instrument. Nakabe *et al.* pointed out the OH radical emission on the flame surface had a peak intensity, which was suitable for detection of successful ignition and flame structure [82]. In their work, OH PLIF was used to find the correlation between the emission intensity of OH radicals and the temperature and composition of gases. Müller *et al.* used OH PLIF to detect the flame kernel development in engines [83]. Therefore, OH PLIF has the ability to detect the ignition that is not easy to detect by other optical techniques. The simultaneous OH PLIF and CH_2O PLIF system will permit local heat release rate measurement that has been proved in the works done by Ayoola *et al.* [84] and Osborne

et al. [85]. The measurement of local heat release rate can be used to verify and improve Minimized Ignition Energy (MIE) models.

6.2.2. Recommendations on the experimental research

In the presented work, only three *n*-alkanes were examined to validate the concept of transition droplet size range and aerosol flame speed. However, there are many types of fluids used and stored in the process industries capable of forming aerosol clouds. Therefore, it is important to understand how the different types of flammable and combustible materials behave in the form of aerosol.

In addition to aerosol flame speed, it is equally important to understand the flammable range. As mentioned in Chapter II, the flammability limit of aerosol is still not clear, and efforts should be made to map out the flammable zone so prevention and mitigation strategies can be planned accordingly. The study of flammability limit may be realized after instrumental upgrade outlined in Chapter 6.2.1.

Although the formation of aerosol usually occurs in the normal atmospheric condition, it is interesting to understand aerosol behavior under different conditions and it may have great applications to manage aerosol hazards. As proposed in Chapter 6.2.1, the aerosol chamber can be upgraded to a close system. Temperature and pressure in the chamber can be controlled to mimic certain release conditions, which helps understand the effect of

temperature and pressure on aerosols. In addition, some other flammable gases can be added in the chamber to create a hybrid system as the presence of flammable gas may worsen the aerosol hazards. The humidity in the chamber can also be varied to understand the inhibition ability of water vapor. In the Chevron Richmond incident [14], the aerosol cloud was only ignited partially and the fire damage was not very severe. It may get the benefit from the fire department spraying a lot of water in the area as the leakage was identified at the early phase. Another application of a closed system is to study the limiting oxygen concentration (LOC). At the LOC, the flammable or combustible plume cannot be ignited by the fixed amount of energy. This information can promote safer handling of aerosol formation.

With regard to inherently safer concept, it is great to have an aerosol cloud which could not be ignited or has very low flame propagation speed if the aerosol formation is unavoidable. The idea is to blend a small amount of nanoparticles which can render the aerosol flammability. Nanoparticles have been studied as fire retarder in the polymer. However, it has not been seen in the flammable or combustible liquid and the corresponding aerosol form. The tentative candidates to inhibit aerosol flammability are nano-SiO2, nano-Sodium bicarbonate (SBC), nano-boron nitride (BN) and more.

The current ignition source is a propane pilot flame with 0.5 cm length. It is difficult to quantify the input energy and also difficult to vary its energy level. Therefore, the electrical spark ignition (ESI) system is proposed. With the modification, minimum

ignition energy (MIE) can be researched. Moreover, the relationship between energy level and above mentioned aerosol experimental properties can be studied to contribute to a comprehensive aerosol flammability database.

Once the laboratory research has been explored, the field medium and large scale experiment may be necessary to simulate the real aerosol release scenarios. Combing the knowledge of laboratory scale and theoretical understanding, the aerosol hazards can be managed and studied appropriately.

6.2.3. Recommendations on the theoretical models

Laser diagnostics on radical formation can provide valuable information about heat release, ignition delay time and possible kinetic mechanisms. This can advance the understanding of aerosol flammability and help the theoretical simulation. As demonstrated in Chapter V, theoretical calculation and empirical analysis have been used to describe the trend of aerosol flame propagation. More efforts are needed to improve the prediction model about the transition range and aerosol flame speed. Similarly, the prediction model about MIE, ignition delay time and other important properties in literature should also be improved to promote the understanding of aerosol flammability and thus help manage aerosol hazards.

REFERENCES

[1] NFPA30, Flammable and combustible liquids code, National Fire Protection Association, Quincy, MA., 2015.

[2] GHS, Globally harmonized system of classification and labelling of chemicals, 6th ed., United Nations, New York and Geneva, 2015.

[3] H.L. Febo, J.V. Valiulis, Recognize the potential for heat-transfer-fluid mist explosions, Chemical Engineering Progress, 92 (1996) 52-55.

[4] T.H. Miller, Live Oak/Milstar Complex and Carpet Service Center, United States Fire Administration, 1995.

[5] S.-y. Huang, X. Li, S. Mannan, Paratherm-NF aerosol combustion behavior simulation: ignition delay time, temperature distribution of flame propagation, and heat kernel hypothesis of combustion process analysis, Journal of Loss Prevention in the Process Industries, 26 (2013) 1415-1422.

[6] P. Sukmarg, K. Krishna, W.J. Rogers, K.D. Kihm, M.S. Mannan, Non-intrusive characterization of heat transfer fluid aerosol sprays released from an orifice, Journal of Loss Prevention in the Process Industries, 15 (2002) 19-27.

[7] K. Krishna, Measurement and prediction of aerosol formation for the safe utilization of industrial fluids, in: Chemical Engineering, Texas A&M University, College Station, TX, 2003.

[8] K. Krishna, T.K. Kim, K.D. Kihm, W.J. Rogers, M.S. Mannan, Predictive correlations for leaking heat transfer fluid aerosols in air, Journal of Loss Prevention in the Process Industries, 16 (2003) 1-8.

[9] P. Lian, D. Ng, A.F. Mejia, Z.D. Cheng, M.S. Mannan, Study on flame characteristics in aerosols by industrial heat transfer fluids, Industrial & Engineering Chemistry Research, 50 (2011) 7644-7652.

[10] P. Lian, A.F. Mejia, Z.D. Cheng, M.S. Mannan, Flammability of heat transfer fluid aerosols produced by electrospray measured by laser diffraction analysis, Journal of Loss Prevention in the Process Industries, 23 (2010) 337-345.

[11] S.-y. Huang, X. Li, M.S. Mannan, The characterization of heat transfer fluid P-NF aerosol combustion: Ignitable region and flame development, Journal of Loss Prevention in the Process Industries, 26 (2013) 1134-1144.

[12] P.J. Bowen, L.C. Shirvill, Combustion hazards posed by the pressurized atomization of high-flashpoint liquids, Journal of Loss Prevention in the Process Industries, 7 (1994) 233-241.

[13] Appendix 2 - Flixborough A2 - Mannan, Sam, in: Lees' Loss Prevention in the Process Industries (4th Edition), Butterworth-Heinemann, Oxford, UK, 2012, 2605-2623.

[14] CSB, Chevron richmond refinery investigation report in, Washington, DC, 2015.

[15] HSE, Offshore hydrocarbon releases statistics and analysis, in, Bootle, Merseyside, UK, 2002.

[16] C.E. Polymeropoulos, Flame propagation in aerosols of fuel droplets, fuel vapor and air, Combustion Science and Technology, 40 (1984) 217-232.

[17] K.K. Chan, C.S. Jou, An experimental and theoretical investigation of the transition phenomenon in fuel spray deflagration: 1. The experiment, Fuel, 67 (1988) 1223-1227.

[18] T. Niioka, Flame propagation in sprays and particle clouds of less volatile fuels, Combustion Science and Technology, 177 (2005) 1167-1182.

[19] V. Cleary, P. Bowen, H. Witlox, Flashing liquid jets and two-phase droplet dispersion: I. experiments for derivation of droplet atomisation correlations, Journal of Hazardous Materials, 142 (2007) 786-796.

[20] G.M. Faeth, Structure and atomization properties of dense turbulent sprays, Twenty-Third Symposium (International) on Combustion, 23 (1991) 1345-1352.

[21] G.M. Faeth, L.P. Hsiang, P.K. Wu, Structure and breakup properties of sprays, International Journal of Multiphase Flow, 21 (1995) 99-127.

[22] K. Krishna, W.J. Rogers, M.S. Mannan, The use of aerosol formation, flammability, and explosion information for heat-transfer fluid selection, Journal of Hazardous Materials, 104 (2003) 215-226.

[23] D.W. Johnson, J.L. Woodward, RELEASE: A model with data to predict aerosol rainout in accidental releases, Center for Chemical Process Safety of the American Institute of Chemical Engineers, New York, NY, 1999.

[24] H. Witlox, P. Bowen, Flashing liquid jets and two-phase dispersion — a review, Health and Safety Executive, Merseyside, UK, 2002.

[25] H. Witlox, M. Harper, P. Bowen, V. Cleary, Flashing liquid jets and two-phase droplet dispersion: II. Comparison and validation of droplet size and rainout formulations, Journal of Hazardous Materials, 142 (2007) 797-809.

[26] Factory Mutual Engineering Corporation, Accident prevention manual for industrial operations, National Safety Council, Chicago, IL, 1974.

[27] R.C. Santon, Mist fires and explosions - an incident survey, in: Proceeding IChemE Hazards XXI Symposium & Workshop, Manchester, UK. , 2009.

[28] D.R. Ballal, A.H. Lefebvre, Ignition and flame quenching of flowing heterogeneous fuel-air mixtures, Combustiom Flame, 35 (1979) 155-168.

[29] A.K. Singh, C.E. Polymeropoulos, Spark ignition of aerosols, Symposium (International) on Combustion, 21 (1988) 513-519.

[30] A.M. Danis, I. Namer, N.P. Cernansky, Droplet size and equivalence ratio effects on spark-ignition of monodisperse n-heptane and methanol sprays, Combustion Flame, 74 (1988) 285-294.

[31] S.K. Aggarwal, K. Nguyen, Ignition behavior of a fuel spray flowing in a tube, Chemical Engineering Communications 88 (1990) 23-29.

[32] U. von Pidoll, The ignition of clouds of sprays, powders and fibers by flames and electric sparks, Journal of Loss Prevention in the Process Industries, 14 (2001) 103-109.

[33] J. Eichhorn, Careful! Mists can explode, Petroleum Refiner, 34 (1955) 194-196.

[34] J.H. Burgoyne, L. Cohen, The effect of drop size on flame propagation in liquid aerosols, Proceedings of the Royal Society of London Series a - Mathematical and Physical Sciences, 225 (1954) 375-392.

[35] C.C. Miesse, Inhibition of flashing of aerosols, Armour Research Foundation of Illinois Institute of Technology, Arlington, VA, 1961.

[36] J.H. Burgoyne, The flammability of mists and sprays, in: Second Symposium of Chemical Process Hazards, 1963, pp. 1-5.

[37] S.J. Cook, C.F. Cullis, A.J. Good, The measurement of the flammability limits of mists, Combustion Flame, 30 (1977) 309-317.

[38] S. Hayashi, S. Kumagai, T. Sakai, Propagation velocity and structure of flames in droplet-vapor-air mixtures, Combustion Science and Technology, 15 (1977) 169-177.

[39] D.R. Ballal, A.H. Lefebvre, Flame propagation in heterogeneous mixtures of fuel droplets, fuel vapor and air, Eighteenth Symposium (International) on Combustion, 18 (1981) 321–328.

[40] K.-K. Chan, S.-R. Wu, An experimental and theoretical investigation of the transition phenomenon in fuel spray deflagration: 2. The model, Fuel, 68 (1989) 139-144.

[41] Y. Nunome, S. Kato, K. Maruta, H. Kobayashi, T. Niioka, Flame propagation of n-decane spray in microgravity, Proceedings of the Combustion Institute, 29 (2002) 2621-2626.

[42] M.V. Sullivan, J.K. Wolfe, W.A. Zisman, Flammability of the higher boiling liquidsand their mists, Industrial and Engineering Chemistry, 39 (1947) 1607-1614.

[43] W.W. Deng, J.F. Klemic, X.H. Li, M.A. Reed, A. Gomez, Liquid fuel microcombustor using microfabricated multiplexed electrospray sources, Proceedings of the Combustion Institute, 31 (2007) 2239-2246.

[44] M. Mikami, Y. Maeda, K. Matsui, T. Seo, L. Yuliati, Combustion of gaseous and liquid fuels in meso-scale tubes with wire mesh, Proceedings of the Combustion Institute, 34 (2013) 3387-3394.

[45] K.Q. Tang, A. Gomez, Monodisperse electrosprays of low electric conductivity liquids in the cone-jet mode, Journal of Colloid and Interface Science, 184 (1996) 500-511.

[46] W.W. Deng, J.F. Klemic, X.H. Li, M.A. Reed, A. Gomez, Increase of electrospray throughput using multiplexed microfabricated sources for the scalable generation of monodisperse droplets, Journal of Aerosol Science, 37 (2006) 696-714.

[47] M.S. Agathou, D.C. Kyritsis, Electrostatic atomization of hydrocarbon fuels and bio-alcohols for engine applications, Energy Conversion and Management, 60 (2012) 10-17.

[48] Malvern, Spraytec user manual, Malvern Instruments Ltd., Worcestershire, UK, 2007.

[49] M. Bumiller, The importance of refractive index when using laser diffraction, HORIBA, Ltd., 2011.

[50] C.V. Mashuga, D.A. Crowl, Application of the flammability diagram for evaluation of fire and explosion hazards of flammable vapors, Process Safety Progress, 17 (1998) 176-183.

[51] P. Lian, Flammability and combustion behaviors in aerosols formed by industrial heat transfer fluids produced by the electrospray method, in: Chemical Engineering, Texas A&M University, College Station, TX, 2011.

[52] Y.-R. Lin, H. Chen, C. Mashuga, M.S. Mannan, Improved electrospray design for aerosol generation and flame propagation analysis, Journal of Loss Prevention in the Process Industries, 38 (2015) 148-155.

[53] A.S. Dukhin, P.J. Goetz, How non-ionic "electrically neutral" surfactants enhance electrical conductivity and ion stability in non-polar liquids, Journal of Electroanalytical Chemistry, 588 (2006) 44-50.

[54] The HLB SYSTEM, a time-saving guide to emulsifier selection, ICI Americas Inc., 1980.

[55] J.M. Crosthwaite, S.N.V.K. Aki, E.J. Maginn, J.F. Brennecke, Liquid phase behavior of imidazolium-based ionic liquids with alcohols: effect of hydrogen bonding and non-polar interactions, Fluid Phase Equilibria, 228–229 (2005) 303-309.

[56] Y.-H. Yu, A.N. Soriano, M.-H. Li, Heat capacities and electrical conductivities of 1-ethyl-3-methylimidazolium-based ionic liquids, The Journal of Chemical Thermodynamics, 41 (2009) 103-108.

[57] S.A. Dharaskar, Ionic liquids (a review): the green solvents for petroleum and hydrocarbon industries, Research Journal of Chemical Sciences, 2 (2012) 80-85.

[58] S.E. Friberg, Q. Yin, F. Pavel, R.A. Mackay, J.D. Holbrey, K.R. Seddon, P.A. Aikens, Solubilization of an ionic liquid, 1-butyl-3-methylimidazolium hexafluorophosphate, in a surfactant-water system, Journal of Dispersion Science and Technology, 21 (2000) 185-197.

[59] A. Heintz, Recent developments in thermodynamics and thermophysics of non-aqueous mixtures containing ionic liquids. A review, The Journal of Chemical Thermodynamics, 37 (2005) 525-535.

[60] L. Alonso, A. Arce, M. Francisco, A. Soto, Thiophene separation from aliphatic hydrocarbons using the 1-ethyl-3-methylimidazolium ethylsulfate ionic liquid, Fluid Phase Equilibria, 270 (2008) 97-102.

[61] T.M. Letcher, A. Marciniak, M. Marciniak, U. Domańska, Determination of activity coefficients at infinite dilution of solutes in the ionic liquid 1-butyl-3-methylimidazolium octyl sulfate using gas−liquid chromatography at a temperature of 298.15 K, 313.15 K, or 328.15 K, Journal of Chemical & Engineering Data, 50 (2005) 1294-1298.

[62] U. Domańska, A. Pobudkowska, F. Eckert, Liquid–liquid equilibria in the binary systems (1,3-dimethylimidazolium, or 1-butyl-3-methylimidazolium methylsulfate + hydrocarbons), Green Chemistry, 8 (2006) 268–276.

[63] U. Domańska, A. Pobudkowska, A. Wiśniewska, Solubility and excess molar properties of 1,3-dimethylimidazolium methylsulfate, or 1-butyl-3-methylimidazolium methylsulfate, or 1-butyl-3-methylimidazolium octylsulfate ionic liquids with n-alkanes and alcohols: analysis in terms of the PFP and FBT models, Journal of Solution Chemistry, 35 (2006) 311-334.

[64] L. Yuliati, T. Seo, M. Mikami, Liquid-fuel combustion in a narrow tube using an electrospray technique, Combustion Flame, 159 (2012) 462-464.

[65] A.J.F. Bombard, A. Dukhin, Ionization of a nonpolar liquid with an alcohol, Langmuir, 30 (2014) 4517-4521.

[66] I. Hayati, A.I. Bailey, T.F. Tadros, Investigations into the mechanisms of electrohydrodynamic spraying of liquids: I. effect of electric field and the environment on pendant drops and factors affecting the formation of stable jets and atomization, Journal of Colloid and Interface Science, 117 (1987) 205-221.

[67] B.E. de Cominges, M.M. Pineiro, E. Mascato, L. Mosteiro, T.P. Iglesias, J.L. Legido, Relative permittivities of binary mixtures of 1-butanol + n-alkane at 298.15 k, Journal of Thermal Analysis and Calorimetry, 72 (2003) 129-133.

[68] J.B. Greenberg, I. Silverman, Y. Tambour, A new heterogeneous burning velocity formula for the propagation of a laminar flame front through a polydisperse spray of droplets, Combustion Flame, 104 (1996) 358-368.

[69] M. Zhu, B. Rogg, Modelling and simulation of sprays in laminar flames, Meccanica, 31 (1996) 177-193.

[70] X. Liu, Q. Zhang, Y. Wang, Influence of particle size on the explosion parameters in two-phase vapor–liquid n-hexane/air mixtures, Process Safety and Environmental Protection, 95 (2015) 184-194.

[71] N.N. Smirnov, V.N. Pushkin, V.R. Dushin, A.V. Kulchitskiy, Microgravity investigation of laminar flame propagation in monodisperse gas–droplet mixtures, Acta Astronautica, 61 (2007) 626-636.

[72] F. Atzler, F.X. Demoulin, M. Lawes, Y. Lee, N. Marquez, Burning rates and flame oscillations in globally homogeneous two-phase mixtures (flame speed oscillations in droplet cloud flames), Combustion Science and Technology, 178 (2006) 2177-2198.

[73] P. Lian, X. Gao, M.S. Mannan, Prediction of minimum ignition energy of aerosols using flame kernel modeling combined with flame front propagation theory, Journal of Loss Prevention in the Process Industries, 25 (2012) 103-113.

[74] W.A. Sirignano, Fluid dynamics and transport of droplets and sprays, Cambridge University Press, Cambridge, U.K., 2010.

[75] A. Williams, Combustion of liquid fuel sprays, Butterworth & Co Ltd, London, UK, 1990.

[76] B. Abramzon, W.A. Sirignano, Droplet vaporization model for spray combustion calculations, International Journal of Heat and Mass Transfer, 32 (1989) 1605-1618.

[77] C. Ji, E. Dames, Y.L. Wang, H. Wang, F.N. Egolfopoulos, Propagation and extinction of premixed C5–C12 n-alkane flames, Combustion Flame, 157 (2010) 277-287.

[78] W. Deng, A. Gomez, Influence of space charge on the scale-up of multiplexed electrosprays, Journal of Aerosol Science, 38 (2007) 1062-1078.

[79] K. Chae, Mass diffusion and chemical kinetic data for jet fuel surrogates in: Mechanical Engineering, University of Michigan, Ann Arbor, MI, 2010, pp. 184.

[80] P. Lozano, M. Martínez-Sánchez, J.M. Lopez-Urdiales, Electrospray emission from nonwetting flat dielectric surfaces, Journal of Colloid and Interface Science, 276 (2004) 392-399.

[81] W. Deng, C.M. Waits, A. Gomez, Digital electrospray for controlled deposition, Review of Scientific Instruments, 81 (2010) 035114.

[82] K. Nakabe, Y. Mizutani, T. Hirao, S. Tanimura, Burning characteristics of premixed sprays and gas-liquid coburning mixtures, Combustion Flame, 74 (1988) 39-51.

[83] S.H.R. Müller, B. Böhm, M. Gleißner, S. Arndt, A. Dreizler, Analysis of the temporal flame kernel development in an optically accessible IC engine using high-speed OH-PLIF, Applied Physics B, 100 (2010) 447-452.

[84] B.O. Ayoola, R. Balachandran, J.H. Frank, E. Mastorakos, C.F. Kaminski, Spatially resolved heat release rate measurements in turbulent premixed flames, Combustion Flame, 144 (2006) 1-16.

[85] J.R. Osborne, S.A. Ramji, A.M. Steinberg, C.D. Carter, S. Peltier, S. Hammack, T. Lee, Measurement of local flame speeds in the thickened flamelet regime using simultaneous 10 kHz TPIV and OH/CH2O PLIF, in: 51st Joint Propulsion Conference, AIAA/ASME/SAE/ASEE, Orlando, FL., 2015.